DRD No. SE-7
DRL No. 58

LOW COST SOLAR ARRAY PROJECT
Large Area Silicon Sheet Task

Dist. Category UC-63
ERDA/JPL 954654- 79/1

SILICON WEB PROCESS DEVELOPMENT

QUARTERLY REPORT

October 1, 1978 - December 31, 1978

C. S. Duncan, R. G. Seidensticker, R. H. Hopkins,
J. P. McHugh, F. E. Hill, M. E. Heimlich, J. M. Driggers
Westinghouse Research & Development Center
Pittsburgh, Pennsylvania 15235

Contract No. NAS 954654

"The JPL Low-Cost Silicon Solar Array Project is sponsored by the U. S. Department of Energy and forms part of the Solar Photovoltaic Conversion Program to initiate a major effort toward the development of low-cost solar arrays. This work was performed for the Jet Propulsion Laboratory, California Institute of Technology by agreement between NASA and DOE."

(NASA-CR-158376) SILICON WEB PROCESS DEVELOPMENT Quarterly Report, 1 Oct. - 31 Dec. 1978 (Westinghouse Research and) 118 p HC A06/MF A01 CSCL 13H

N79-20282

Unclas
G3/31 16682

Westinghouse R&D Center
1310 Beulah Road
Pittsburgh, Pennsylvania 15235

TECHNICAL CONTENT STATEMENT

TABLE OF CONTENTS

TABLE OF CONTENTS (Cont.)

LIST OF FIGURES

LIST OF FIGURES (Cont.)

LIST OF FIGURES (Cont.)

LIST OF FIGURES (Cont.)

1. SUMMARY

Silicon dendritic web is a ribbon form of single crystal silicon produced directly from the melt without the use of dies or shapers. Solar cells fabricated on web have exhibited conversion efficiencies of 15.5%- the highest yet for a ribbon form of silicon. The primary objectives of this program are to develop techniques to grow silicon web at 25cm^2/min output rate and demonstrate the feasibility of web growth with simultaneous melt replenishment. The methods developed are to be compatible with efficient solar cell performance.

During this quarter the focal points of the effort have been: (1) tests of aftertrimmers to improve web width (2) evaluation of growth lid designs to raise speed and output rate (3) tests of melt replenishment hardware and (4) investigation of directed gas flow systems to control unwanted oxide deposition in the system and to improve convective cooling of the web.

The results of both computer simulations and experimental tests of a heated aftertrimmer to control deformation of wider web crystals were negative. The heated aftertrimmer actually raises stress in the material and by itself does not contribute to increasing web width. Analysis of these results led to the design, debugging and test of a water-cooled aftertrimmer. Initial computer simulations of this equipment were verified-webs grown with the cold aftertrimmer exhibited low residual stress. This work is continuing.

Systematic studies of growth lid bevel and slot width produced web growth rates up to 7cm/min and output rates on a number of occasions between 12 and 13cm^2/min, (as this report was being prepared a value over 15cm^2/min was achieved).

The control of the melt level has been identified as a critical requirement for web growth for technical, as well as economic reasons. As the melt is transformed to crystal, the position of the solid-liquid interface falls deeper into the hot growth cavity. This produces two adverse effects: (1) a reduction in growth speed and (2) an eventual increase in web stress (which limits web widening). Increased emphasis must be placed on the establishment of an operational melt replenishment system to provide the stable thermal conditions required for high output operation.

As a first step in the development of replenishment technology, we have successfully tested a manually-operated melt replenishment system. The equipment embodies a two compartment crucible design in which the melt level is self equilibrating. The silicon pellets injected to replenish the melt are kept from the growing crystal by a quartz barrier. One drawback to the system is the occasional carry over to the growth chamber of minute oxide particles by the gas jet used to keep the feed port clean. The particles attach to the web and hinder further growth.

We have examined two directed gas flow systems to control oxide deposition within the growth system. A venturi arrangement which draws gas away from the growth slot and web keeps the web and furnace shields oxide-free for long periods. The approach appears applicable to controlling oxide carry-over during feeding and will be tested in that context shortly. An alternative procedure, directing the gas through a cavity beneath the shields toward the web, produced very stable growth conditions but severely degraded cell performance. Apparently, contact of the argon with the hot molybdenum furnace parts transported impurities to the web surface, contaminating the material. This type of impurity transport if unrecognized could be a problem in other silicon growth systems. Replacement of the flooding system with an improved venturi arrangement produced solar cells with $\sim$ 14% AM1 efficiencies (with AR coating).

Web solar cell efficiency monitored to characterize the experimental crystal growth runs is typically 12.5-14%. When efficiency does fall below the higher values, deep level spectroscopy reveals impurity trap levels present in both the as-grown web and cells processed from that material. This raises the possibility of improving web cell efficiency still further by optimizing growth and cell process operations.

2. INTRODUCTION

Silicon dendritic web is a ribbon form of silicon single crystal shaped by a natural crystallographic and surface tension forces as the material is drawn from the liquid phase. The web process has a number of inherent advantages to achieve or better the 1986 Low Cost Solar Array (LSA) Project cost objective of 50 cents per peak watt of photovoltaic output power. Web solar cells have demonstrated the highest conversion efficiency-15.5% AM1-for any silicon ribbon material. The web faces are crystal facets, smooth enough as grown that they are essentially ready for cell fabrication. Costly slicing and etching are not required. The thin, 100 to 200 μm web conserves expensive silicon. Moreover, the refining action of the growth process makes feasible the use of cheaper, less pure "solar" grade silicon as it becomes available. Finally, the form of the product, long flexible strips, facilitates automation of the crystal growth and cell process operations. Taken together, these characteristics point to large savings in labor, equipment and silicon for solar cells made from silicon dendritic web.

The primary objectives of the present program are the development of technologies to raise the output rate of the web process and to show the feasibility of melt replenishment so that stable growth conditions can be maintained for practical periods. The results of previous SAMICS-IPEG economic analyses show that the LSA 1986 combined wafer and polysilicon cost goal can be met at a silicon web output rate of $25cm^2/min$ when the cost of polysilicon is \$25/kg, the web cell efficiency is 15% and a three day growth cycle is carried out. A projected wafer cost below the JPL goal can of course be achieved with these same operating parameters when \$10/kg silicon becomes available. Thus the goals of this Phase II program are to demonstrate a $25cm^2/min$ web output rate, grow crystals over 10 meters long with replenishment while maintaining the dislocation density of the material below $10^4 cm^{-2}$ and the web thickness in the range 100 to 200 μm.

The program approach involves the use of dynamic thermal trimming and special growth lid designs to increase web width and growth velocity while minimizing stress in the material. Development of the techniques is an interactive process in which computer simulation of the growing ribbon is coupled with empirical evaluation of system parameters and hardware to improve web output rate. Development of melt replenishment capability has included investigations of mechanical and thermal requirements to feed pelletized silicon to the melt while simulataneously growing web crystal. The impact of changes in growth system parameters on web seeding and web quality are monitored by structural, electrical, and device measurements to assure that the material remains compatible with the fabrication of efficient solar cells. Finally, the economic analysis is updated to reflect the progress in web technology development.

The effort this quarter has centered primarily on (1) the test of aftertrimmers to increase web width (2) design and test of high speed growth lids (3) test of pellet injection methods and crucible designs for melt replenishment and (4) the evaluation of directed gas flow systems to eliminate oxide deposition inherent with some lid-shield configurations and to improve convective gas cooling of the web. The highlights of these experiments which involved some 150 experimental runs are described in the following sections; the details of individual runs are collected in the Appendix.

3. TECHNICAL PROGRESS

3.1 Development of Techniques for High Output Web Growth

A brief review of the parameters controlling the web output rate (area grown per unit time) is a useful prelude to the discussion of recent experimental results. Figure 1 depicts the essential features of a silicon web growth furnace. Heat is introduced to the system by induction coupling to a molybdenum susceptor. The outflow of heat is controlled by a slotted molybdenum susceptor lid and heat shields through which the growing web also passes. The lid and shields shape the liquid isotherms so the center region is supercooled while the periphery remains hot enough to prevent freezing at the quartz crucible-melt interface. These elements in combination with thermal trimmers placed above the shields also define the temperature profile in the web crystal itself.

The rate at which liquid silicon is converted to web single crystal is determined by the attainable web width and growth velocity. Crystal width depends dominantly on the lateral temperature profile in the liquid while the dissipation of the latent heat of fusion controls the growth velocity. Both processes are influenced strongly by system heat flow, but in different ways. For example, the growth slot width, bevel angle, and lid thickness (and the level of the liquid in the cavity) have profound effects on web growth velocity, while the slot length, area and hole size are more important for controlling the melt temperature profile. To the first order, the two problems, (1) heat flow in the melt/crucible/susceptor system and (2) heat loss from the web and meniscus, can be decoupled and treated separately. Thus, initially techniques to raise width and speed have been investigated independently to be later coupled to maximize output rates. Sections 3.1.1 and 3.1.2 describe the individual activities dedicated to web width and speed development; initial experiments to blend the techniques are set forth in Section 3.1.3.

Dwg. 7686A17

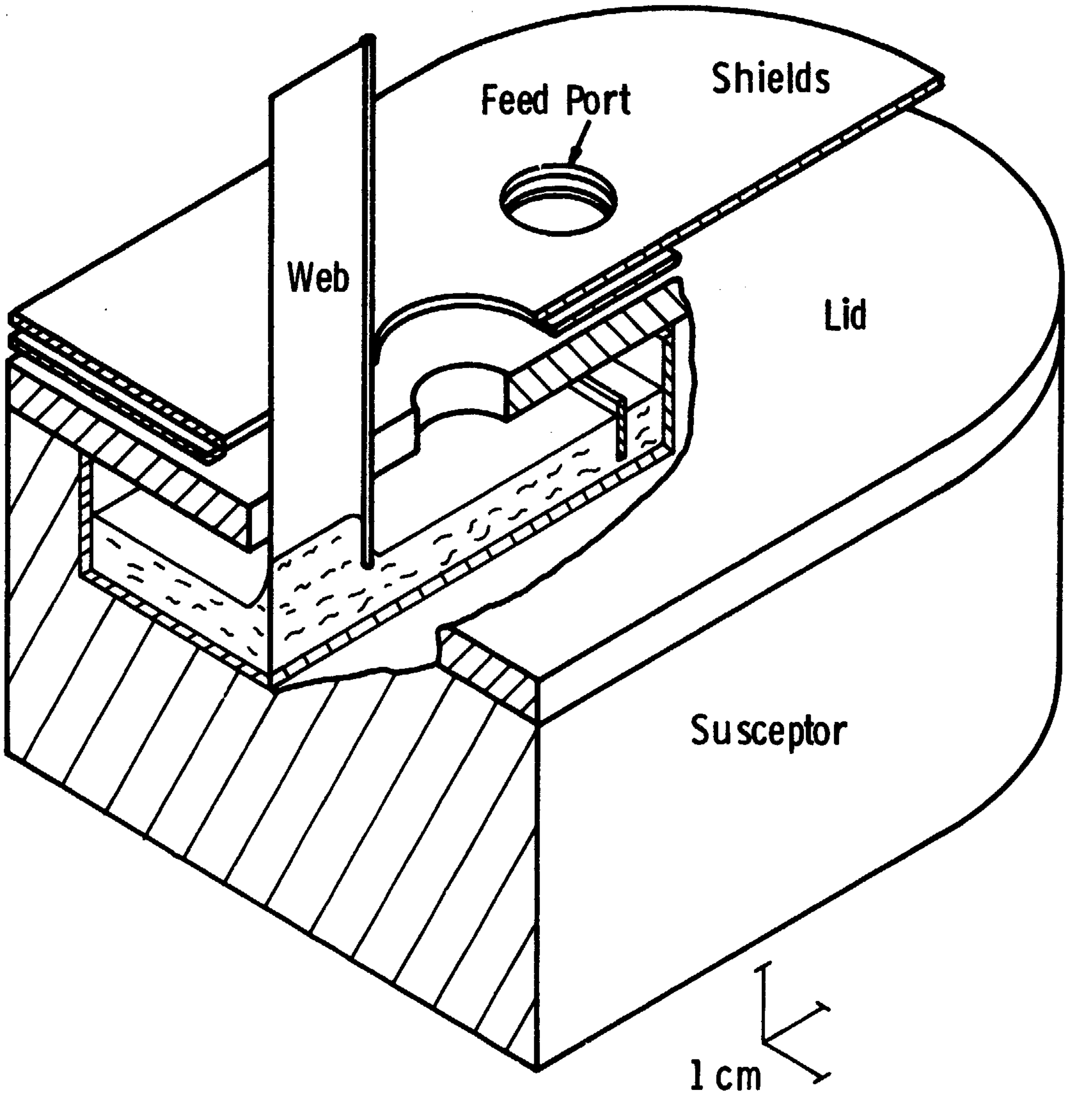

Figure 1 Schematic section of susceptor for web growth fitted with an "RE-1" lid

3.1.1 Methods for Width Enhancement

3.1.1.1 Background

The ultimate web width is dictated by the temperature profile in the melt in the way suggested by Figure 2. Heat loss from the meniscus, however, perturbs the thermal field near the tip of the bordering dendrite so that there is slightly more growth on the outer edge than on the inner edge. This causes a small deviation of the growth direction from the preferred [211] direction and the crystal widens so long as there is a uniform temperature profile in the melt. When the widening web reaches a region of increasing melt temperature as shown in the figure, the intrinsic lateral temperature gradient in the liquid counteracts the temperature gradient created by the meniscus heat loss. The web then ceases to widen and continues to grow at a steady state.

Thus if the melt profile is too steeply concave upward wide web cannot be grown. Web width runs limited by this effect at the beginning of the development program. Through a design program based on experimental development aided by computer simulations, susceptor/crucible/lid designs, which demonstrated flat melt temperature profiles over regions approximately 60 mm in length, were achieved. Figure 3 illustrates the computed and measured profile for two such configurations. As these improvements were made in the thermal profile, the width of the web which could be grown also increased from about 15 mm to over 40 mm, Figure 4.

As wider and wider web was grown, the limitation to further width increase was no longer imposed by the melt profile. Instead, stresses in the wider ribbon crystals caused them to so deform during growth that they could not be pulled through the growth slots. Measurements of some longitudinally split web crystals also indicated that residual stresses remained in the material after growth-even when deformation was not observed.(1) Both of these observations implied thermally generated stresses had to be eliminated to achieve the widest webs.

Dwg. 6438A24

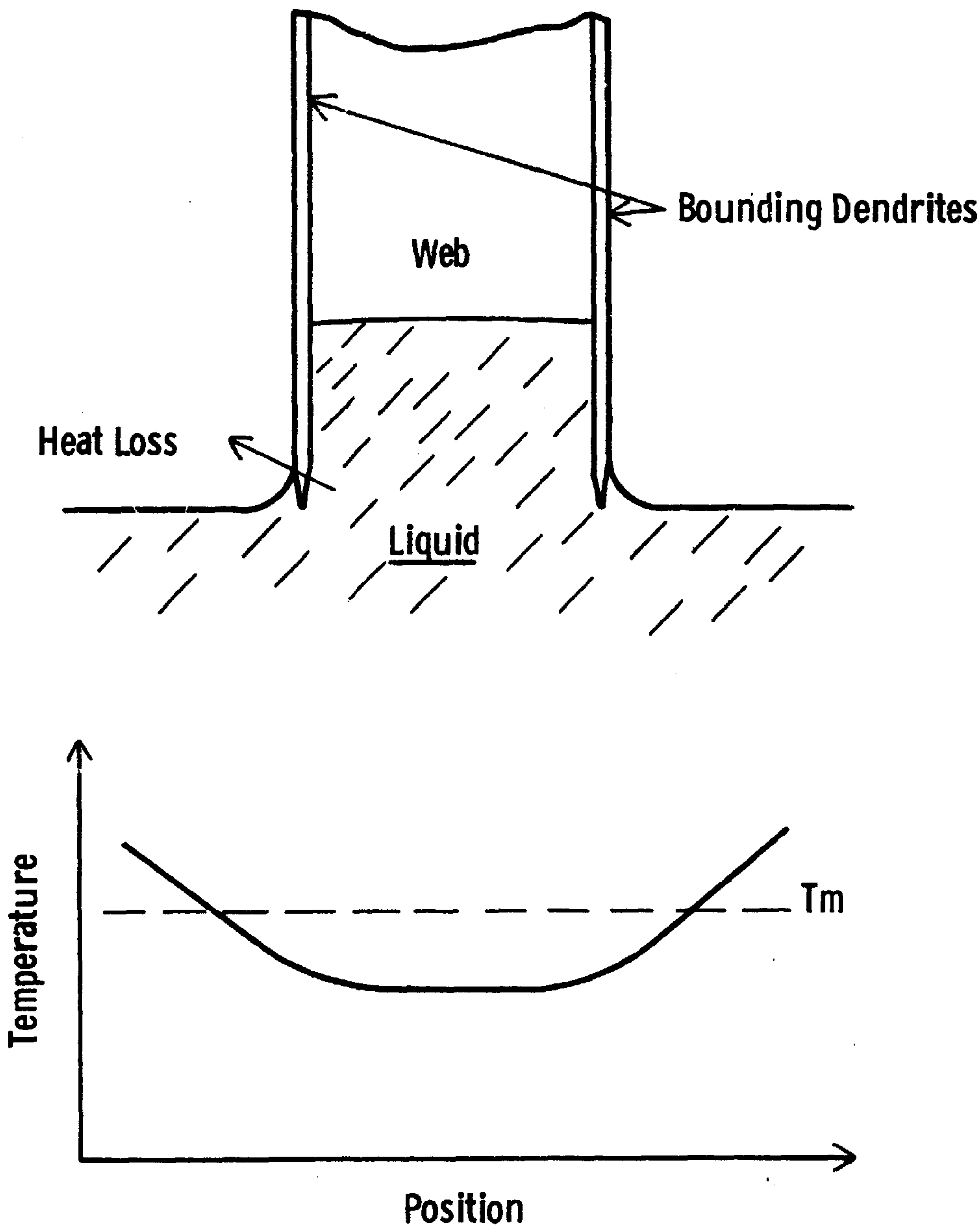

Figure 2 Schematic illustration of a growing web compared with temperature profile at melt surface

Curve 714929-A

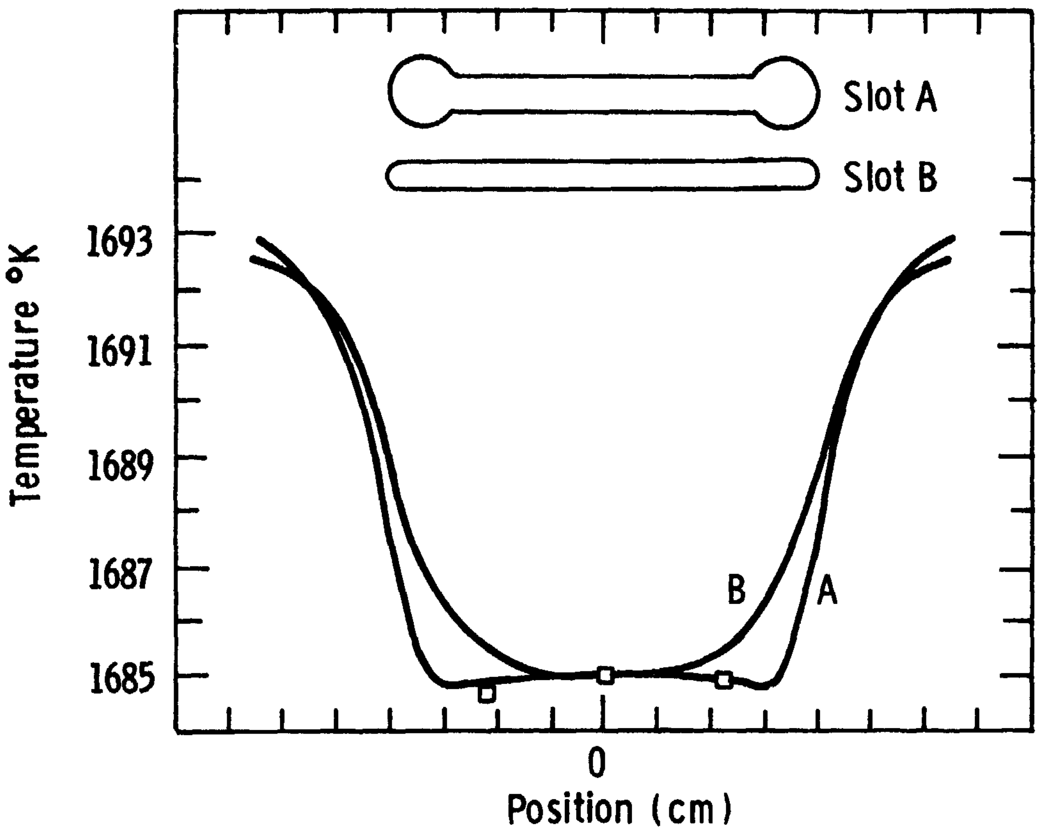

Figure 3 Computed and measured melt temperature profiles for different lid slot geometries

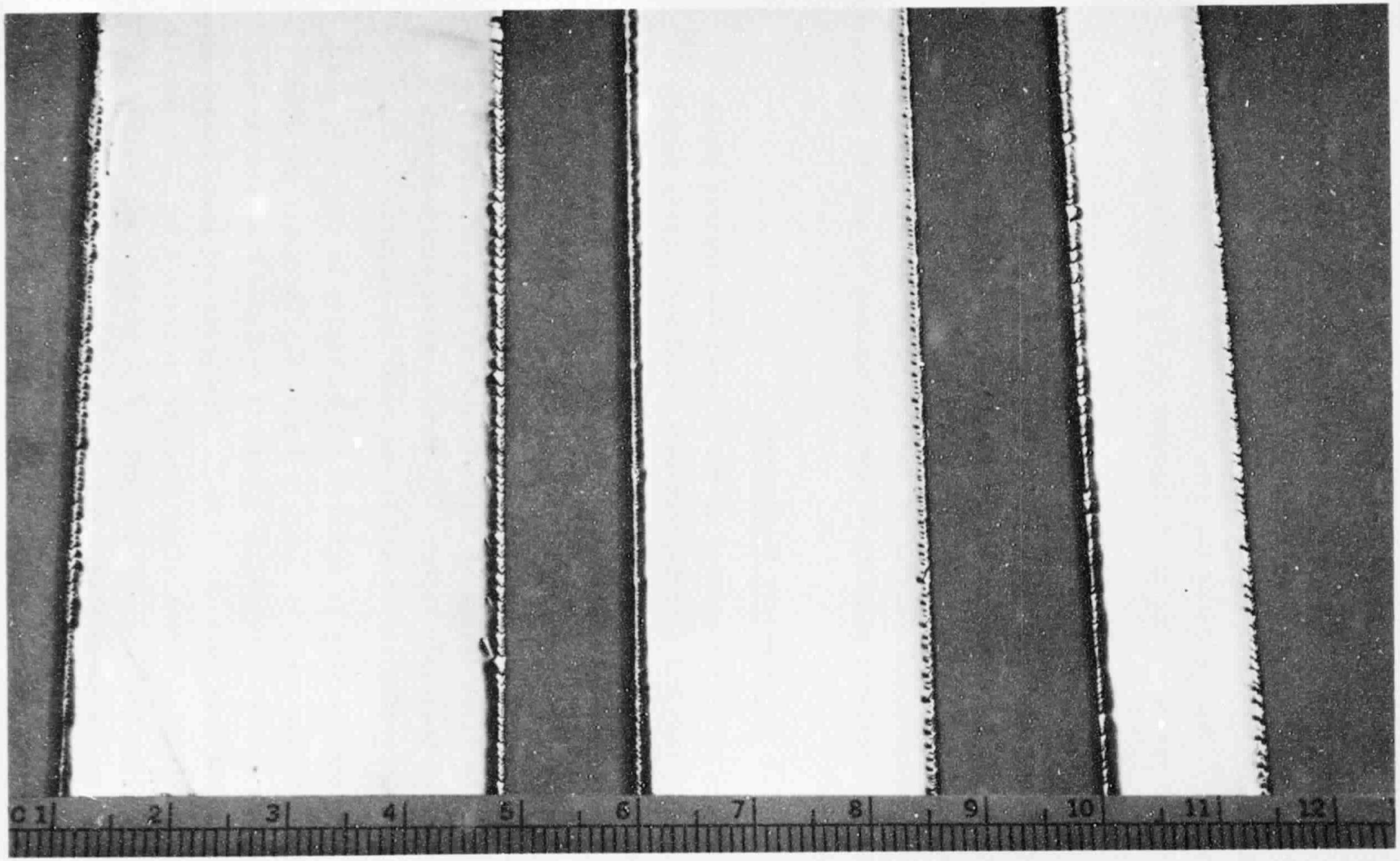

Figure 4 Dendritic web crystals grown from melts with different lateral temperature profiles. Flatter profile produces wider webs.

Measurements of residual stress on material grown from lids with different vertical profiles (straight sides, bevels) and various slot widths, indicated that the details of the slot geometry had a profound effect. The trends of the data collected indicated that what was required to reduce stress was management of the temperature profile in the growing web.[1]

In the present phase of this program, a parallel experimental and analytical approach was taken to identify the sources of and to control the stress in dendritic web crystals. Following the approaches taken by workers with other techniques of ribbon growth,[2,3] an afterheater assembly was designed and constructed for use in the web furnaces. Concurrently, an analytic modeling effort was mounted to aid the application of this equipment.

3.1.1.2 After Heater Development

During the first quarter of the present development phase, several forms of integral afterheaters were tried with little success.[4] These trimmers were heated by induction coupling and by conduction from the lid to which they were attached. The lack of both independent temperature control and heater positioning were obvious deficiencies with the approach, so a new and more flexible apparatus was designed and constructed. The first design of this afterheater was discussed briefly in the preceeding Quarterly Report.[5] Several minor problems were evident with that configuration and it was modified slightly.

The later version is depicted schematically in Figure 5, and a photograph of the equipment is shown in Figure 6. The upper and lower heaters on each side of the web are specially designed immersion heaters capable of operation at more than 1000°C. The upper and lower heater are joined by a thin nickel/chrome alloy sheet to generate a vertical temperature gradient along the length of the web. Each of the four heaters is equipped with its own power supply and temperature measurement and control so that a range of temperatures and temperature gradients can be obtained in practice. The vertical position of the entire assembly is also

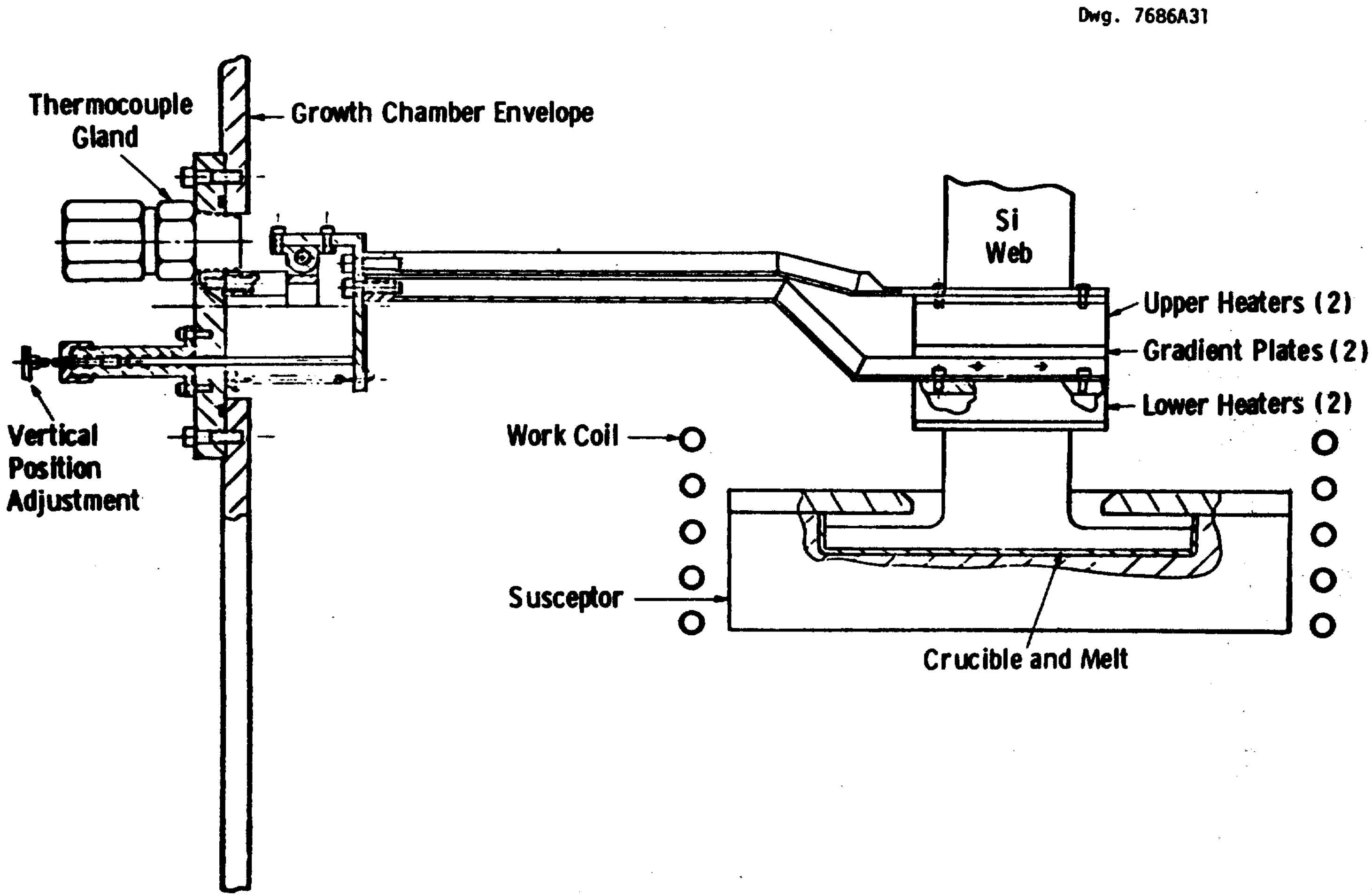

Figure 5 Schematic drawing of afterheater system used to modify vertical profile of a growing web crystal.

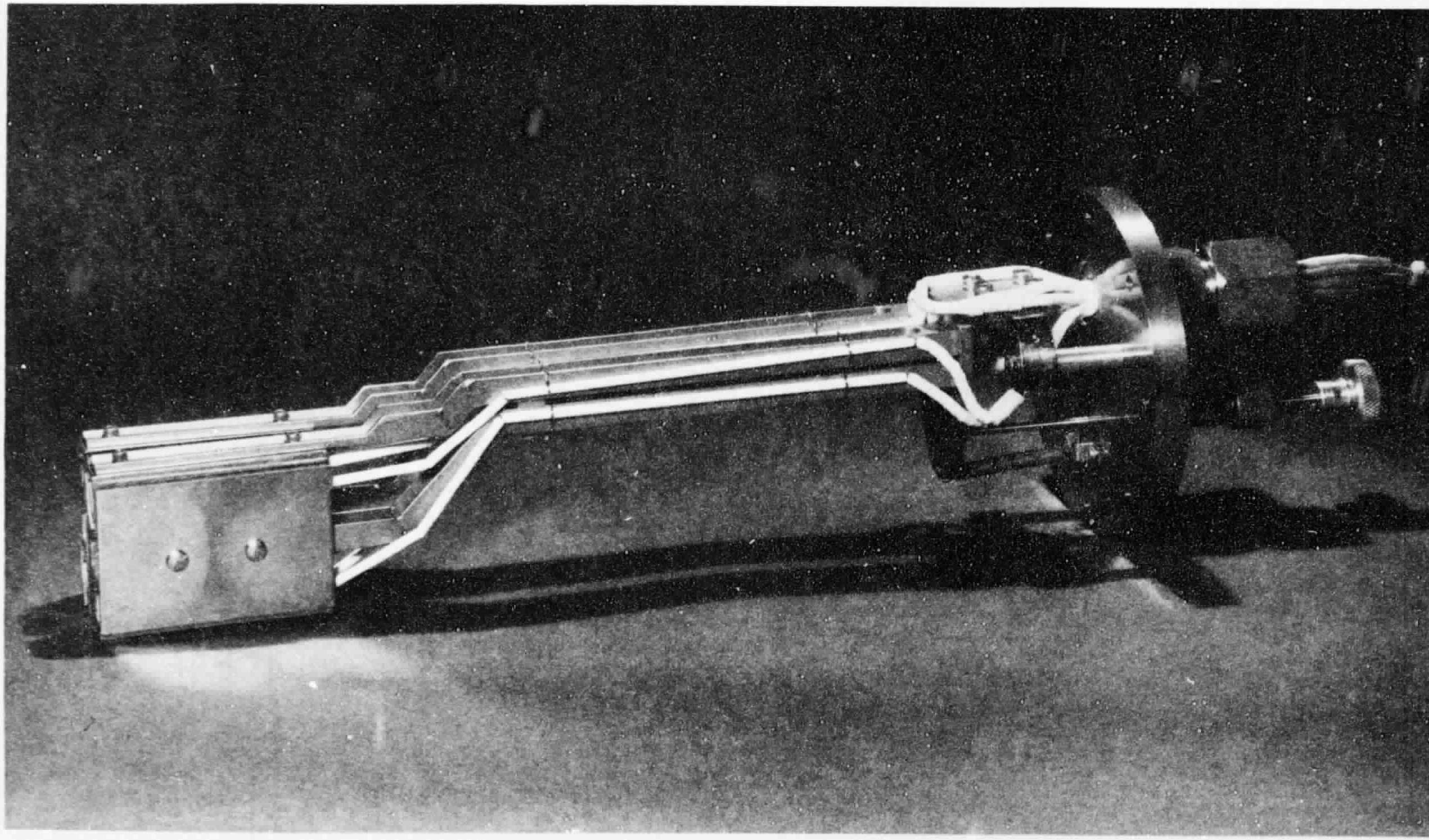

Figure 6   Photograph of Afterheater System Depicted in Figure 5.

adjustable to supply an additional control parameter for experiments. All chamber penetrations required to position and power the afterheater are vacuum tight.

Most of the operating runs with the afterheater apparatus were conducted with the bottom of the assembly about 25 mm above the top of the susceptor shields. With this arrangement, the maximum temperature difference between the bottom and top of the afterheater (full power on the bottom heater and zero power to the top heater) was 350°C or a gradient of 70°C/cm. Due to radiation coupling between the susceptor and the afterheater, the minimum temperature at the bottom of the afterheater was approximately 780°C; with full power to the heater, the maximum temperature was about 930°C. In order to increase the temperature range of the apparatus, radiation shields were added to the assembly to isolate the afterheater from the susceptor. With these shields in place, the minimum temperature was reduced to about 745°C.

The operating range of the equipment was deemed sufficient for the initial experiments. These tests were carried with the afterheater positioned above a susceptor with an "RE-1" lid assembly (Figure 7). This lid was chosen as a baseline since it produced a flat melt temperature like Figure 3A and because a wealth of growth data had been accumulated against which to compare the performance of the afterheaters.

The most compelling results of the study were that stresses, especially the residual stresses, in the web crystals increased markedly for every combination of afterheater operating conditions that was tried. For example, from previous measurements, the characteristic residual stress for the RE-1 configuration was $\sigma/W^2 = 9 \pm 8 \times 10^5$ dynes/cm^4. Measurements of crystals grown with the afterheater operated in a number of conditions were $\sigma/W^2 = 2.1 \pm 1.0 \times 10^7$ dynes/cm^4, a factor of about 20 greater than without the afterheater. Some of the reasons for this behaviour were clarified by the modeling results which became available about the time these initial afterheater tests were run.

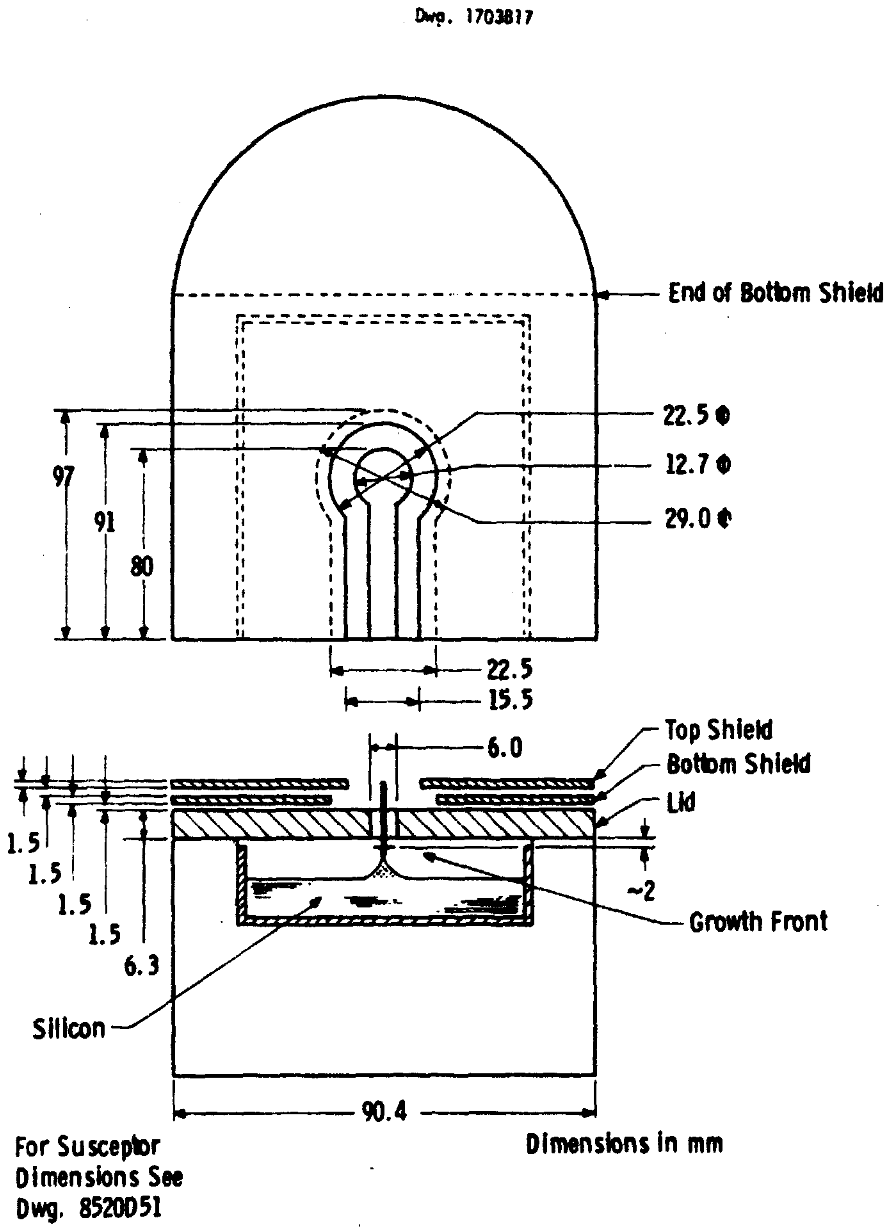

Figure 7 "RE-1" growth lid configuration (schematic).

3.1.1.3 Thermal Stress Analysis in Silicon Web

The modeling procedure for calculating the thermally-generated stress in the dendritic web crystals was discussed in the previous Quarterly Report.[5] Briefly, the temperature profile for a given lid and afterheater configuration is computed using a numerical integration of the heat flow equation in a moving coordinate system. The calculated temperatures in the ribbon are then used as input data for a finite element analysis of the stresses. In this analysis technique, the ribbon is represented by a grid of rectangular elements and each element is given its proper temperature. The size of the element changes due to thermal expansion, and the analysis program computes the stresses necessary to give continuity to the boundaries of adjacent elements. The program output then gives the stress components, principal stresses, and stress intensity for each element as well as contour plots for these variables.

The general geometry for the analysis of the afterheater case was given in the previous report[5] as were some of the preliminary results. In that discussion, emphasis was placed on the longitudinal stress component, σ_{ZZ}. It was also noted that the greatest stress difference in the longitudinal components occurred where the web was relatively cool, and thus was unlikely to be responsible for the residual stress which requires some plastic deformation of the lattice. (A large longitudinal stress, however, may induce elastic deformation, a topic considered in the next section).

In order to understand the source of residual stress, data is needed on the yield stress of silicon as a function of temperature; such data is available from the work of Graham et al. on the hot rolling of polycrystalline silicon.[6] Their results for visco-elastic flow can be summarized by the equation

$$\sigma_{YP} = 2.57\text{x}10^{-5}\ \exp(49459/T)\ \text{dynes/cm}^2. \qquad (1)$$

With this information, and the temperature profiles in the web due to the afterheater, the stress condition in the web can be reanalyzed.

Consider the three conditions depicted in Figure 8. The curves represent, respectively, the longitudinal (Z) variation in temperature along the web for the case of (1) no afterheater (2) an afterheater operating at 1100°K and (3) an afterheater operating at 300°K (the latter case is analogous to shielding the growing web from the heat radiated to it by the susceptor lid). For each temperature profile we have computed the lateral stress (σ_{YY}) and the edge to center difference in the longitudinal stress σ_{ZZ} as a function of distance above the solid liquid interface. These relationships are plotted in Figures 9 and 10, respectively. Superposed on each curve (accented lines) are the regions for which the estimated silicon yield stress (Equation 1) is exceeded. Only the lateral stresses, Figure 9, exceed the yield point. More important, the stresses in the web are highest when an afterheater is employed.

The model thus provides the explanation for our experimental result: with the dendritic web geometry an afterheater system by itself serves only to accentuate the problem of thermal stress. The model result also suggests a further line of experiment to resolve the problem.

3.1.1.4 Design and Test of "Cold" Aftertrimmers

Besides providing an explanation for the observed stress increase with the afterheater, the model curves of Figure 9 and 10 show that the distribution, which gives the lowest stress values is that with a "room temperature" afterheater, or more properly, an aftertrimmer. Further analysis of this approach lends to a conceptual design of a "cold" aftertrimmer which was then fabricated and installed in the J-Furnace. Beyond a reduction in residual stress, the cold aftertrimmer should also reduce web bending due to what we believe is elastic deformation.[5] The logic for this approach is outlined briefly below.

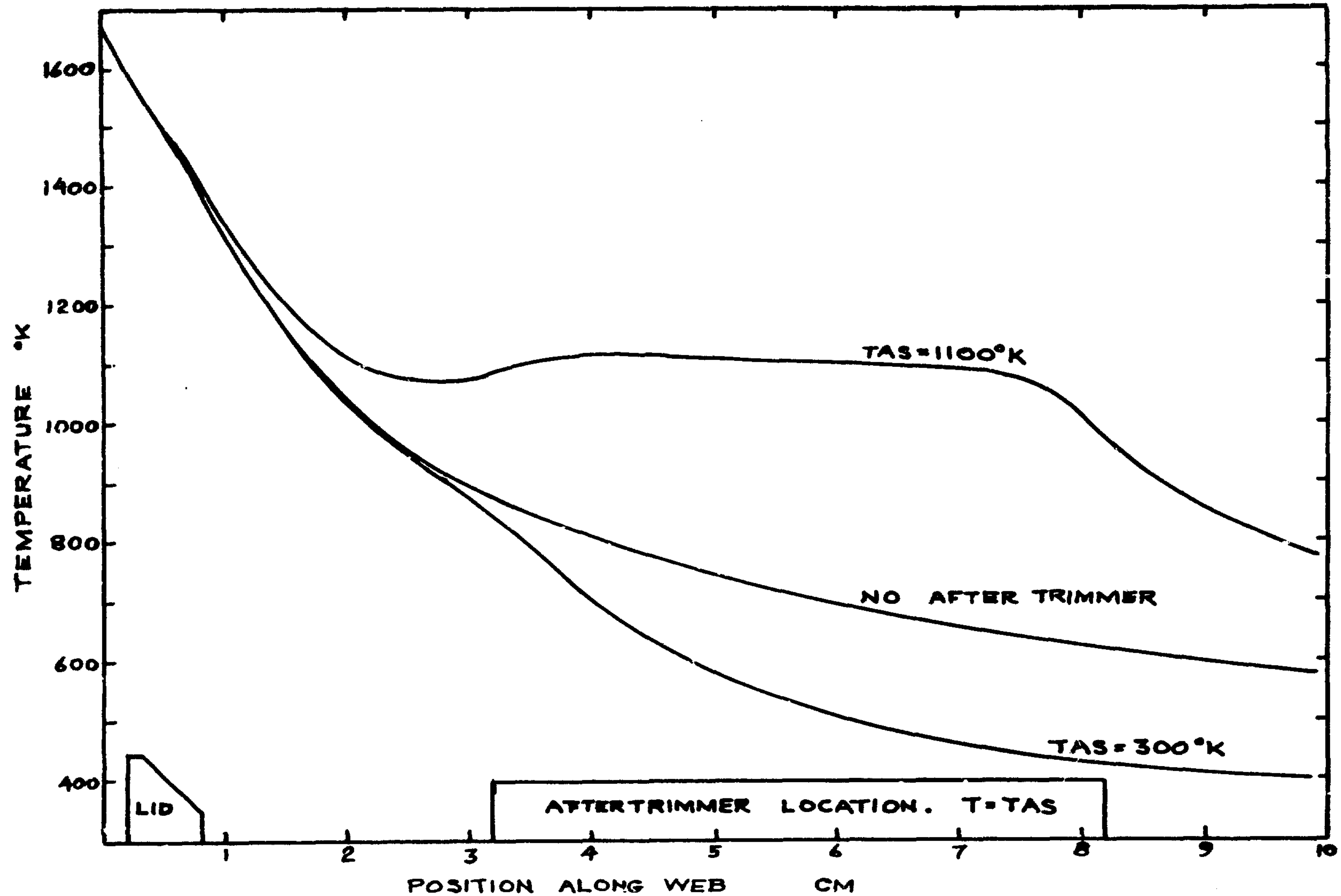

Figure 8 Computed longitudinal temperature profiles in silicon web crystals. Temperature as a function of position along web for three cases: no aftertrimmer, 300°K aftertrimmer (TAS - 300°K), and 1100°K aftertrimmer (TAS = 1100°K).

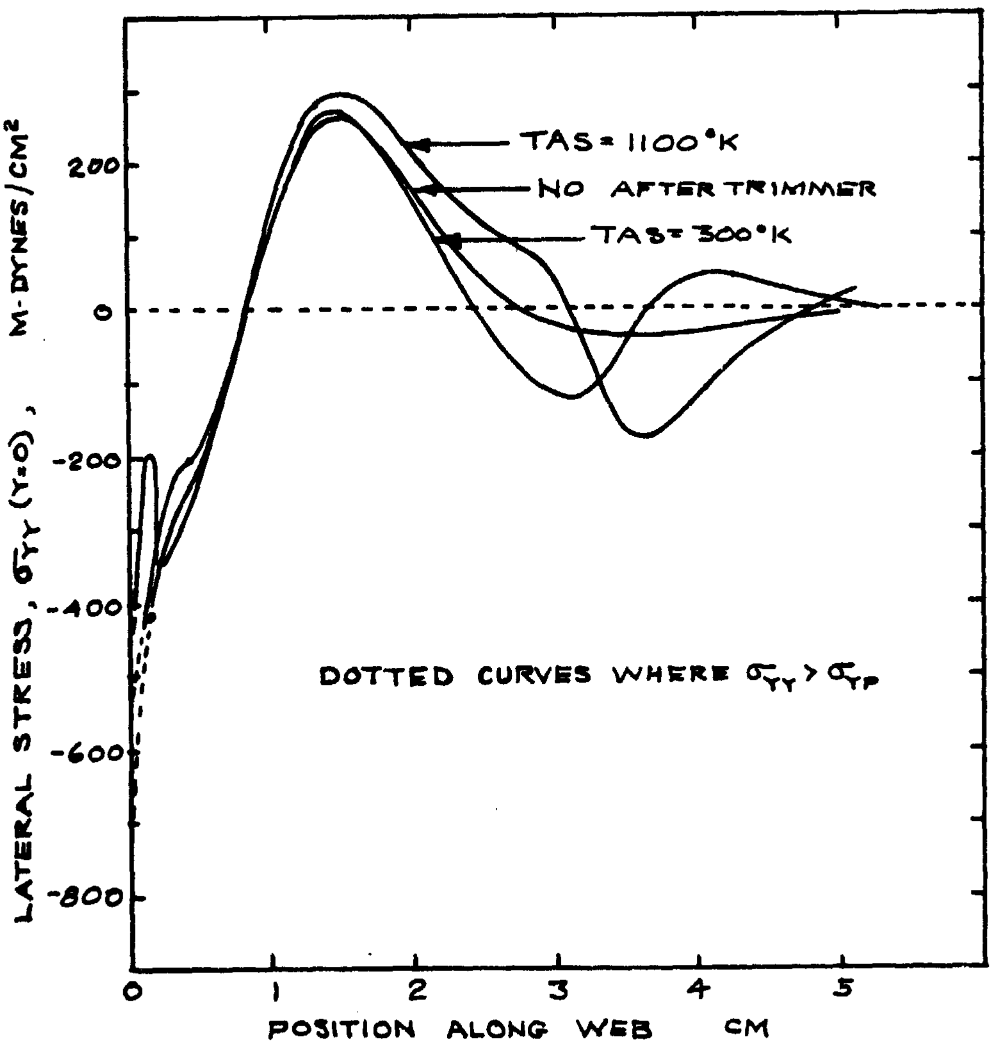

Figure 9 Computed lateral stress distribution in silicon web crystals. Lateral stress (σ_{YY}) at web centerline as a function of position above the crystal-liquid interface. Curves are dotted at positions where σ_{YY} exceeds. The silicon yield stress (σ_{YP}).

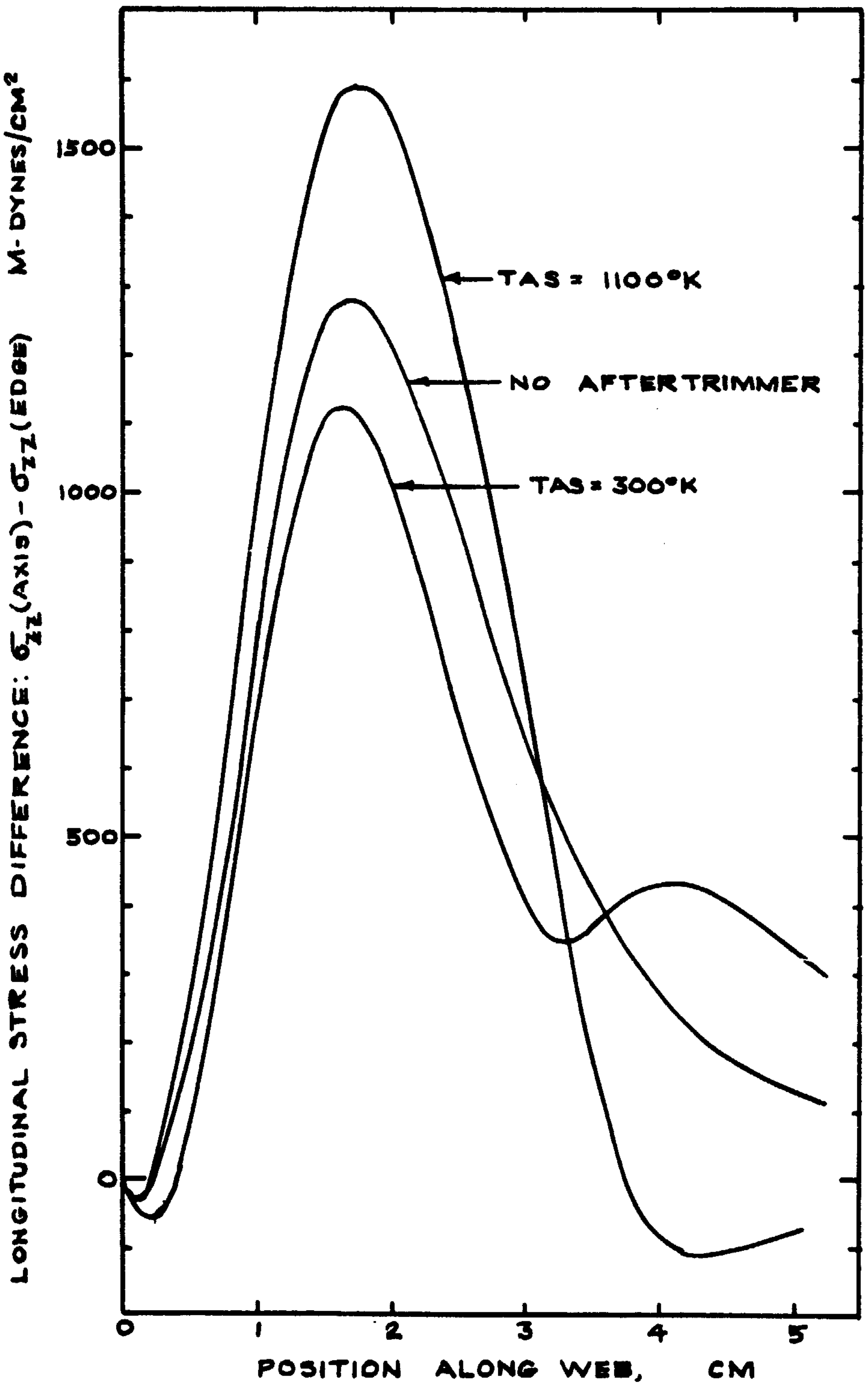

Figure 10 Computed variation in longitudinal stress difference (σ_{ZZ} axis - σ_{ZZ} edge) as a function of position about the crystal-liquid interface for three cases: no after-trimmer, 300°K after trimmer, and 1100°K after trimmer.

We have observed on a number of occasions that crystals grown from "low stress" lids are stilled deformed. Samples taken from these crystals just before the deformed regions had low residual stress levels as well as low dislocation densities. After the deformation event, the residual stress and dislocation density increased often by several orders of magnitude. These precipitous changes suggested that the deformation was due to elastic buckling of the ribbon by the large longitudinal stress fields well above the growth front. (e.g. Figure 10).

The process we envisage is illustrated schematically in Figure 11. Initially, the web grows without deformation as in Figure 11a, although stress fields are present. The largest lateral stresses are at "P" where plastic flow can occur, and the largest longitudinal stress is at E where only elastic deformation is possible. As the crystal widens, the magnitude of the stresses increases[1] and the resistance of the ribbon to buckling decreases so that at some critical point in growth (Figure 11b) the ribbon buckles with the greatest (elastic) deformation at "E", and with some lesser deformation at "P"; in addition to the curvature shown by the sections, there would also be a curvature out of the plane of the figure.

At this point, the deformation may be purely elastic, or some plastic flow may also occur at "P". In any case, the twin planes in the material must also curve and remain locally parallel to the crystal faces. However, as the ribbon continues to propagate, the new material will tend to grow in a straight line between the bounding dendrites due to surface forces in the meniscus as shown in Figure 11c. This new material cannot contain the twin plane which will emerge as a roughly parabolic trace on the ribbon surface (Figure 11d); the dislocation density and slip will also increase at this point. These "wishbone" configurations are in fact frequently observed in deformed web crystals[1,5] as is the increase in dislocation density and slip. Further, once the dislocation pinning effect of the twin planes is gone, the deformation mode of the ribbon frequently changes to a rippled morphology.

Dwg. 7686A18

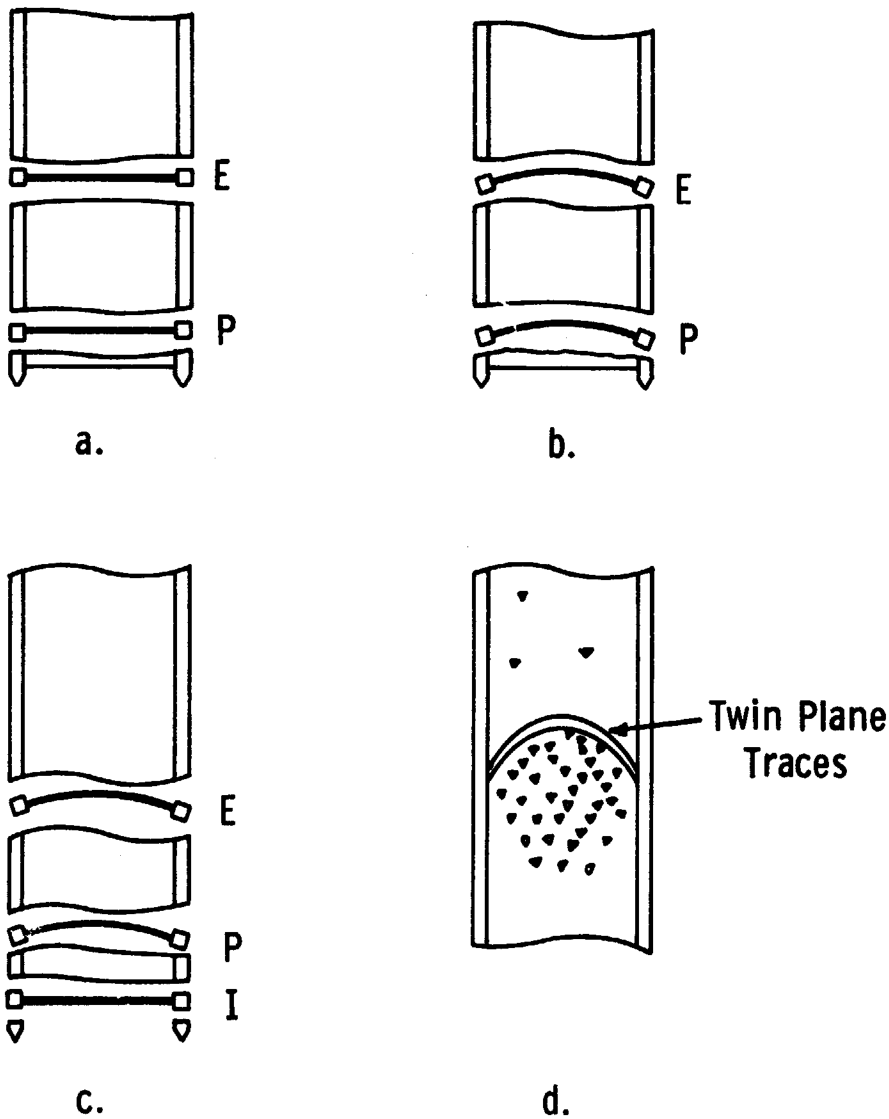

Figure 11 Hypothesized Elastic Deformation Process occurring during the growth of web crystals (see text)

Other modes which are seen include a twist, probably the result of lateral thermal asymmetry, and a long period waviness. The cold aftertrimmer functions to linearize the vertical temperature profile above the suceptor lid. This in turn reduces the stress in the material, (Figures 9 and 10), and minimizes the possibility of web buckling.

The first version of the cold aftertrimmer is shown schematically in Figure 12; two water cooled copper plates about 4x8x.3 cm mounted at a 45° angle above the susceptor assembly. Perforated tubing which was brazed to the bottom edges of the plates provided an argon flow curtain to prevent any accumulation of oxide on the aftertrimmer.

Webs grown in the first few runs of this apparatus were subject to frequent pull outs; and the formation of third dendrites. The temperature distribution on the melt surface was then carefully measured by determining the melting point of a thin dendrite at several melt positions. This test revealed that the temperature profile had been drastically altered by the presence of the aftertrimmer. Since the aftertrimmer itself was essentially at the chamber wall temperature, this perturbation should not have been the result of changes in the heat loss from the liquid. Rather the presence of the copper plates perturbed the induction heating field.

For this reason a second version of the aftertrimmer, (Figure 13), was constructed. In this design the copper plates were arranged vertically above the susceptor to have a much smaller effect on the induction field. Indeed, dendrite probes indicated that the melt temperature profile closely approximated the expected distribution for the RE-1 configuration of the susceptor assembly, although a slight right-left asymmetry still existed. Reversing the trimmer support arms so they no longer parallel the induction power leads, (by remounting the aftertrimmer in the opposite side of the chamber) eliminated the remaining assymetry.

Dwg. 7686A30

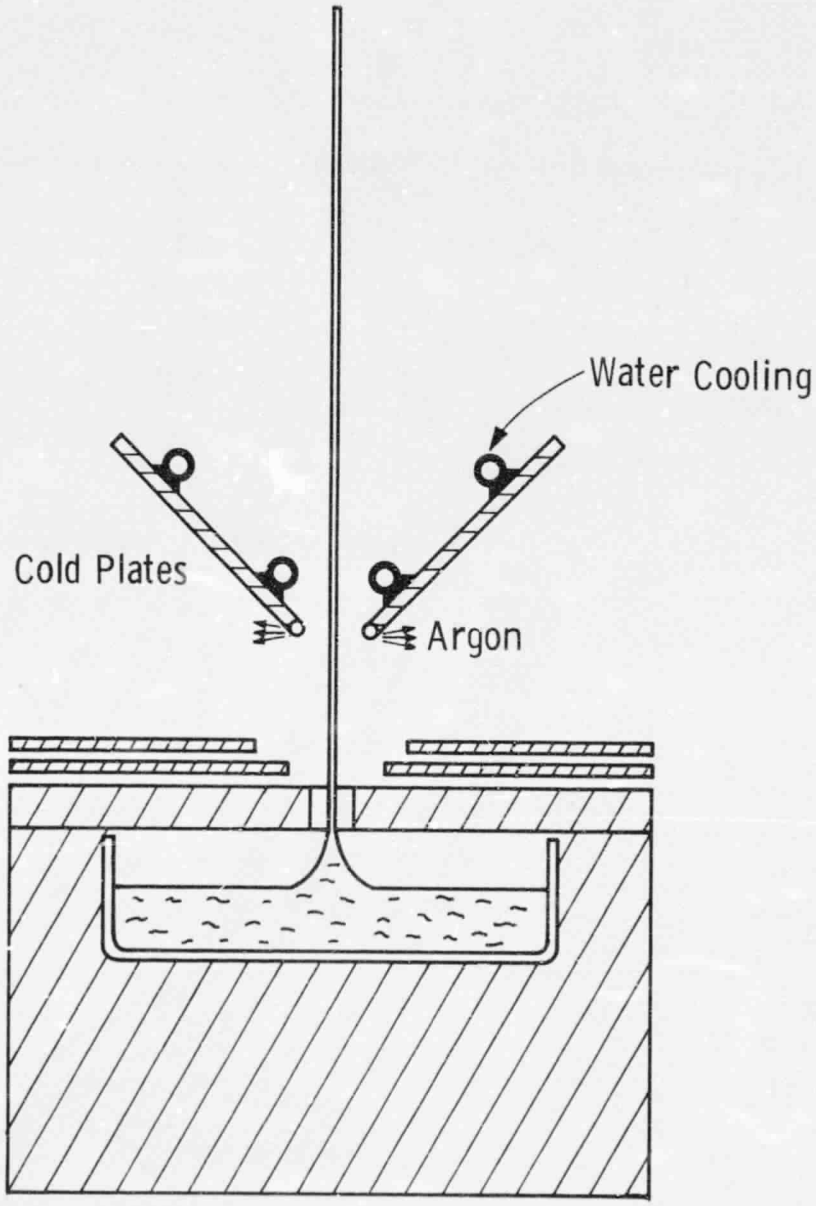

Figure 12 Schematic drawing of cold aftertrimmer with cold shield plates mounted 45° to the vertical axis.

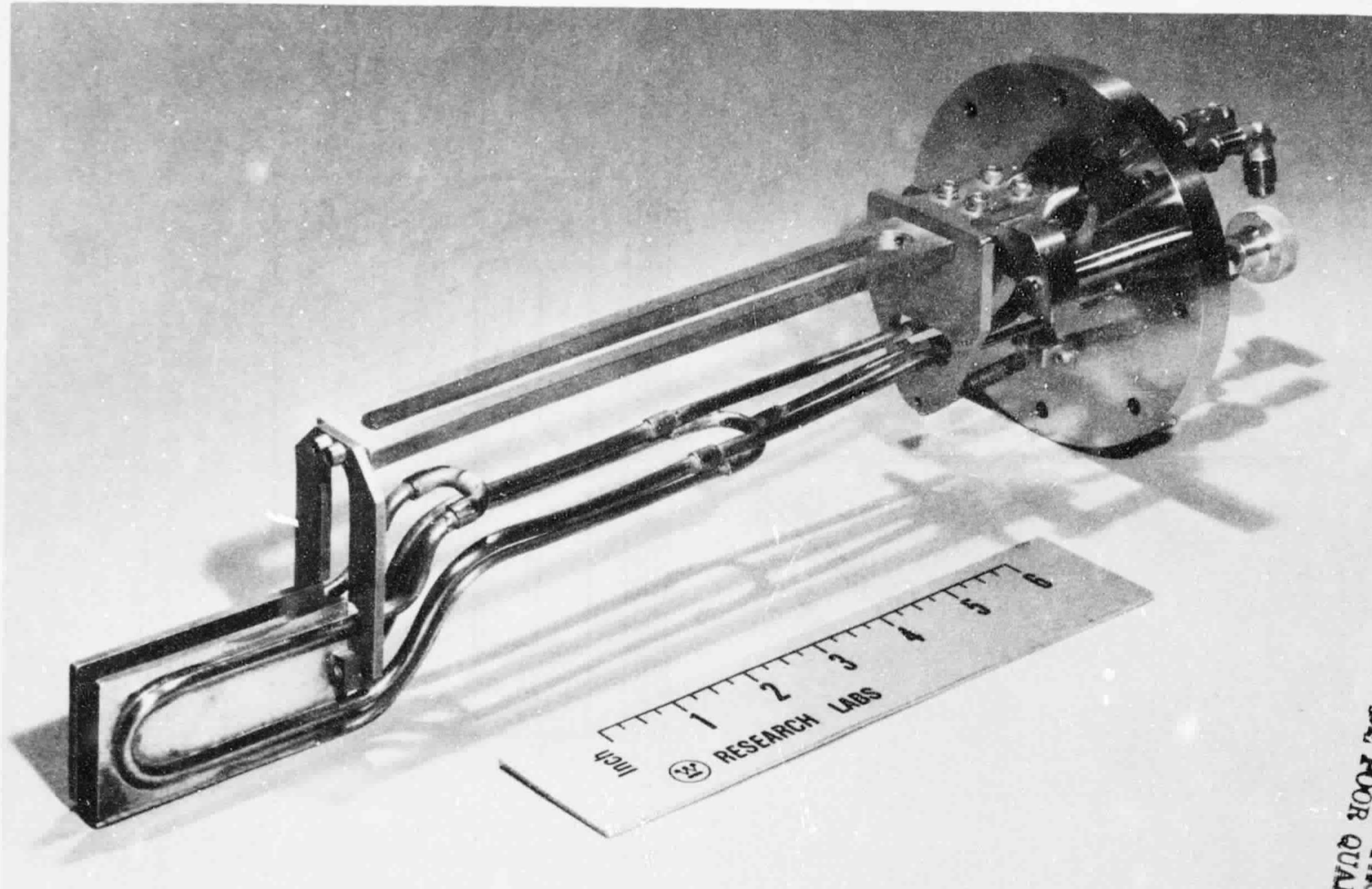

Figure 13 Photograph of Cold Aftertrimmer with Parallel Cold Plates

A final set of adjustments must be implemented to fully utilize the trimmer as designed. This is necessary because there is an interaction dependent on the height of the induction coil, a parameter used to "trim" the growth conditions. The melt temperature profile will be satisfactory at one coil height, but will shift slightly if the coil height is changed. Elimination of this interaction is the subject of continuing design development.

Initial growth experience with the cold aftertrimmer has been very promising. Measurements of the residual stress in a number of crystals indicate that it is compatible with the stresses found with the RE-1 lid alone. Measurements of a number of crystals gave a specific residual stress $\sigma/W^2 = 2.6 \pm 7.8 \times 10^6$ dynes/cm^4. (The large standard deviation of this data reflects the fact that various aftertrimmer conditions, e.g vertical position, were included in the measurements.

These first experiments confirm as predicted by the model, that the cold trimmer produces low residual stress. We have not yet completed enough experiments to assess its performance with regard to the elastic stress situation. This evaluation will continue during the next quarter.

3.1.1.5 Effect of Melt Level on Web Stress

In most cases the specific residual stress, i.e. the actual residual stress divided by the square of the sample width, serves as a good characteristic parameter of the lid and slot design. However,we have noted in some cases appreciable variation in a specific stress between different crystals grown from the same system. This happens primarily during a run when there has been a significant melt level change between crystals grown. We used the thermal stress model to investigate this phenomenon in more detail. Again, the configuration chosen for analysis was the RE-1 lid since a good data base was available for comparison with the model predictions. Temperature distributions in the web were calculated for crystal-liquid interface positions at 0, 1, 2, and 4 mm below the bottom of the susceptor lid with no aftertrimmer. For the RE-1 lid these positions roughly correspond to the interface position at the start of growth and the positions after 2,4, and 8 meters of material have been grown.

Only the lateral stress component exceeded the yield stress for plastic flow in this particular lid, Figure 14. This occurred for the most extreme melt positions, consistent with actual growth experience. The sign of the lateral stress also changes as the melt level falls. We have occassionally measured negative residual stresses which we attributed to uncertainty in the data, especially at low stress values. This now appears to have been a real effect due to melt depletion.

The most important result of this analysis is that the stress distribution and hence ultimate web width can be very dependent on the melt level during growth as well as the lid geometry and thermal trimmer profile. Since we now do not replenish the melt in most of our run we may, in fact, be negating the beneficial effects of low stress lids and thermal trimmers designed to provide wide web. As we discuss in the next sections melt level control is perhaps even more important for maintaining the conditions required to grow web at high speeds.

3.1.1.6 Summary

Both experimental results and computer simulation indicate that afterheaters placed above the susceptor lid raise rather than reduce the residual stress in web crystals. Afterheaters *per se* are not a viable technique to promote the growth of wide web crystals. Instead, analyses show that a susceptor lid designed for low stress (no plastic deformation) coupled with a cold aftertrimmer (to minimize elastic bending of the web above the lid) should promote conditions for wide web growth. A cold trimmer has been designed and given preliminary tests. Residual stress is low for this system and experiments are underway to test its effect on elastic deformation. Control of the melt level in the web growth system is important if the benefits of low stress lids and thermal trimmers are to be fully achieved. If the melt is depleted by crystal growth, stress levels rise and web deformation is expected.

Curve 714928-A

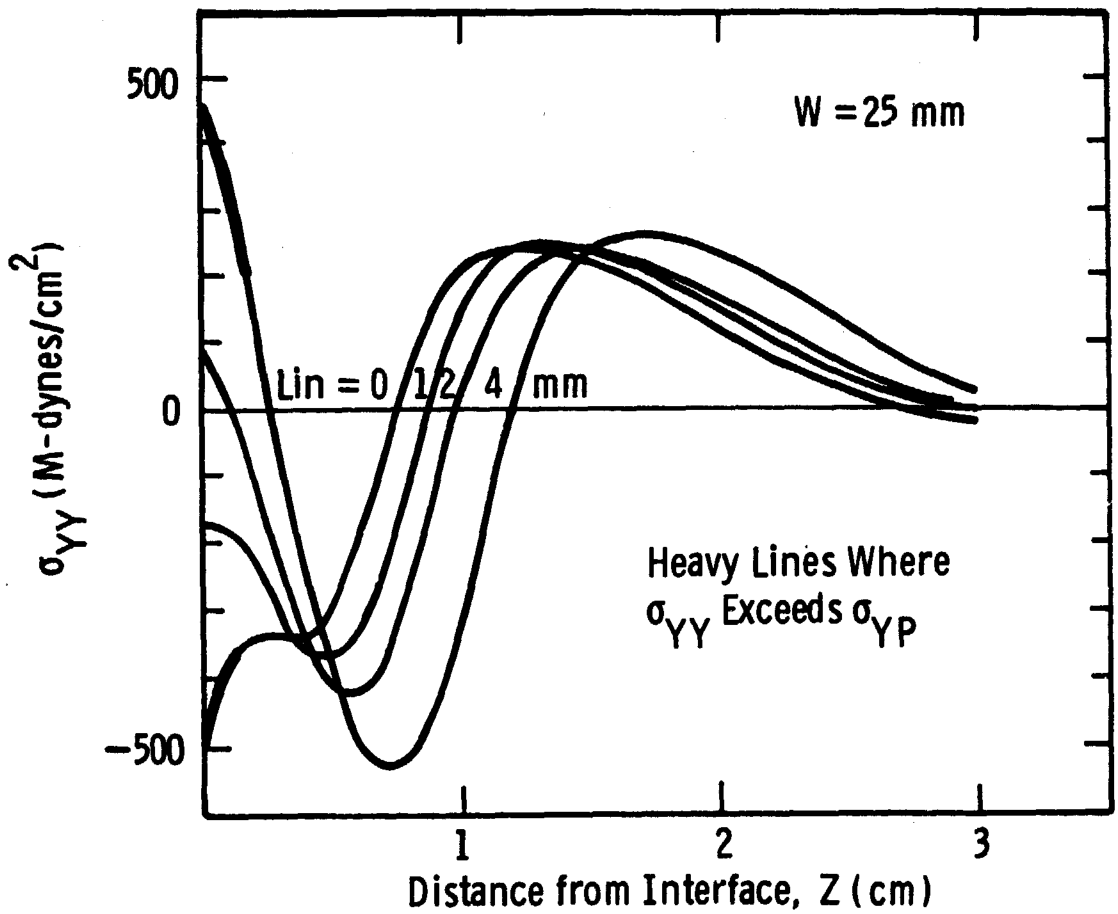

Figure 14 The variation of lateral stress, σ_{YY}, at the centerline of a growing silicon web crystal as a function of distance from the crystal-liquid interface. Heavy lines delineate regions where the lateral stress exceeds the yield point of silicon, σ_{YP}.

3.1.2 Methods to Enhance Web Growth Velocity

3.1.2.1 Background

The maximum crystal growth velocity in general depends on how effectively the latent heat of fusion can be dissipated from the crystal-liquid interface. For dendritic web, unlike other ribbon techniques, the latent heat can be liberated in two ways: to the supercooled liquid from which the crystal grows and to the crystal itself. The portion of the total web velocity attributable to heat loss to the melt may be as high as 2cm/min at melt undercoolings near 6-8°C (undercooling >10°C risks spontaneous crystallization of the liquid silicon). The remaining and major portion of the total velocity is due to heat loss by radiation from the web (This may be augmented by convective cooling). Total velocities up to 10 cm/min[1] have been achieved albeit on relatively thin ribbons.

The experiments described in this section deal mainly with experiments to improve radiative loss (and to a lesser extent convective loss) from the silicon web and thus to improve practical growth speed. We have previously developed a mathematical model[1] to assess the effects of furnace parameters, e.g susceptor lid thickness, growth slot width, shield and aftertrimmer temperatures, on web growth rate. The situation can be visualized with the aid of Figure 15 from an earlier report. As the model analyses, and intuition would suggest, radiative loss from the web can be improved in several ways:

(1) Lower the temperature of the top radiation shield, e.g. by using stacks of radiation shields above the susceptor lid.

(2) Increase the width of the growth slot.

(3) Increase the view angle in the susceptor lid, e.g. by beveling the slot.

(4) Raise the position of the growth front closer to the susceptor lid.

(5) Reduce the thickness of the susceptor lid.

Dwg. 6439A08

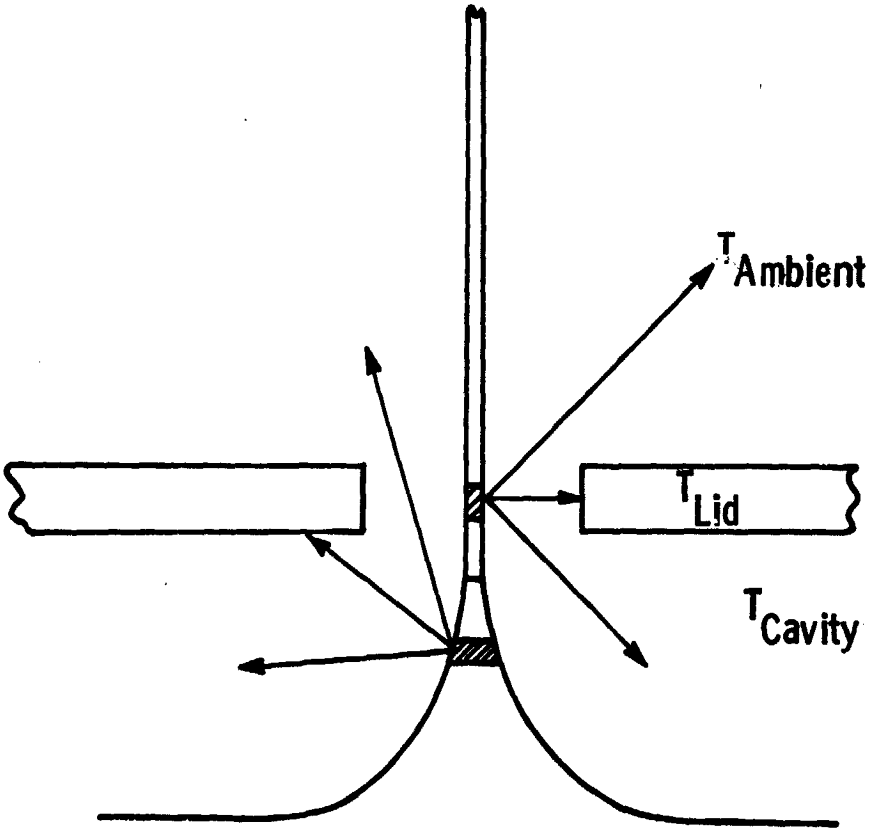

Figure 15 Paths for heat loss from the web crystal and adjacent liquid meniscus.

Our recent experiments centered primarily on approaches (2) to (4). The thermal model for the web system predicts that for a given furnace geometry the relationship between web thickness and velocity will be of the form

$$v = a + \frac{b}{t} \tag{2}$$

where t is the web thickness and a and b are constants specific to the growth configuration (for a given t, a system which more effectively dissipates heat will produce a higher growth velocity). Thus by measuring the thickness of webs grown from a fixed furnace condition as a function of the pull speed, a velocity-thickness plot is developed which is characteristic of that condition. We evaluated a number of furnace geometries this way to determine their effectiveness to raise growth speed. The model output was used to guide the initial choice of configuration to be tested. The following sections highlight the results of these studies; details of the specific runs, most of which were carried out primarily in the J furnace, are tabulated in the Appendix.

3.1.2.2 Effect of Lid Slot Design on Growth Speed

We carried out a series of experiments to evaluate how beveled lids and slot width effected growth speed. Melt to lid height was also investigated by employing a lid which was recessed into the cavity above the melt. A thick, straight slot lid (like Figure 7, but 9mm thick instead of 6mm) was used as a reference case.

Figure 16 depicts the improvement in speed gained by introducing beveled sections along the lid profile as illustrated by the lid cross-sections in Figure 17. Speed increments of 2 to 3 times the base case were achieved. That is, the velocity-thickness curve for a beveled lid shifts vertically up the speed axis as the amount of bevel section is increased. Speeds over 5cm/min have been achieved this way. (The data points in the figure are from experiments, the curve calculated from theory; agreement between the two is excellent.)

Curve 714924-A

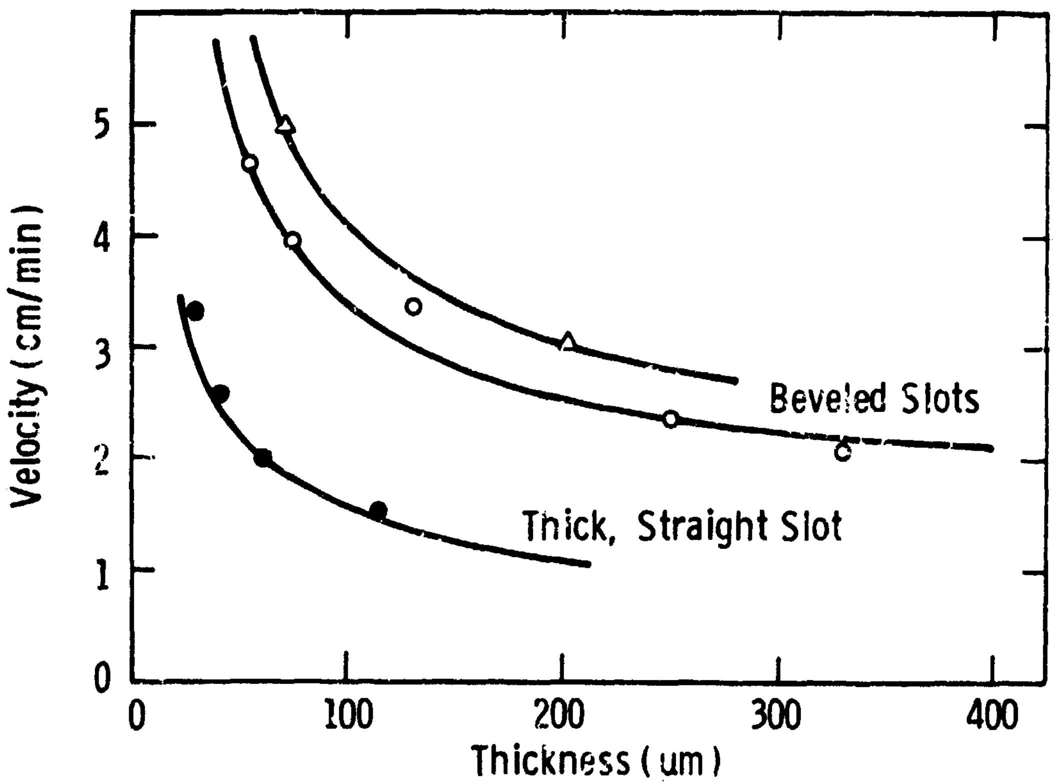

Figure 16 Calculated and observed velocity-thickness relationships for different lid slot designs. Figure illustrates how an increase in heat loss (e.g by increasing the radiation view factor by a beveled lid) raises growth speed for a given thickness of crystal.

Dwg. 1703B16

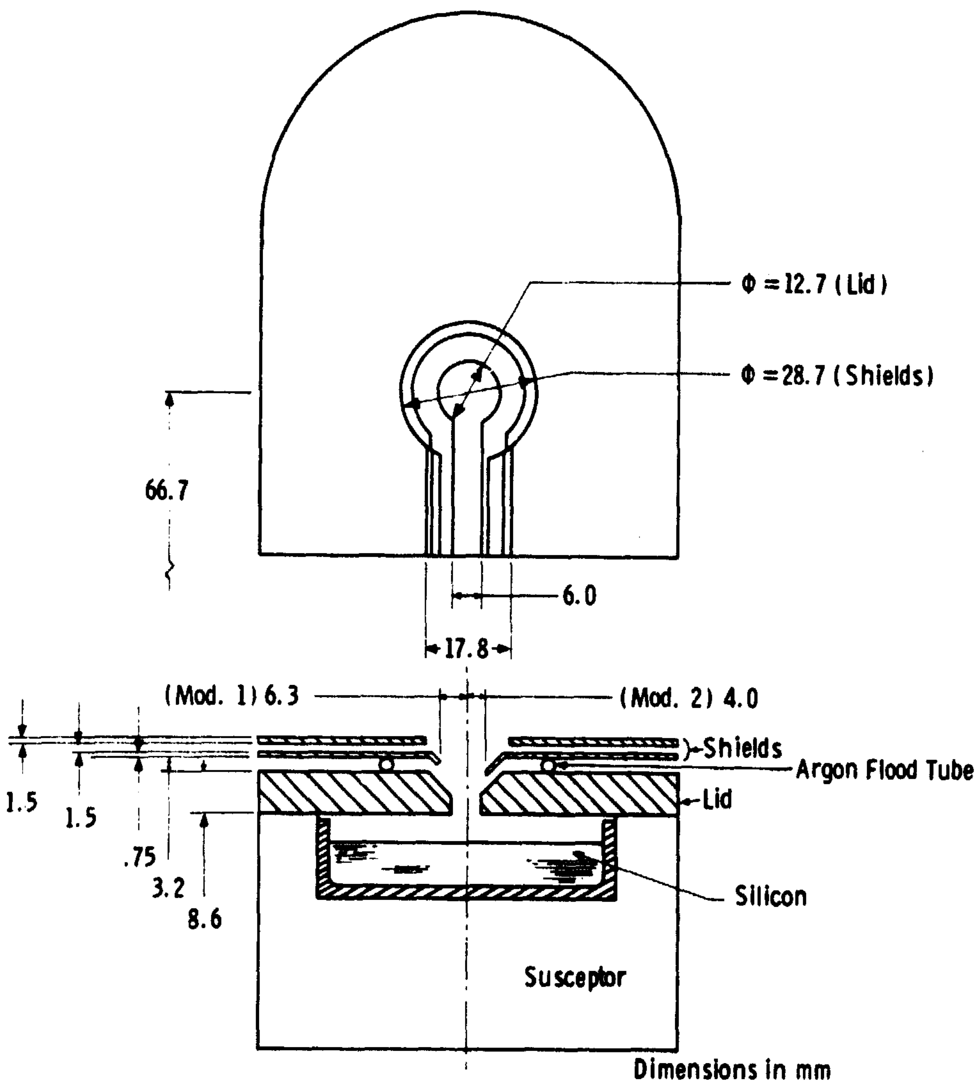

Figure 17 Examples of a growth lid which is beveled to increase radiative heat loss from the web. Mod. 1 and Mod. 2 depict different shield arrangements.

A further increase in speed can be gained by shielding the hot lip of the growth slot from the growing web. This situation is depicted by Mod 2 (right side) of Figure 17. The drawback to this approach is that an overhanging lid like that shown in the figure can collect oxide. To circumvent this problem we introduced a pair of argon flow tubes parallel to the growth slot (see Figure17). Argon purged between the lid and shield can then be employed to prevent oxide deposits. A series of runs in the RE furnace, (Appendix) proved the validity of the approach (two other argon flow techniques have also been tested on the W furnace, viz. section 3.1.4, but the method which is still undecided. This now makes possible the use of high speed lid configurations previously unfeasible. It also provides a means to introduce convective cooling of the web, an approach we have not previously explored.

A further evolution of the beveled lid concept is shown in Figure 18. The bevel is recessed with only a small straight lip over the liquid. Radiative transport was increased so that growth rates over 6cm/min could be achieved on webs over 2.5cm wide. By increasing the slot width of this design growth speed was raised to 7cm/min.

While we can achieve speeds commensurate with high overall output rates there are two difficulties which must be overcome to make such procedures routine and to stabilize growth conditions for longer periods. One of these is to better control the seeding operation for "fast" lids which provide greater radiative heat transport. Typically, during seeding both melt undercooling and growth speed are adjusted during a short transient to produce the button and initiate web growth. The added heat loss in a fast lid makes this adjustment more difficult for the operator to reproduce. Thick buttons may result. Within these buttons, extra twins (Figure 19) form, causing lineage structure to propagate into the web. Alternatively, the situation may be overcorrected; the web then thins under the bottom, the twins outcrop, and lineage again is created[1]. Improved parameter readout and control should resolve this difficulty.

Dwg. 7686A09

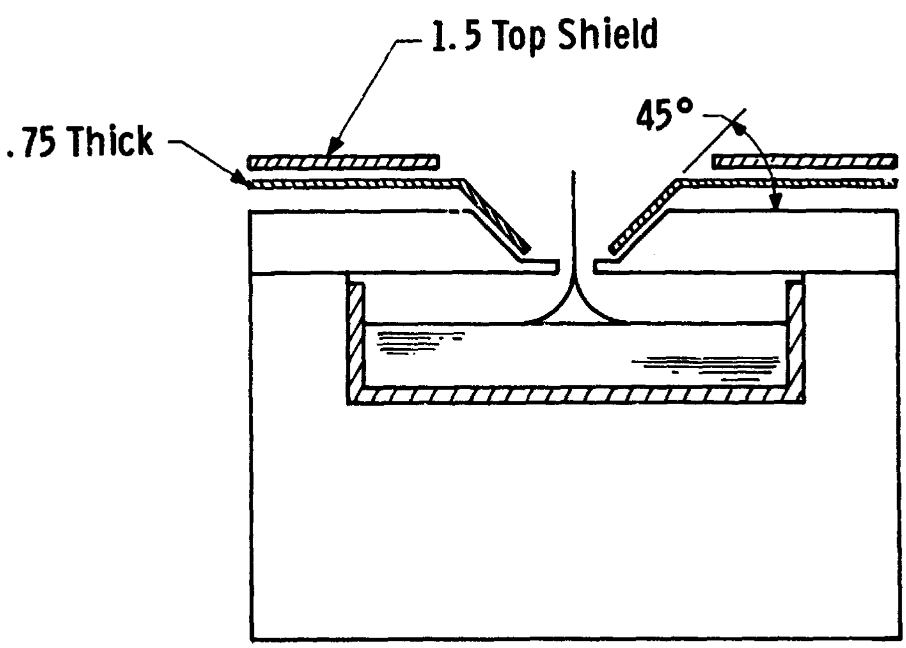

Figure 18 Lid slot design with large radiative view factor.

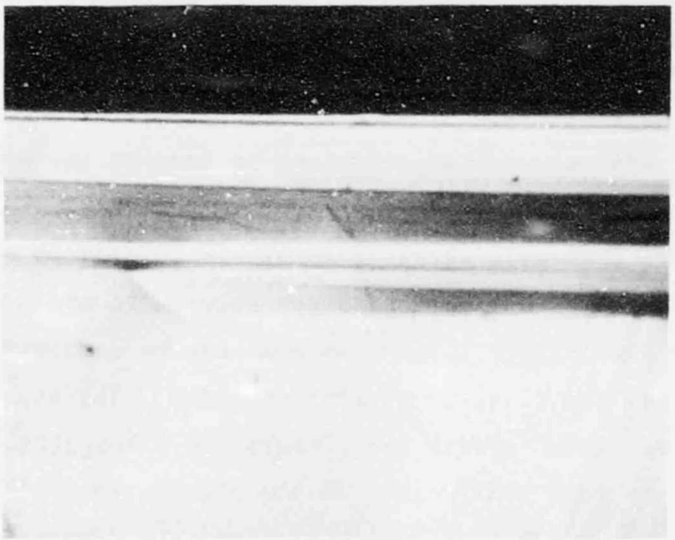

Figure 19 Extra twins formed during the seeding process when the crystal is excessively cooled.

Another way to increase web growth velocity is to raise the melt level closer to the lid slot. This may be accomplished by recessing the lid itself or by feeding silicon to the melt. One set of experiments conducted with a recessed lid produced speeds over 5cm/min. These early experiments were terminated by a lid wetting accident.

The critical importance of constant melt height to sustain growth speed and thermal stability is considered in the next section.

3.1.2.3 Effect of Melt Height on Growth Velocity

By means of our thermal model we have calculated web growth velocity as a function of the distance between the melt level and the lid for several slot designs. The model predictions indicate that a given growth rate only can be sustained so long as the melt level remains fixed. For example, Figure 20 depicts how the temperature profile in the web changes with melt height. As liquid silicon is removed by crystal growth, the freezing front drops lower into the hot cavity below the susceptor lid (Figure 15). Less heat can be dissipated so that the web must thin if the velocity remains constant. The experimental data from a baseline "slow" growth lid (Figure 21), illustrate that this prediction is in fact realistic. In the figure, we plot web thickness as a function of growth time (which is inversely proportional to melt height). As the melt is depleted the web becomes thinner and thinner. The implications of this result are that high growth rates obtainable with proper lid design can only be sustained for short periods early in a run unless some control action is taken.

One way to compensate for melt drop is by adjusting the melt temperature and hence supercooling. This is because the latent heat of fusion can be dissipated to the melt as well as the surroundings during web growth. The extent to which this can be carried out is limited by nucleation in the melt when supercooling becomes excessive. Moreover, the approach is not entirely satisfactory because adverse stresses develop in the web as the melt level falls (Section 3.1.1). Melt replenishment in fact is a far more elegant and necessary solution to the problem. Recent results on this subject are covered in Section 3.2.

Curve 714927-A

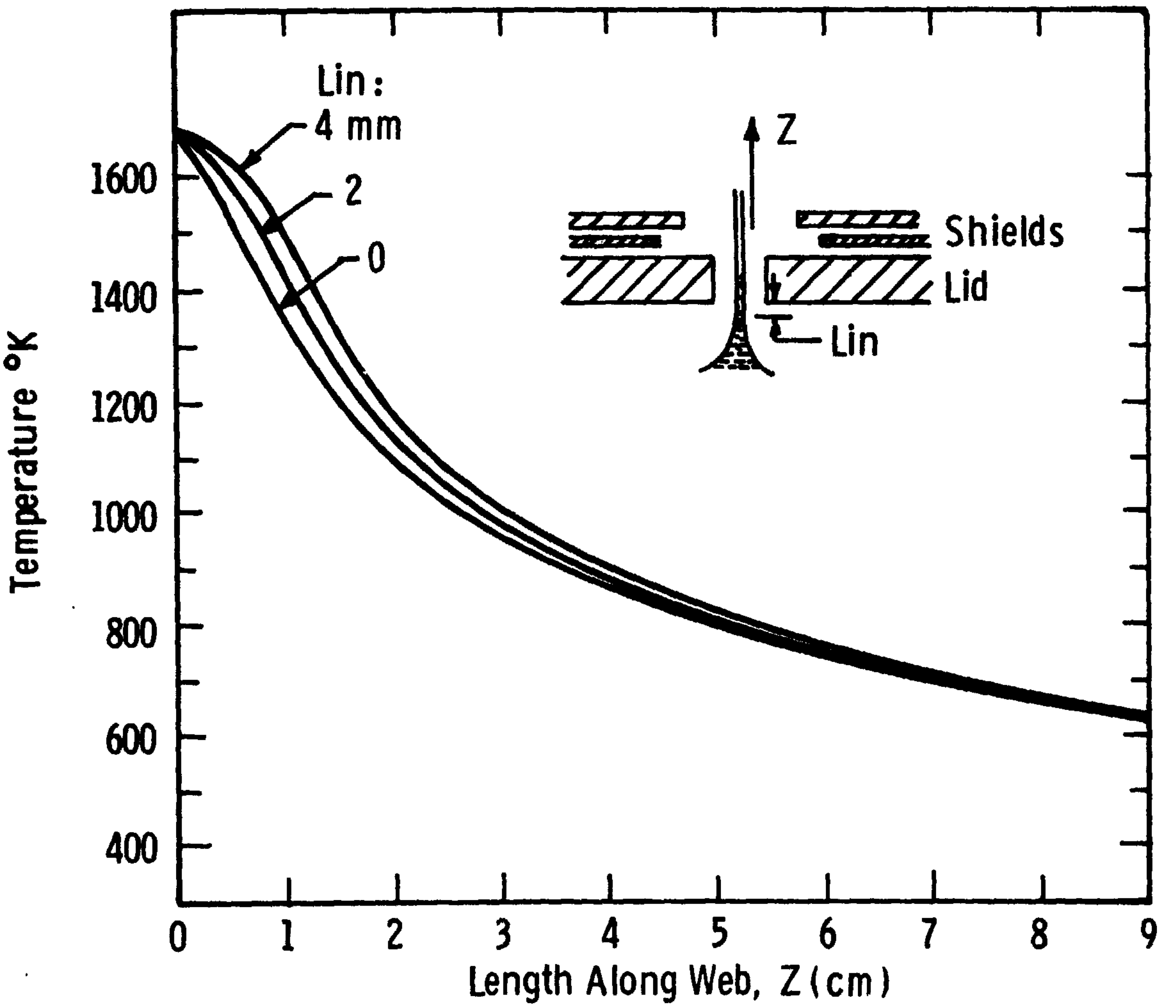

Figure 20 Temperature profiles for an "RE1" lid as a function of interface position

Curve 714925-A

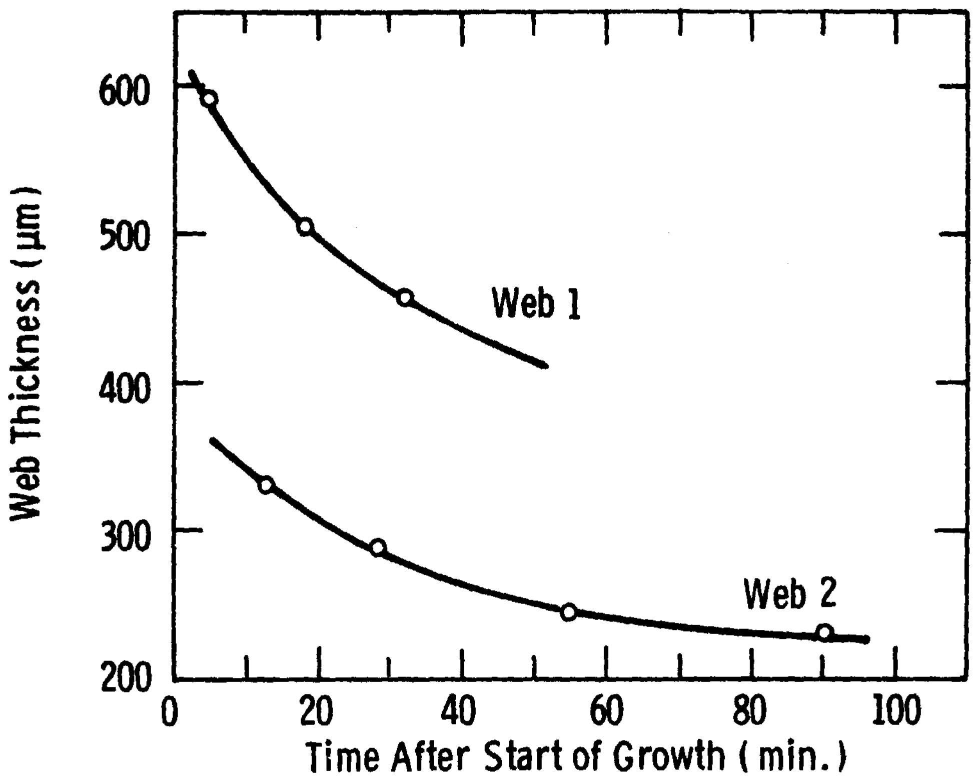

Figure 21 Variation of web thickness with growth time for crystals from two different runs. As the melt is depleted by crystal growth, the crystal thins at constant growth speed.

3.1.2.4 Summary

By suitable design of the growth slot width, slot profile, and adjustment of height, web growth speeds up to 7cm/min have been achieved. Rates to 5cm/min can be repeatably obtained. For some of the high speed lid configurations, stable seeding conditions are difficult to maintain. This situation can be improved with signal indicators to give real time output of undercooling and pull speed during the seeding transient. With this information, appropriate seeding conditions can be controlled and reproduced. A more overriding concern is to provide a nearly constant melt level during growth. A melt drop of a mm or more significantly alters heat loss from the web; high speed growth can then no longer be maintained without web thinning. Continuous thermal adjustments are also required as the melt drops. If improperly carried out this corrective action may actually destabilize growth at high output rates. An operational melt replenishment system with level control is the long run solution to this problem.

3.1.3 Combined Configurations to Raise Output Rate

Because techniques to increase web width and speed can be investigated in tandem, parallel efforts have been carried out to use program resources effectively. By this approach speeds (7cm/min) and widths (4.1cm) have been independently demonstrated which if achieved together would exceed the output rate goal of 25cm^2/min. During this period we have begun uniting these techniques to achieve this end. Experiments have been carried out using lid designs which give relatively flat melt profiles, yet exhibit good radiative loss and low stress characteristics. In this way output rates between 12 and 13cm^2/min have been demonstrated on a number of occasions (15 cm^2/min was achieved as this report was being prepared).

Future effort will focus on blending these lid configurations with the aftertrimmer designed to reduce elastic bending of the web. We believe that $25cm^2$/min output rates can be achieved this way. However, our recent experiments clearly indicate that melt replenishment will be required if stable growth at high output rate is to be sustained.

3.1.4 Development of Improved Process Techniques

As noted above, we have found that some combinations of growth lid and shield arrangements which gave improvements in web width, speed or stress were difficult to employ in practice because oxide collected on the furnace components during growth. This caused changes in growth conditions or, sometimes worse, spalling of oxide into the melt and termination of growth. For this reason a series of experiments was carried out in the W furnace on gas flow systems to eliminate oxide deposition. A second aspect of the experiments was to investigate the conditions required for stable growth with directed gas flow.

Two systems were tested to redirect the gas flow: a novel venturi technique and a more conventional argon purge or flooding. In the first approach (Figure 22), argon gas is forced into a pair of venturi flow tubes (chimneys). This aspirator effect creates a suction which drains argon down across the web, through the melt cavity where it is then exhausted out the chimneys. The venturi arrangement is extremely effective. For example, Figure 23 illustrates how oxide collected in the growth slot, almost completely blocking the ends, before the venturi was installed. In contrast, no oxide accumulated after an eight hour run (Figure 24), when the venturi was used to redirect the gas flow. A second advantage of this system is that the web surface is kept clean and oxide free as well, Figure 25.

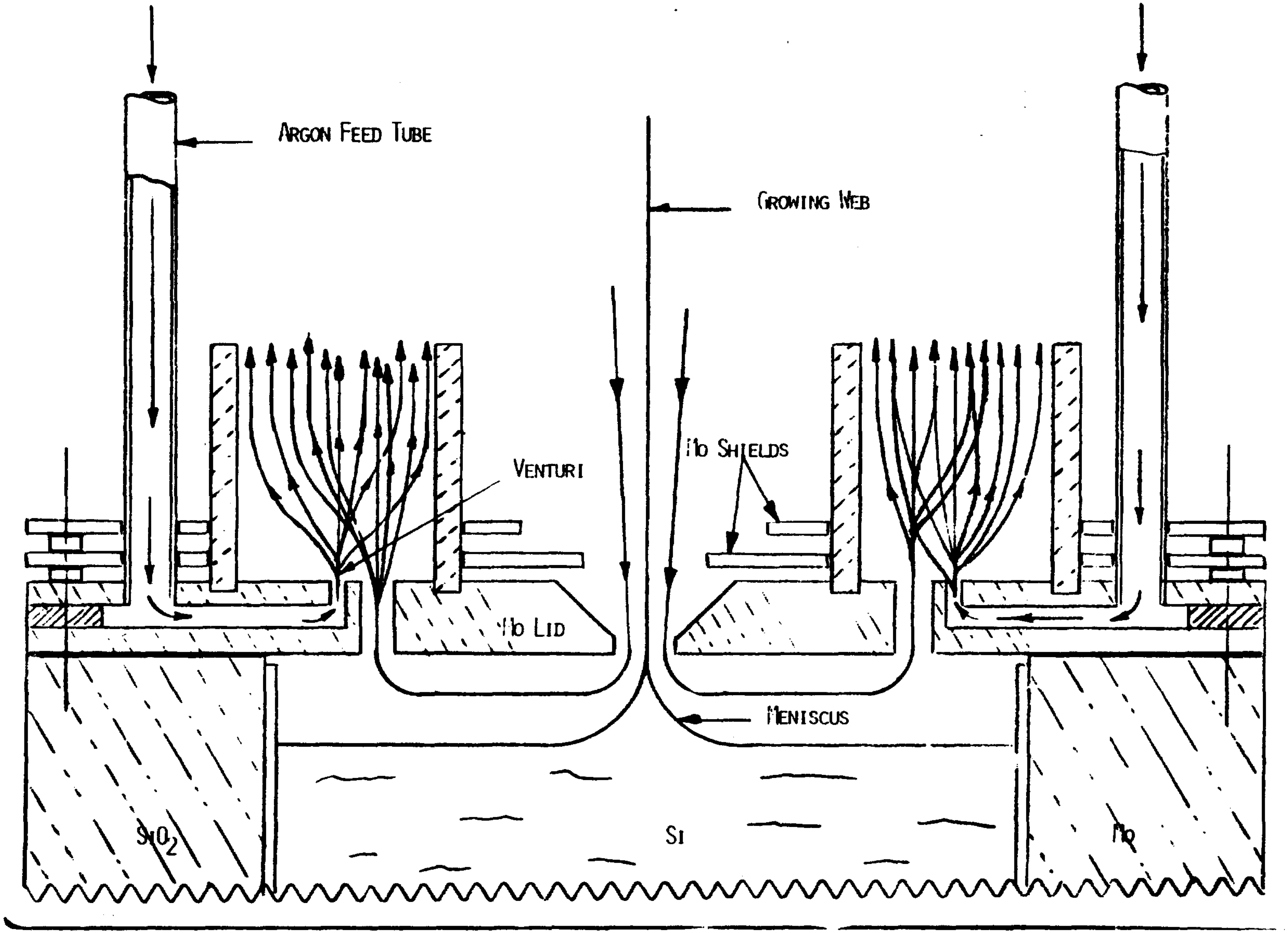

Figure 22 First venturi lid design tested to control gas flow in a web growth system.

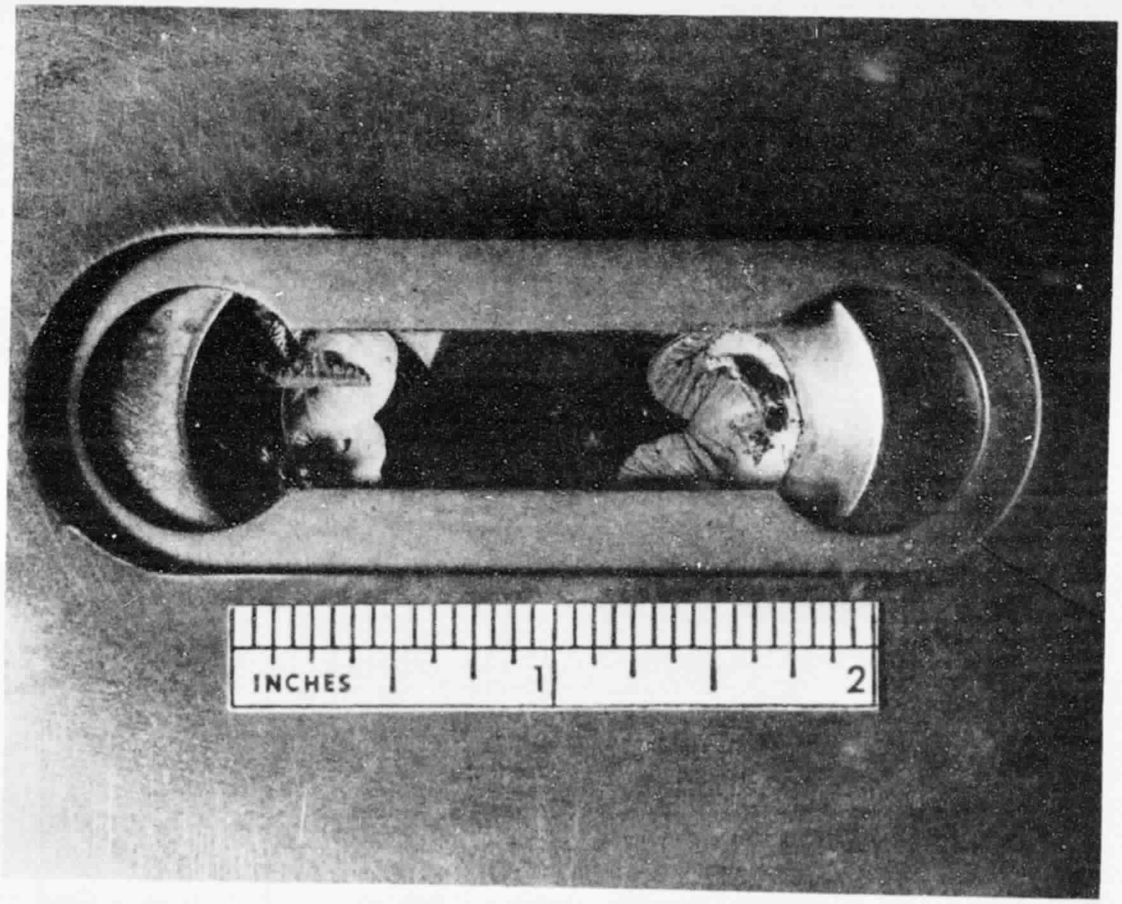

Figure 23 Collection of oxide at the ends of the "dogbone" shields when no gas flow control was employed.

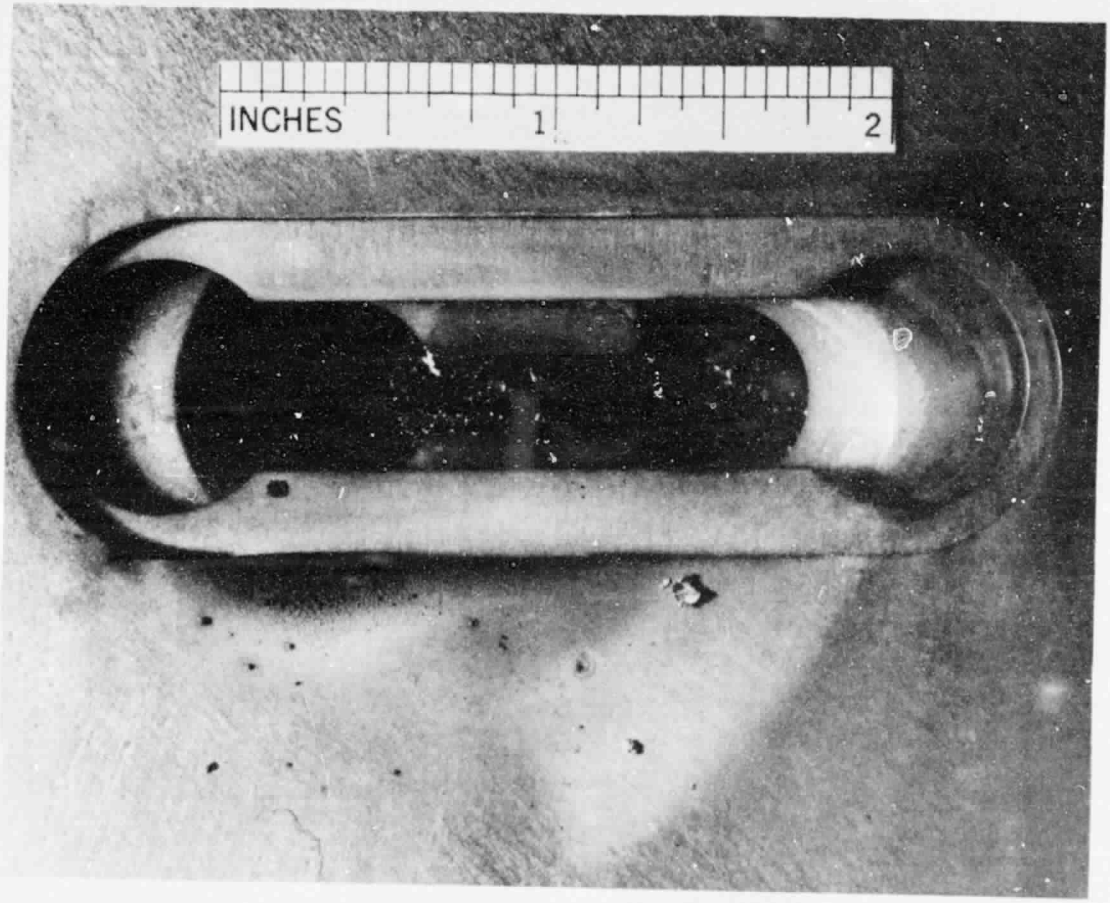

Figure 24 Shields remain free of oxide with venturi gas flow control.

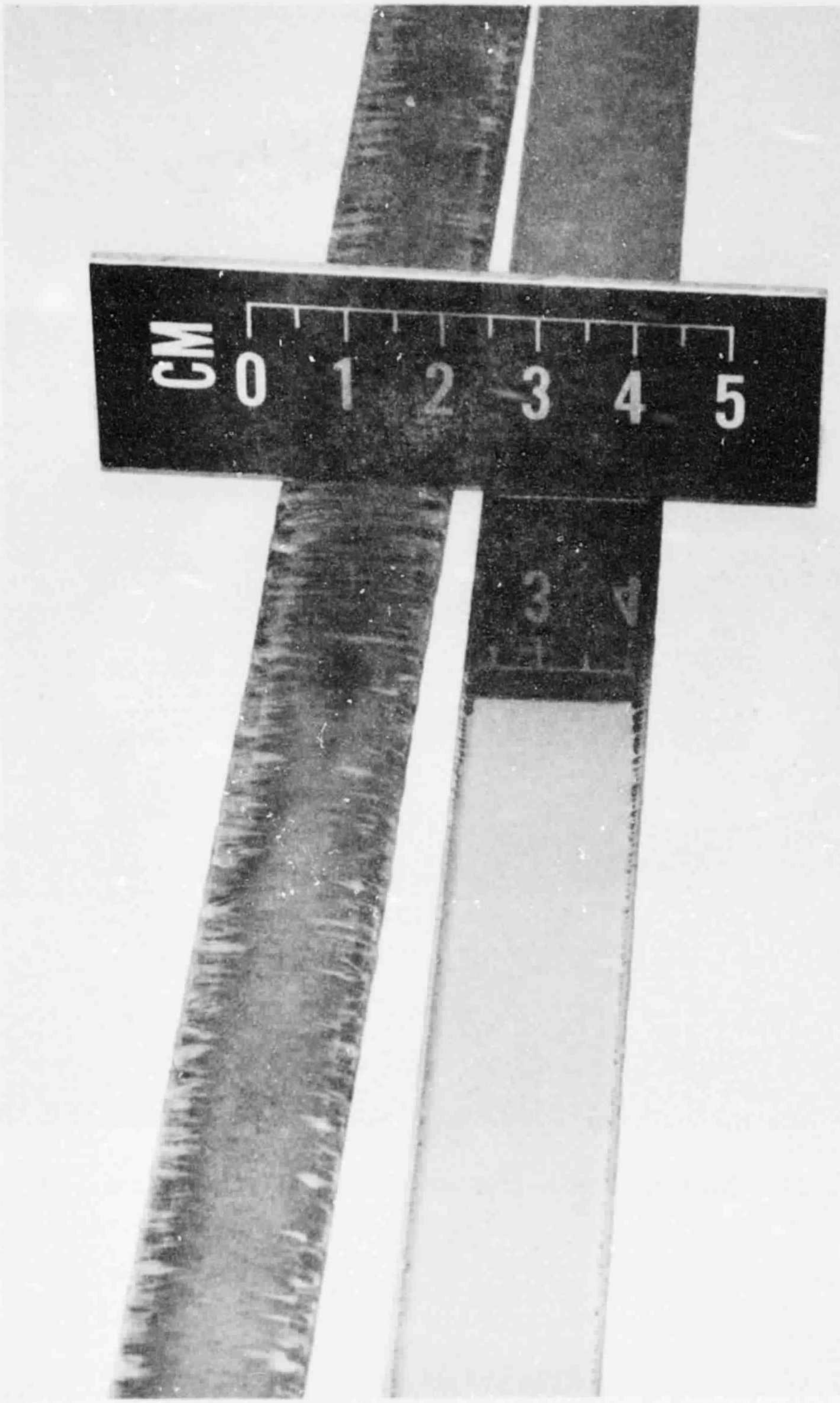

Figure 25 Web crystals grown with (right) and without gas flow control. As grown crystal has mirror like surface when the venturi system is employed.

The major drawback to the first venturi configuration was that the high gas flow rates in the vicinity of the crystal-liquid interface perturbed the temperature stability. Pull outs or extra dendrites resulted when growth was not controlled. An alternative method, argon flooding, was tested while a new venturi arrangement was being designed. The basic components of the flooding system are depicted in Figure 26. Argon is introduced at the edge of the cavity formed between the hot susceptor lid and the intermediate shield. The argon flows through the cavity, and then over the web as indicated in the figure. A variety of positions of the feed tube and gas flow rate were tried. Extremely stable growth conditions were achieved with the opposed flow geometry illustrated in Figure 26. Lengths of web several meters long with widths controlled to $\pm$ 1mm were grown. Subsequent characterization of the web (Section 3.3) indicated, however, that solar cell efficiency was impaired in material grown this way. The characterization data suggested that surface contamination had occurred, possibly by Mo transport in the hot argon gas.

A new venturi system, Figure 27, was then designed based on the results of the early venturi and flooding system results. The argon flow path of the new system was detoured away from the immediate vicinity of the freezing front. Early results with the system are encouraging and indicate that growth can be controlled. Moreover, cell efficiencies measured on the webs grown this way are excellent ($\eta_{AR} \sim 14\%$). We believe the venturi system has direct applicability in web systems designed for melt replenishment (Section 3.2). The use of the technique for convective gas cooling will also be assessed.

3.2 Melt Replenishment Studies

3.2.1 Background

It is well recognized now that melt replenishment (or some equivalent procedure) will be required to achieve process economics for almost all of the ingot, sheet and ribbon growth technologies if the 1986 LSA wafer cost objectives are to be met. For web growth melt replenishment is mandatory not only for cost reasons, but for sustenance of conditions for high output operation as described in Section 3.1.

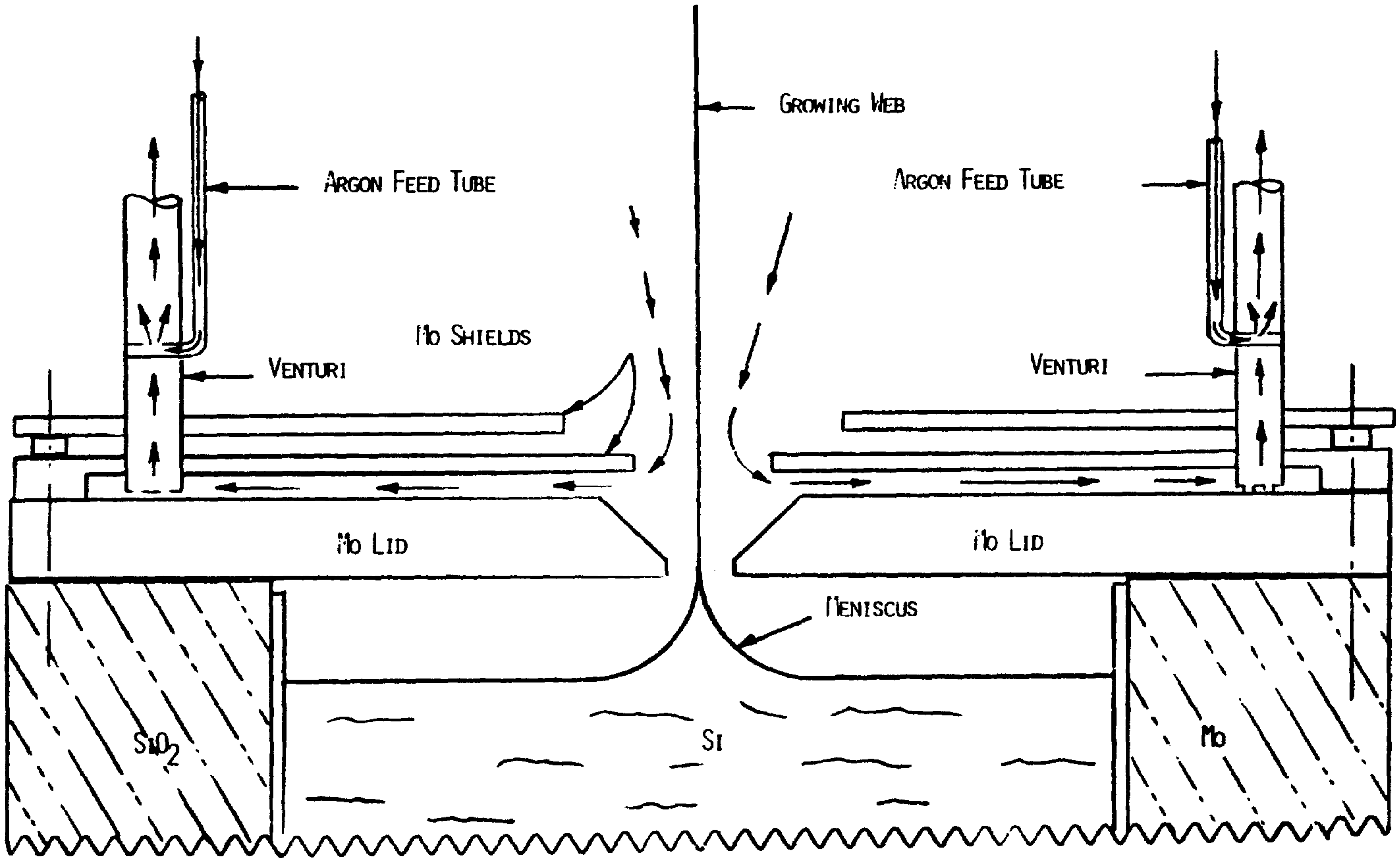

Figure 26 Schematic depiction of lid design for argon flooding experiments.

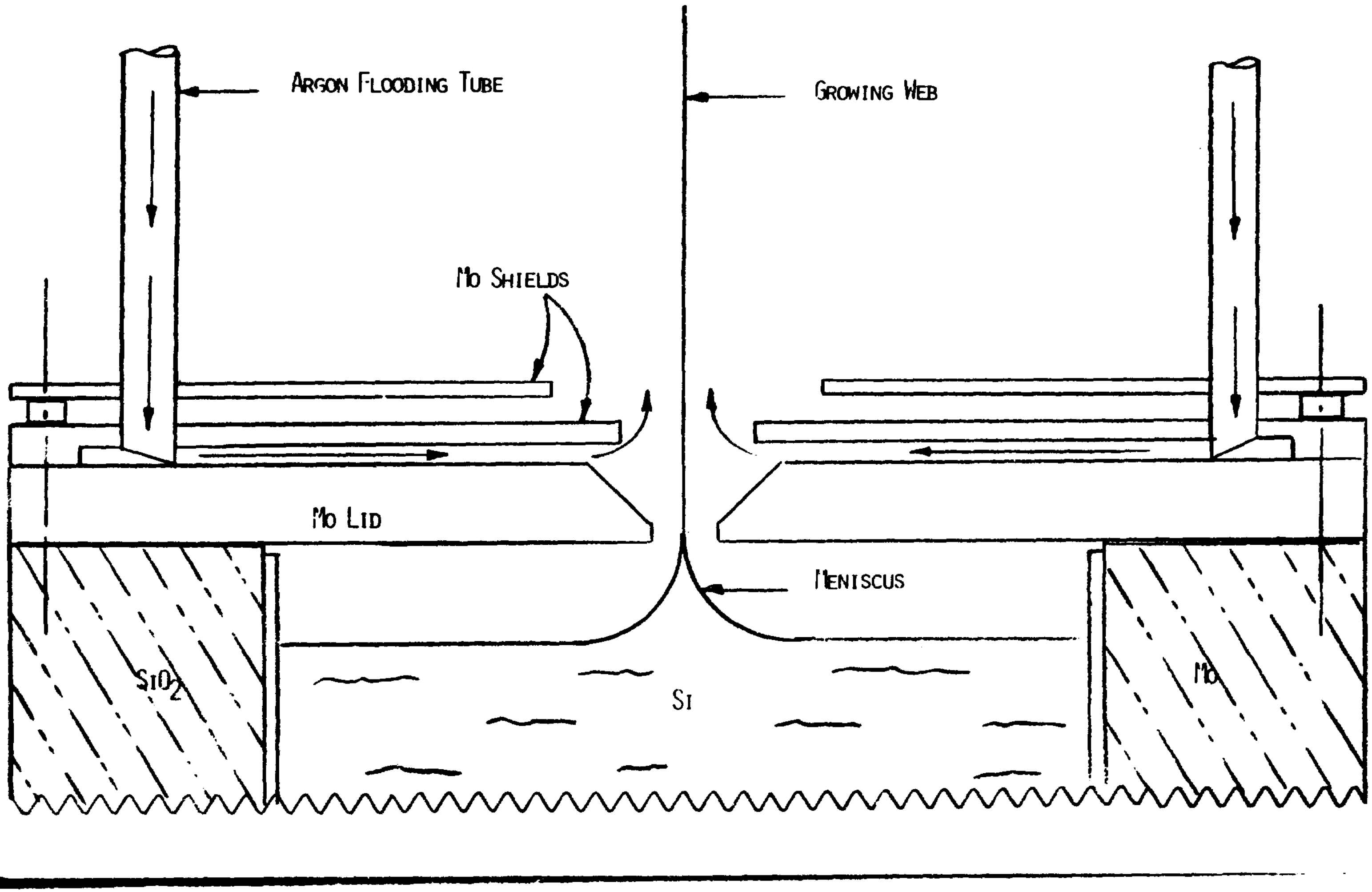

Figure 27 Improved venturi lid design. Gas flow restricted in vicinity of web-liquid interface.

As part of this program, our objective is to demonstrate the feasibility of simultaneous web growth with melt replenishment. Initially, we fabricated a manually-activated system to replenish the melt with silicon pellets. During this quarter we have concentrated on the development of methods to feed pellets without disturbing the growing web. A variety of barrier-crucible designs have been tested in runs on the RE furnace (the details are given in the Appendix). A successful approach has been identified. Recently, a manually-activated feed system has also been tested to improve feeding and experiment efficiency. We describe below the system hardware and the results of these recent studies.

3.2.2 Description of System Elements

3.2.2.1 Manually-activated System

The principal features of the experimental melt replenishment system, Figure 28a and 28b are:

Utilization of Polysilicon Pellets. The systems use polysilicon pellets 2 to 4 millimeters in cross-section. Pellets this size are sufficiently small to cause only slight temperature perturbation in the thermal system during web growth. The pellets are stored in a pellet reservoir and are fed one at a time as required. The vacuum valve and the ports to argon and vacuum sources permit the pellet reservoir to be opened and refilled without interruption of the growth.

Compartmented Crucible. The pellets, on command, are dropped through the valve and feed tube into a melt replenishment compartment of the crucible. The barrier which separates the melt replenishment compartment from the growth compartment is not liquid-tight so that the melt level equilibrates continuously between the two compartments. The barrier prevents the pellets, themselves or ripples caused by the pellets, from disturbing web growth.

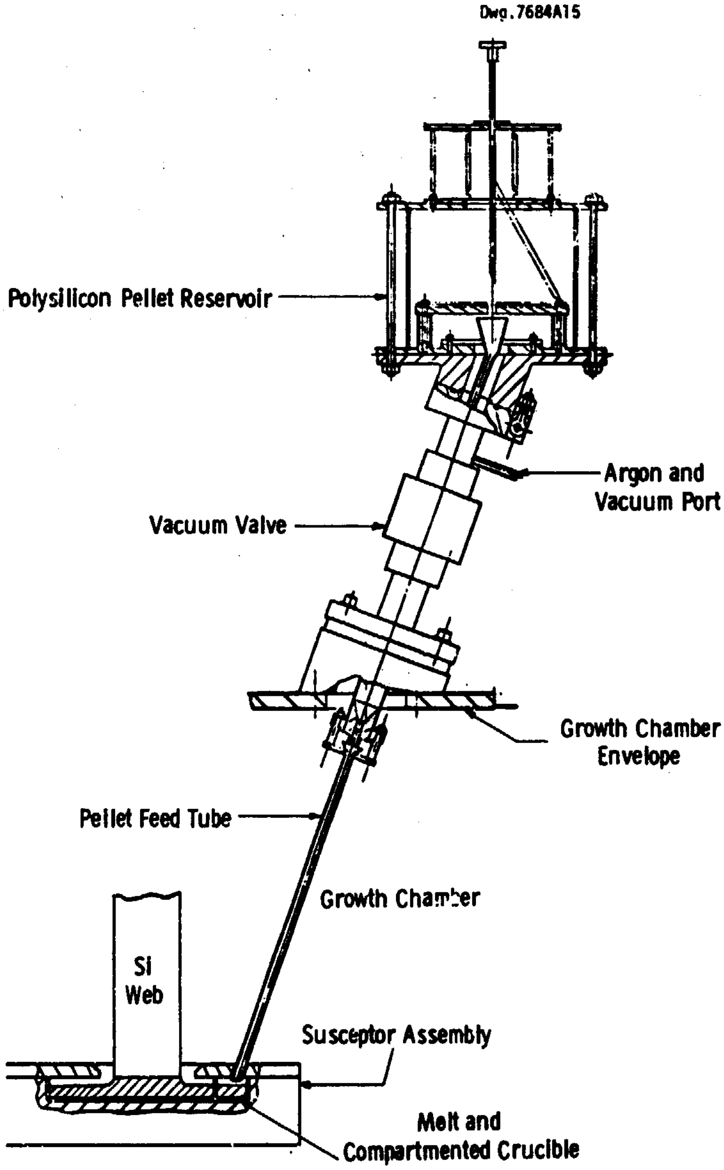

Figure 28a Schematic of manually actuated melt replenishment system.

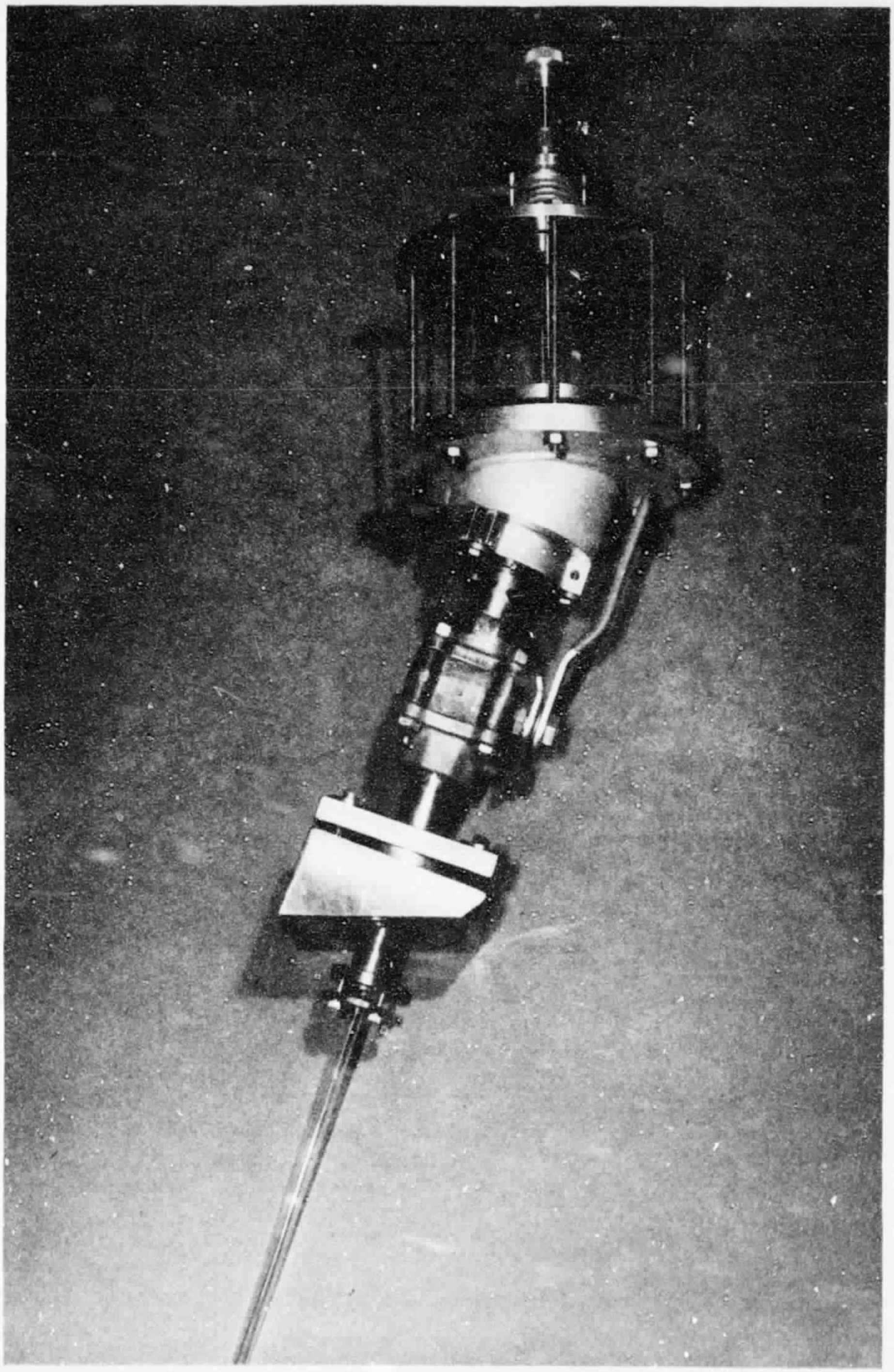

Figure 28b Photograph of manually actuated melt replenishment system.

RM-78768

Argon Flow. The argon port and valve shown enable argon to be purged through the feed tube. This prevents oxide accumulation at the exit end of the tube. A flow gauge (not illustrated) is provided, so that an adequate but minimum argon flow rate may be set. By minimizing the flow rate, thermal effects in the growth region are avoided.

3.2.2.2 Mechanically Activated System

A mechanically operated pellet reservoir has been developed and built to replace the manually operated system shown in Figure 28. The bench model of this unit which was described in an earlier report[5] has been developed into a full working model, as shown schematically in Figure 29 and the photograph of Figure 30. The mechanically activated melt replenishment system provides all of the function of the manually operated system and, in addition, pellets now can be fed on command and at a programmable rated. This improves experiment efficiency since the operator is freed from the laborious task of feeding individual pellets while monitoring web growth. Since the pellets can be fed at variety of rates it is considerably easier to approximate and replenish silicon consumed during growth. Finally, with appropriate level sensing a truly operational replenishment system could be implemented.

3.2.3 Development of Compartmented Crucible for Feeding

If feed material is introduced into an ordinary single compartment crucible, the pellets will, before they melt, quickly float to the cooler regions of the liquid, i.e. the growth region. There the partially-melted material may be picked up by the growing web, generally causing structural degradation of the crystal. Thus it is necessary to isolate the melt in the feed region of the crucible from the place where the web grows. This can be accomplished by introducing a barrier in the crucible. As noted, the barrier must be "leaky" so that the level of molten silicon can equilibrate between the feed and growth compartments of the crucible.

Dwg.7684A14

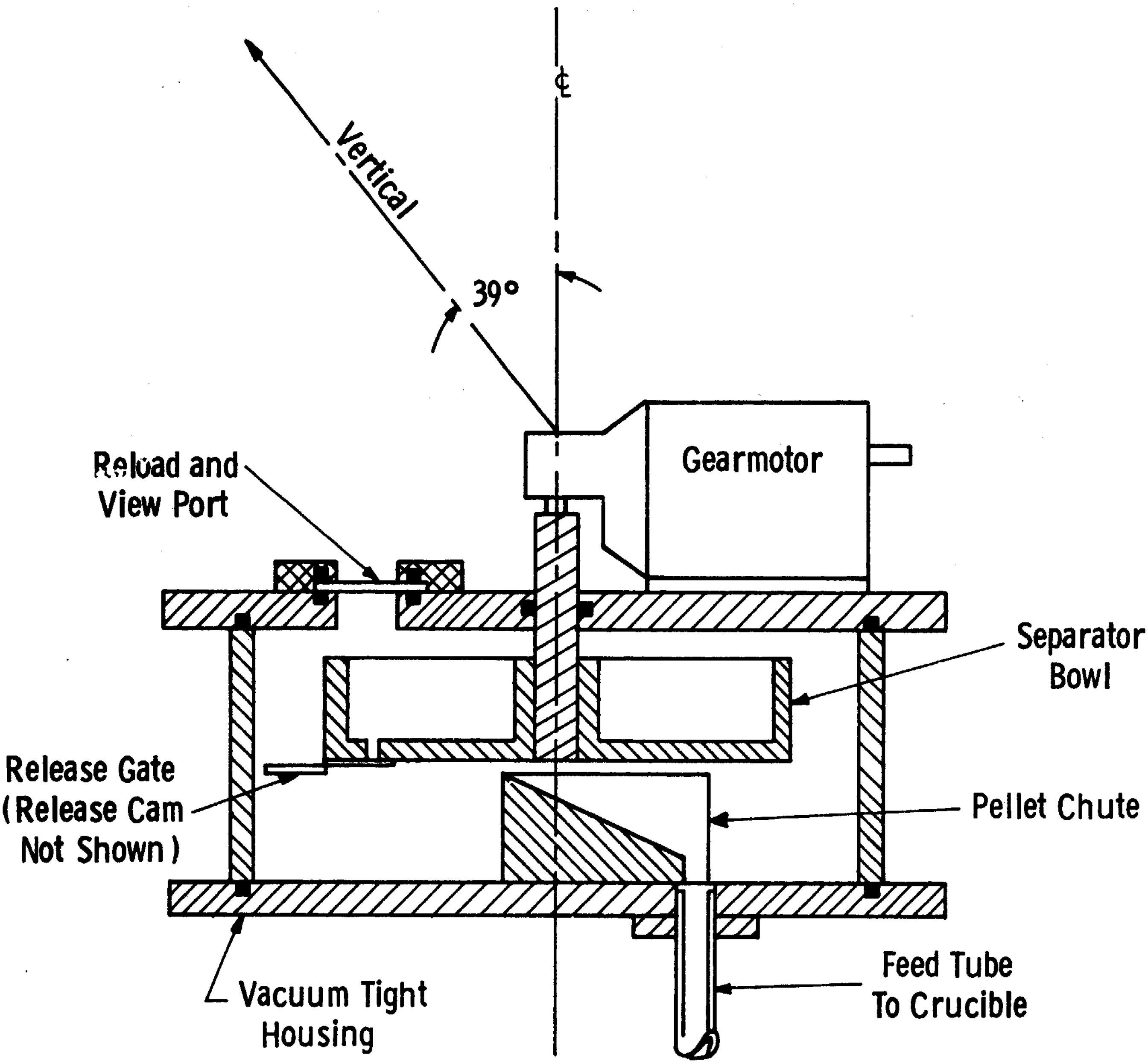

Figure 29 Mechanically actuated pellet reservoir and feeder.

ORIGINAL PAGE IS
OF POOR QUALITY

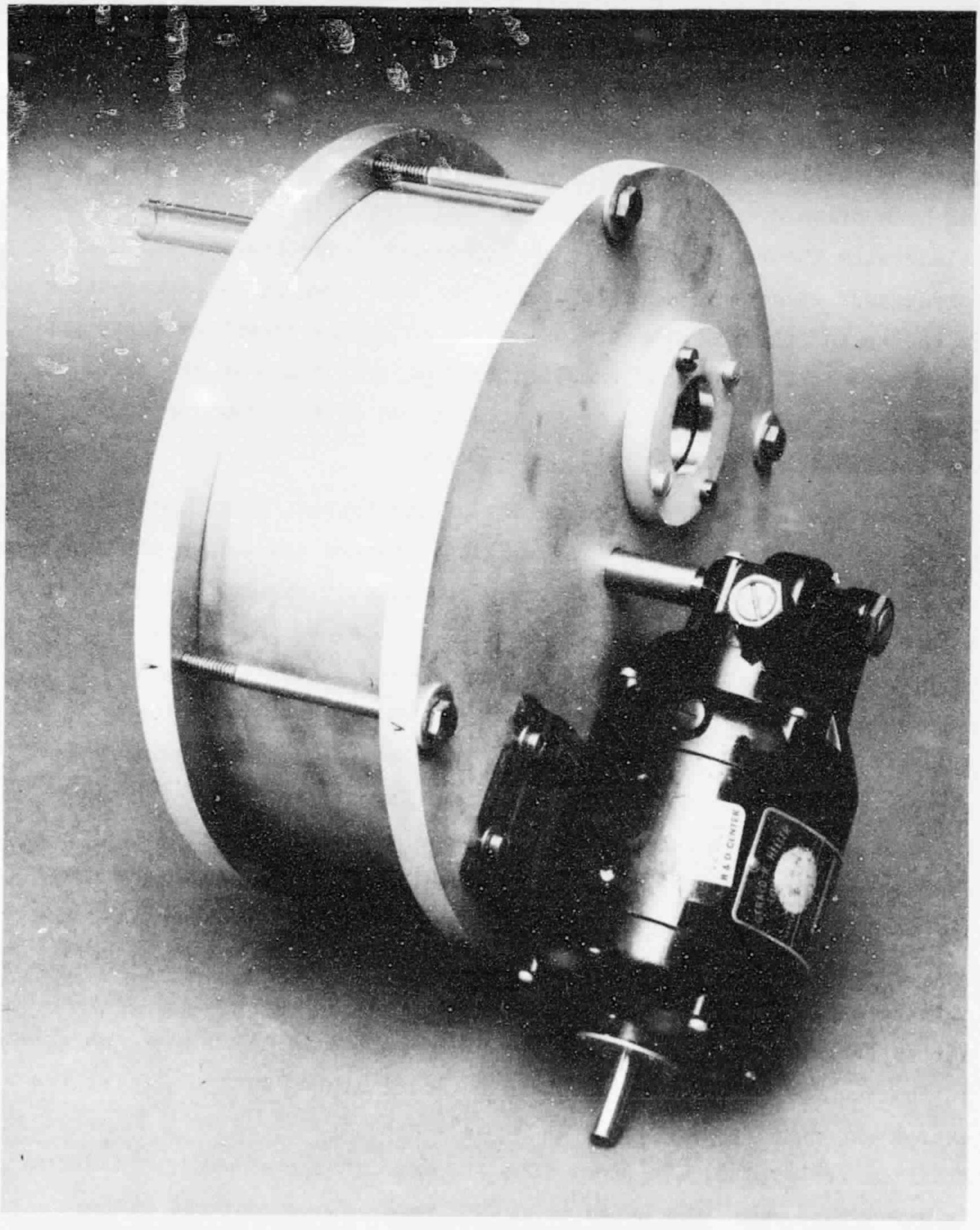

Figure 30 Mechanically actuated pellet reservoir and feeder.

Several ideas for quartz barriers fused to the inside of the crucible were evaluated. During an early series of experiments using a simple plate with a small (∿ 1mm) gap at the bottom, a rather annoying phenomenon was observed. After the completion of the runs, in many cases, the silicon originally placedin the crucible feed compartment had been drawn over into the growth compartment. For example, Figure 31 illustrates the result of one such experiment. The drawing of the feed compartment evidently occurred during the melt down, as a perturbation in end to end thermal symmetry was observed during growth attempts, and there were both melted and unmelted feed pellets found in the feed compartment. This behavior is related to the surface tension and wetting characteristics of molten silicon on quartz.

Several design modification of the barrier were fabricated and tested in an effort to alter the wetting behavior and obtain reproducible conditions in the feed reservoir. In addition to the vertical barrier with a communicating slot on the bottom (Type A design, Figure 32), a barrier set at a 60° slant with the 1mm communicating slit, (Type B, not shown) and a 6x10mm "mouse hole" opening in the barrier (Type C, Figure 33) were each evaluated under a variety of run conditions. For all barrier geometries, the crucible feed compartment was found empty in at least some number of the runs. This behavior suggested that barrier design by itself would not solve the problem. However, the fact that the feed compartment remained full some of the time, suggested that the melt down procedure might influence the wetting behavior. Thus different melt down procedures were tested. In some runs the coil was displaced far to the right (the feed compartment is on the left) so that the silicon in the feed compartment melted before the remaining charge. After the charge was completely melted, the coil was shifted back to a symmetrical position for growth. In other runs the main charge was melted first. In every case where the material in the feed compartment was melted first, the feed chamber remained full during the run, e.g. Figure 34. This was true for both Type A and C barriers. Thus a workable and effective solution to the problem was obtained. In practice Type C barriers are employed and the feed material is now always melted first.

ORIGINAL PAGE IS
OF POOR QUALITY

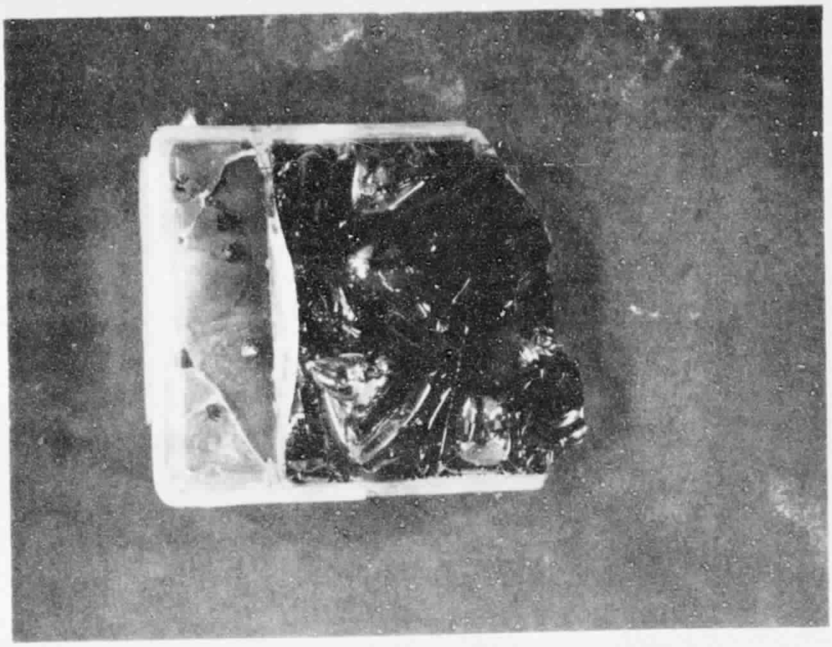

Top View

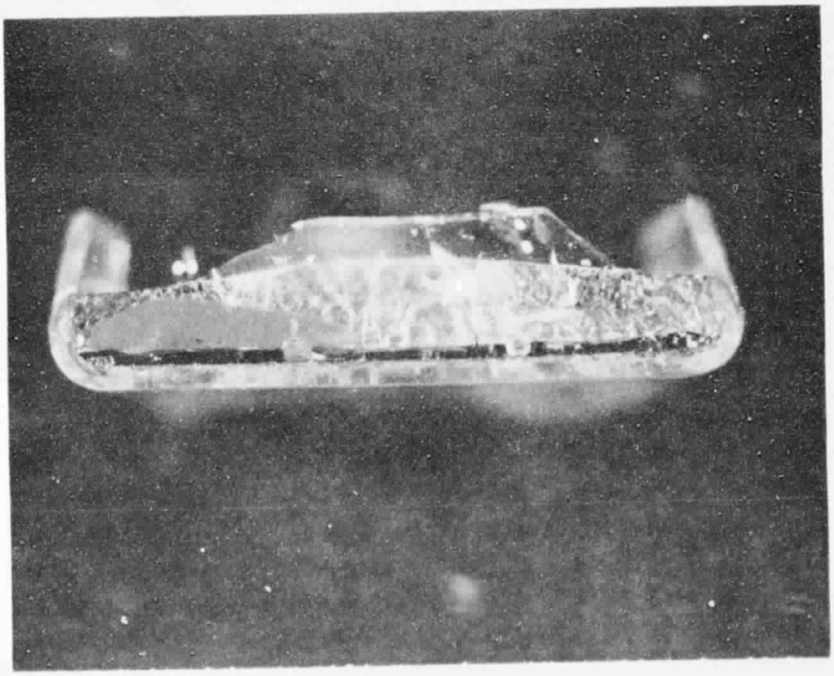

End View

Figure 31   Crucible showing depleted feed compartment.

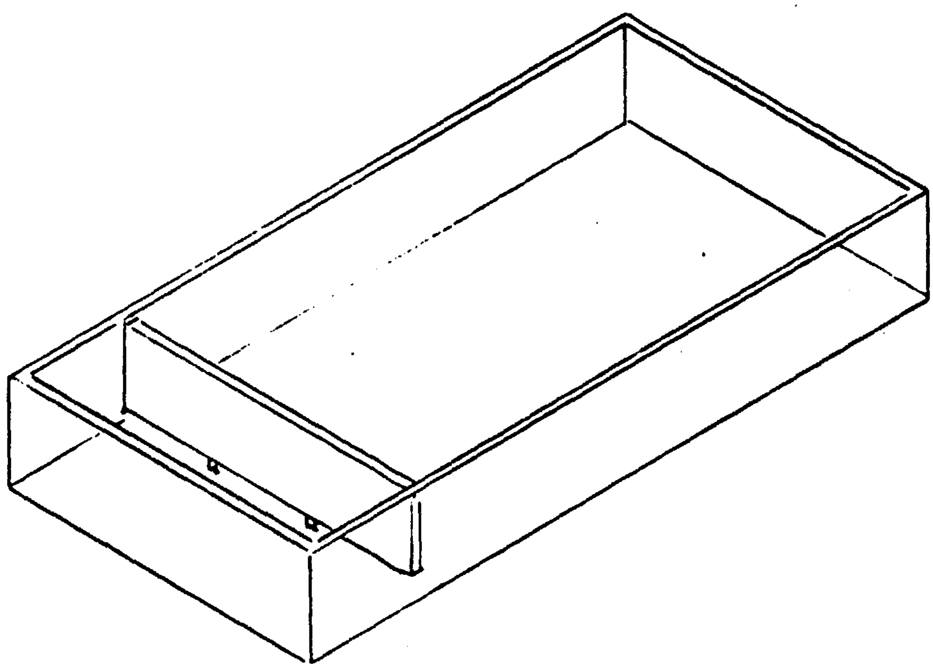

Figure 32 Type "A" barrier in quartz crucible.

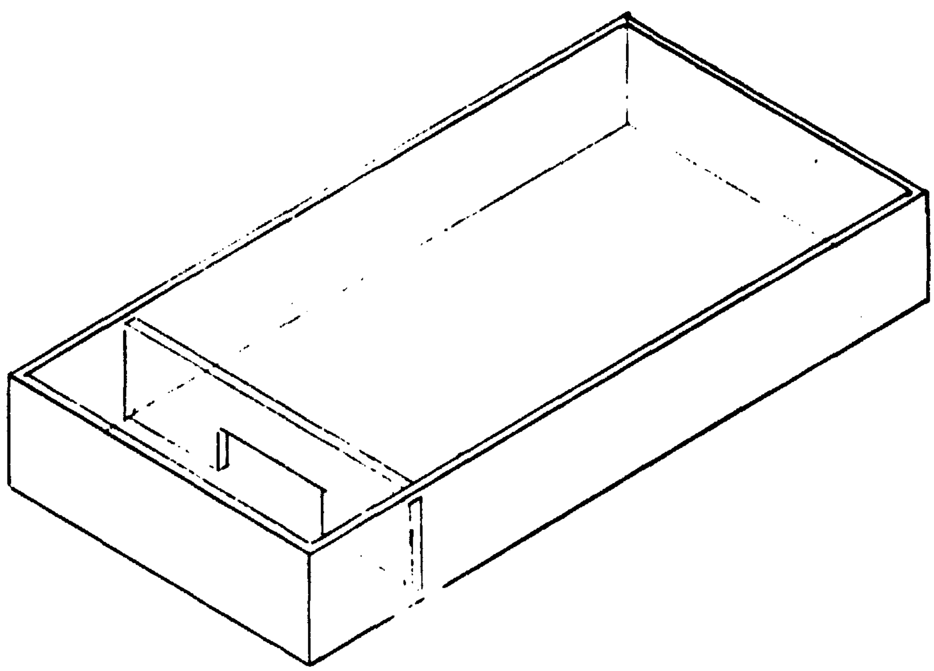

Figure 33 Type "C" barrier in quartz crucible.

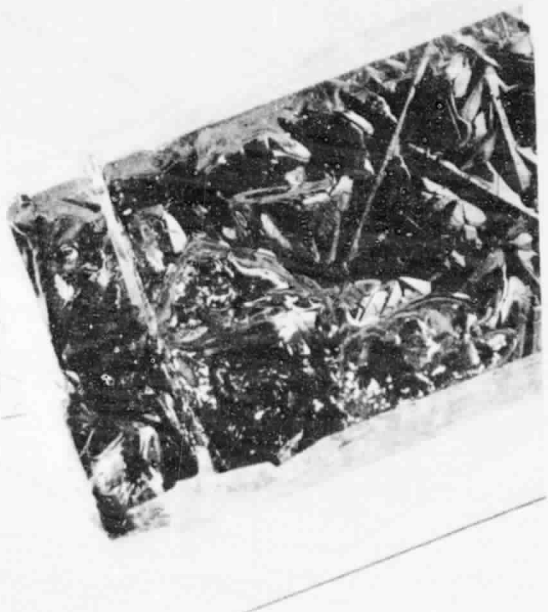

Figure 34 When material in feed chamber is melted first, silicon remains in the compartment throughout the run.

3.2.4 Web Growth with Manual Feeding

A number of experiments have been conducted in the RE furnace to evaluate feed system parameters such as pellet injection rate and argon flow rate through the feed tube. Although not the primary objective of these early runs, feeding with growth for periods over an hour has been demonstrated.

The feed material is cut into pellets from the same polysilicon cylinders used to initially charge the crucible. The knowledge gained from these experiments can be applied to utilize other forms of pelletized silicon when such solar grade feed stock becomes available in the future. Manual feeding rates of one to four pellets per minute have been used. In a production facility, the feeding rate will depend on particle size and would be adjusted so that the silicon added would balance the amount removed in the form of web crystal. In that way the level would be maintained constant.

Our experience indicates that the quartz feed tube in its present configuration requires a small argon flow (50 to 100 cm^3/min) to prevent the accumulation of oxide which would eventually block the tube and stop pellet injection. Since the feed tube penetrates the lid, most of this flow passes over the melt in the growth region.

We have found that from time to time as pellets are fed, tiny particles of silicon nucleate on the surface of the melt, float to the web, and either terminate growth or impair crystal quality. The occurrence is sporadic, sometimes occurring at the initiation of feeding, and sometimes much later in a run. There is considerable circumstantial evidence that the nucleation of silicon is caused by minute oxide particles dislodged by falling pellets then blown by the argon flow into the growth compartment. Particles which fall into the feed chamber are prevented from reaching the growth chamber by the quartz barrier. If this hypothesis is true redirection of the incoming argon gas should alleviate the condition. We plan to carry out experiments of this kind in conjunction with the mechanized feed system.

3.2.5 Mechanized Feed System

The W furnace is already equipped with a tested venturi system which can be used to control and direct gas flow during web growth (Section 3.2). This is therefore a logical place to carry out the first experiments to eliminate the possibility of oxide blowing over into the feed chamber during growth. To expedite these experiments we have mounted the mechanized feeder on the W furnace as shown in Figure 35. The pellets, fed at an adjustable rate, enter the growth chamber by means of gas tight teflon and quartz tubes. The venturi effect should produce counter flow away from growth chamber hindering any particle carry over. These tests will begin during the next quarter.

3.3 Characterization of Silicon Web from Experimental Runs

3.3.1 Solar Cell Characteristics

The principal means of characterization of dendritic web material, other than its physical dimensions, remains the performance of test solar cells. Since the ultimate application of the material is for photovoltaic converters, the cell performance provides a direct operational measure of the material quality. The design and fabrication of the 1x1 cm test cells remains essentially the same as described previously[1] although presently the mask details have been changed to permit the fabrication of two test cells on a 25 mm long sample. This modification permits a larger number of cells to be fabricated during a single processing run and thus improves the statistics of the data. Table 1 gives the resulting cell performance data for the silicon dendritic web crystals evaluated during the report period. The table is arranged by furnace and crystal number, and each entry represents the average of four or more individual cells. In order to provide a baseline for the fabrication run, samples of web crystals with properties known from previous experiments are included in each run: the data for these crystals also are tabulated.

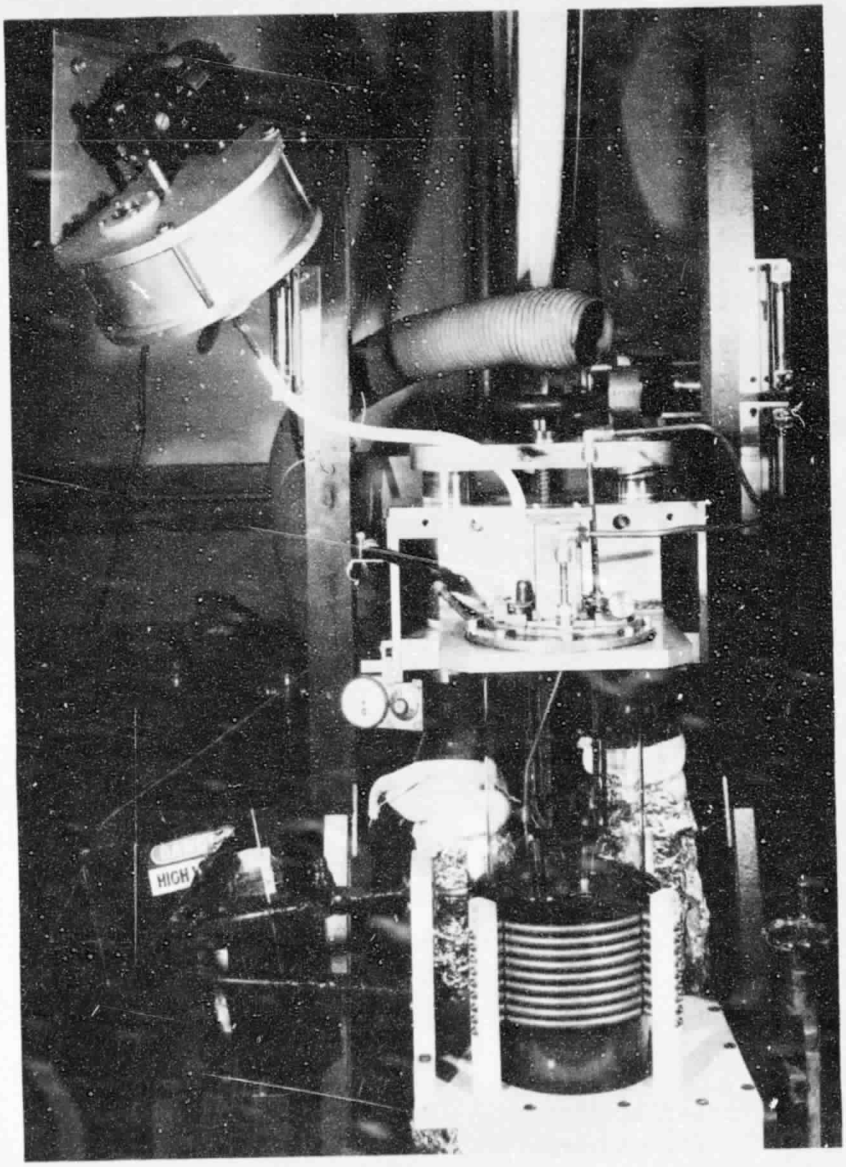

Figure 35 Mechanically activated feeder mounted for use on "W" furnace.

TABLE 1

AVERAGED SOLAR CELL CHARACTERISTICS FOR WEB MATERIAL*

Crystal	Run	I_{sc} mA	V_{OC} Volt	FF	η_o %	η_{AR} %	τ_{OCD} μs	Remarks
RE28-5.2	WQ6	22.8	.567	.749	10.2	14.6	36.1	Std. Mtl.
	WQ15	20.3	.554	.739	8.8	12.6	21.8	"
RE32-5.1	WQ8	22.6	.570	.751	10.2	14.6	23.7	"
	WQ9	22.1	.564	.743	9.8	14.0	22.3	"
	WQ10	22.4	.566	.731	9.8	14.0	23.4	"
	WQ11	21.8	.555	.737	9.4	13.4	20.7	"
	WQ15	20.7	.548	.728	8.7	12.4	17.2	"
RE49-3.5	WQ10	20.4	.526	.717	8.1	11.6	5.5	
RE49-4.4	WQ10	20.3	.506	.708	7.7	11.0	3.6	
RE50-1.3	WQ10	20.5	.522	.719	8.1	11.6	3.9	
RE50-2.1	WQ10	20.3	.519	.702	7.8	11.1	2.8	
RE54-1.2	WQ13	23.0	.550	.740	9.9	14.2	19.5	
RE54-1.3	WQ10	22.3	.555	.735	9.6	13.7	22.6	
RE54-2.1	WQ10	21.1	.530	.729	8.6	12.3	9.1	
RE56-3.2	WQ10	22.2	.570	.745	9.9	14.1	28.3	
RE78-3.3	WQ15	21.5	.542	.727	9.0	12.9	14.2	
RE78-4.3	WQ15	21.1	.533	.731	8.7	12.4	9.0	
J73-5.1	WQ10	20.4	.514	.710	7.9	11.3	2.4	
J78-3.2	WQ10	21.0	.526	.734	8.6	12.3	3.7	
JJ80-4.2	WQ11	19.6	.510	.740	7.8	11.2	2.1	
J80-5.1	WQ10	20.1	.518	.725	8.0	11.4	2.6	
J84-4.3	WQ10	22.1	.550	.736	9.5	13.6	12.1	
J84-4.7	WQ10	21.6	.542	.728	9.1	13.0	10.0	
J95-2.2	WQ15	20.9	.532	.739	8.7	12.4	12.5	
J95-3.2	WQ15	19.1	.513	.735	7.6	10.9	3.0	
J96-3.2	WQ15	20.6	.537	.756	8.9	12.7	10.6	
J96-5.2	WQ15	21.1	.537	.739	8.9	12.7	12.5	
J97-1.3	WQ15	21.2	.548	.743	9.1	13.0	14.7	
J104-2.1	WQ15	21.2	.548	.743	9.1	13.0	22.5	
J106-1.6	WQ15	20.1	.533	.745	8.4	12.0	9.4	
J106-3.4	WQ15	20.3	.522	.741	8.3	11.9	6.0	
W78-1.5	WQ13	20.9	.555	.746	9.1	13.0	13.7	
W87-2.3a	WQ11	20.2	.540	.749	8.6	12.3	2.7	Std. Clean
W87-2.3b	WQ11	20.4	.541	.759	8.9	12.7	2.3	No HF

TABLE 1 (Cont.)

Crystal	Run	I_{sc} mA	V_{OC} Volt	FF	η_o %	η_{AR} %	τ_{OCD} μs	Remarks
W87-2.3c	WQ11	20.3	.546	.763	8.9	12.7	2.8	25 μm CP
W88-2.3	WQ11	20.9	.510	.693	7.8	11.2	1.1	"Clean" Web
W90-3.3	WQ11	20.1	.531	.749	8.4	12.0	4.4	
W91-4.8a	WQ11	20.8	.549	.749	9.0	12.9	8.1	Std. Clean
W91-4.8b	WQ11	20.6	.534	.743	8.6	12.3	5.3	No HF
W91-4.8c	WQ11	20.4	.548	.747	8.8	12.6	7.4	25 μm CP
W94-2.1	WQ15	20.9	.541	.754	9.0	12.9	12.7	
W94-3.2	WQ15	20.5	.532	.747	8.6	12.3	8.2	
W96-1	WQ11	11.4	.361	.590	2.6	3.7	-	
W98-1	WQ13	11.8	.374	.601	2.8	4.0	0.9	
W99-1	WQ13	10.3	.313	.545	1.8	2.6	0.5	
W103-2	WQ13	12.9	.363	.588	3.0	4.3	0.5	
W104-2a	WQ13	10.2	.322	.558	1.9	2.7	0.8	Jcn. on clean side
W104-2b	WQ13	12.3	.339	.558	2.5	3.6	0.8	Jcn. on oxide side
W105-1a	WQ13	10.2	.315	.547	1.9	2.7	0.4	Jcn. on clean side
W105-1b	WQ13	11.9	.377	.600	2.9	4.1	0.8	Jcn. on oxide side
W106-1a	WQ13	11.6	.347	.577	2.5	3.6	0.4	Jcn. on clean side
W106-1b	WQ13	11.2	.332	.563	2.2	3.1	0.4	Jcn. on oxide side
W108-1	WQ13	13.2	.346	.543	2.6	3.7	0.4	
W108-1.3	WQ13	10.8	.330	.558	2.1	3.0	0.4	
W113-1	WQ13	22.3	.563	.738	9.8	14.0	17.9	
W114-2	WQ13	22.2	.564	.744	9.8	14.0	24.7	
W116-1	WQ15	19.9	.516	.735	8.0	11.4	2.9	

CONDITIONS

AM-1 Illumination @ 91.6 mW/cm^2

Cell Area = 1.032 cm^2

η_{AR} is anticipated cell efficiency with an AR coating

*Each entry represents the average value of data on from two to six cells

As the data in Table 1 indicate, the web solar cell performance continues to reflect the high quality of the material. AM1 conversion efficiencies of 13-14% (9-10% without AR coating) are common for crystals grown under a variety experimental conditions.

One group of crystals is an exception to the typical behavior: those webs grown in the W furnace in runs W98 to W108. For this material the solar cell efficiency and OCD (open circuit decay) lifetime were extremely low. <u>A priori</u>, there was no reason to suspect the material was of inferior quality. The residual stress levels were small, avg. $\sigma/W^2 = 1.0\times10^7$ dynes/cm^4, and there was no sign of obvious crystal defects. The only particular characteristic that the crystals had in common was that they were grown from a furnace configuration in which a large gas flow passed between the molybdenum lid and top shield then impinged onto the growing ribbon (see Section 3.2).

The available information suggested that the gas flow had introduced contamination into the webs, possibly a surface deposit of molybdenum in some form. A variety of chemical analysis techniques were tried in an attempt to identify any impurities on the web surface. Neither S.I.M.S., E.S.C.A., nor SEM techniques were sufficiently sensitive to detect what impurities, if any, were present.

For that reason a second set of experiments was conducted as follows. Twelve microns of material were chemically polished from each side of crystal W108 (this crystal had a heavy oxide deposit on one face). Solar cells were fabricated with some of the n^+p junctions on the heavily oxidized side and some on the other. Average cell efficiencies were then compared to efficiencies for the original unetched crystals. The results are given in Table 2.

TABLE 2

CELL DATA FOR W108 EXPERIMENT
(% EFFICIENCY BEFORE AR COATING)

Junction on the Heavy Oxide Side		Junction on the Light Oxide Side	
Etched	Unetched	Etched	Unetched
5.6	2.5	4.8	2.0
5.7	2.6	4.9	2.1
5.6	2.5	---	2.0

The etched crystals have higher efficiencies, supporting the hypothesis that a surface contaminant was present. An interesting observation that the more strongly oxidized side of the web gave higher efficiencies in both the etched and unetched cases. This suggests that the oxide layer may act a a barrier to impurity into the silicon from an external source. Further support for the high gas flow as the source of the contaminant was that when the flooding technique was terminated and the venturi system reinstalled, then cell quality returned to its usual value.

3.3.2 Deep Level Spectroscopy for the Analysis of Web Crystals

Deep Level Transient Spectroscopy (DLTS) is a sensitive method for quantitative evaluation of electrically-active impurities in silicon. The technique can reveal impurities at concentrations well below those detectable by conventional analytic methods.[7,8] This provides a direct way to identify and analyze for impurities inferred to cause cell performance degradation such as that described in the previous section. For this reason we have carried out preliminary experiments to (1) evaluate the applicability of the method specifically to silicon web

(2) identify trap levels which may be reducing carrier lifetime in web (3) determine whether there is any relation between the properties of the as-grown web and subsequently processed solar cells. With a better understanding of the properties of web it should be possible to raise AM1 solar cell conversion efficiency above the 15.5% value so far achieved.

Two types of web material were studied, solar cells from previous characterization runs, and as-grown material from which the cells were originally made. Cells with uncharacteristically poor efficiencies were deliberately selected for analysis to give a range of performance characteristics and to facilitate the observation of any trends in the experimental data. DLTS measurements were made on the cells and the as-grown crystals.* These analyses were supplemented with detailed I-V measurements.(7)

Figure 36 illustrates the transformed I-V characteristics for web solar cells ranging in efficiency from 5.96 to 9.5% (AM1 without AR coating). The upper segment of these curves represents bulk performance (ideality factor n = 1) and the lower segment is indicative of the junction response. A leftward shift in the upper segment indicates a reduction in the bulk lifetime.(7) The I-V analysis showed that the effects of shunt resistance (∿50KΩ) and series resistance (∿0.5Ω) were very small and nearly the same for all the crystals and cells. From the shift observed in the curves in Figure 36, we concluded that differences in bulk lifetime were the primary reason for the spread in cell efficiencies in these devices.(7) The higher efficiency cells had higher lifetime and vice versa.

*We are indebted to Dr. Ram Kachare of JPL for fabricating Schottkey barriers of the as-grown web and performing DLTS analysis of the samples. He also collaborated in the data analysis and confirmed some of our measurements on the web cells.

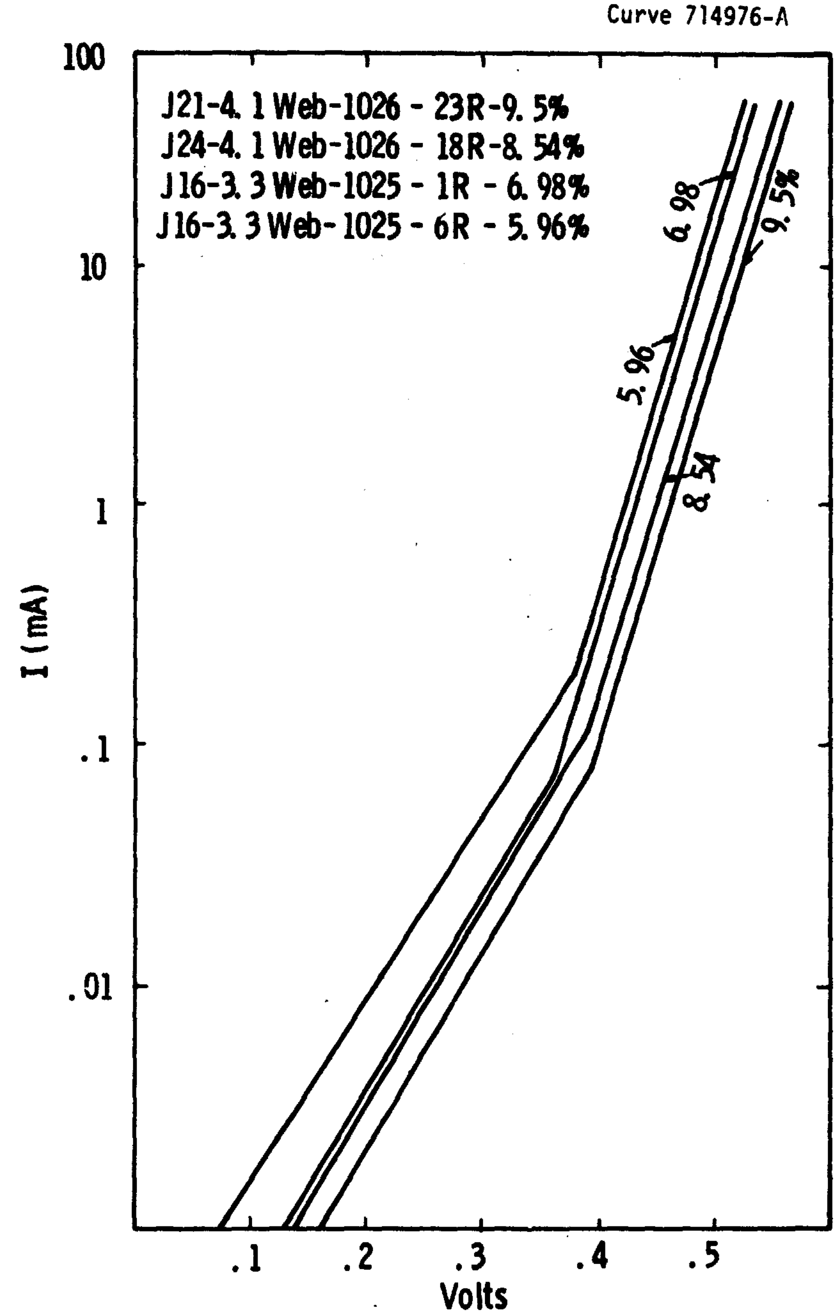

Figure 36 Transformed I-V curves for web solar cells displaying a range of conversion efficiencies. Cells with reduced performance made on webs suspected of surface contamination. (see text). No AR coating on cells.

The next step was to identify the deep level responsible for degrading the bulk lifetime in the poorer cells. Deep level transient spectroscopy (DLTS) was performed on each unprocessed crystal and on solar cells fabricated from them. Measurements on the unprocessed material were done using Ti-Au Schottky barrier diodes about 1.3mm in diameter while 0.7mm diameter mesa diodes were used for the measurements on the solar cells. The key results of the deep level measurements are compiled in Table 3, which gives both the energy and the density of the deep levels detected on the unprocessed web and on the solar cells. All the unprocessed web crystals exhibit a deep level at E_V + 0.3 ev, while most of the solar cells themselves show a level at E_V + 0.4 ev. A distinction is that the cells showing the E_V + 0.4 ev level were all processed from crystals grown in the J-Furnace, while the two cells processed from material grown in the R-Furnace retained the E_V + 0.3 ev level. (The data sample is yet too small to assess the significance of this observation).

Figure 37 relates the logarithm of the reciprocal trap density to the efficiency of the solar cells. Although some data scatter exists, there appears to be a correlation of efficiency with both the E_V + 0.3 ev level in the unprocessed material and with the E_V + 0.4 ev level found in the cells themselves. It is not clear whether the level present in the as-grown material is somehow modified by subsequent processing or by some kind of complexing with other impurities. The available data, Figure 38, do suggest a relationship between these two levels. The line in the figure is a forced fit of slope unity; a slope of 1.22 gives a somewhat better fit. Approximately, each E_V + 0.3 ev level gives rise to 16 E_V + 0.4 ev levels.

Several conclusions can be drawn from this preliminary study. First, the DLTS technique is sufficiently sensitive to detect the impurity levels which degrade solar cell performance in the more inferior web cells. Second, there are apparently levels in the starting material which are relatable to other levels in the finished devices even though the first levels apparently vanish during the processing sequence. Finally, the

TABLE 3

DLTS RESULTS ON WEB CRYSTALS AND CELLS
CONTAINING SUSPECTED CONTAMINATION

Crystal I.D.	Doping cm^{-3}	Run No.	Cell No.	Cell η %	Deep Levels in As-Grown Crystal Energy(ev)	$N_T(Cm^{-3})$	Deep Levels in Solar Cells Energy(en)	$N_T(Cm^{-3})$	Notes
J21-4.1	$7x10^{14}$	1026	23R	9.50			No Level		No CP
					E_V+0.30	$2.48x10^{11}$			
J21-4.1	$7x10^{14}$	1026	18R	8.54			E_V+.40	$2.3x10^{12}$	CP
J-15-1.1	$1.5x10^{15}$	1023	8R	8.47	E_V+.30	$1.17x10^{12}$	E_V+.40	$2.3x10^{13}$	
J-17-2.3	$6x10^{14}$	1023	13R	7.18	E_V+.30	$3.0x10^{12}$	E_V+.40	$4.2x10^{13}$	
							E_V+.30	$5.5x10^{12}$	
J-16-3.2	$1.8x10^{15}$	1025	1R	6.98			E_V+.40	$8.8x10^{13}$	
					E_V+.30	$4.0x10^{12}$			
J-16-3.2	$1.8x10^{15}$	1025	6R	5.96			E_V+.40	$7.5x10^{13}$	
R225-3.2	$1.5X10^{15}$	1026	1R	7.23			E_V+.30	$1.33x10^{13}$	No CP
					E_V+.30	$2.8x10^{13}$			
R225-3.2	$1.5x10^{15}$	1026	5R	9.36			No Level		CP

Curve 715030-A

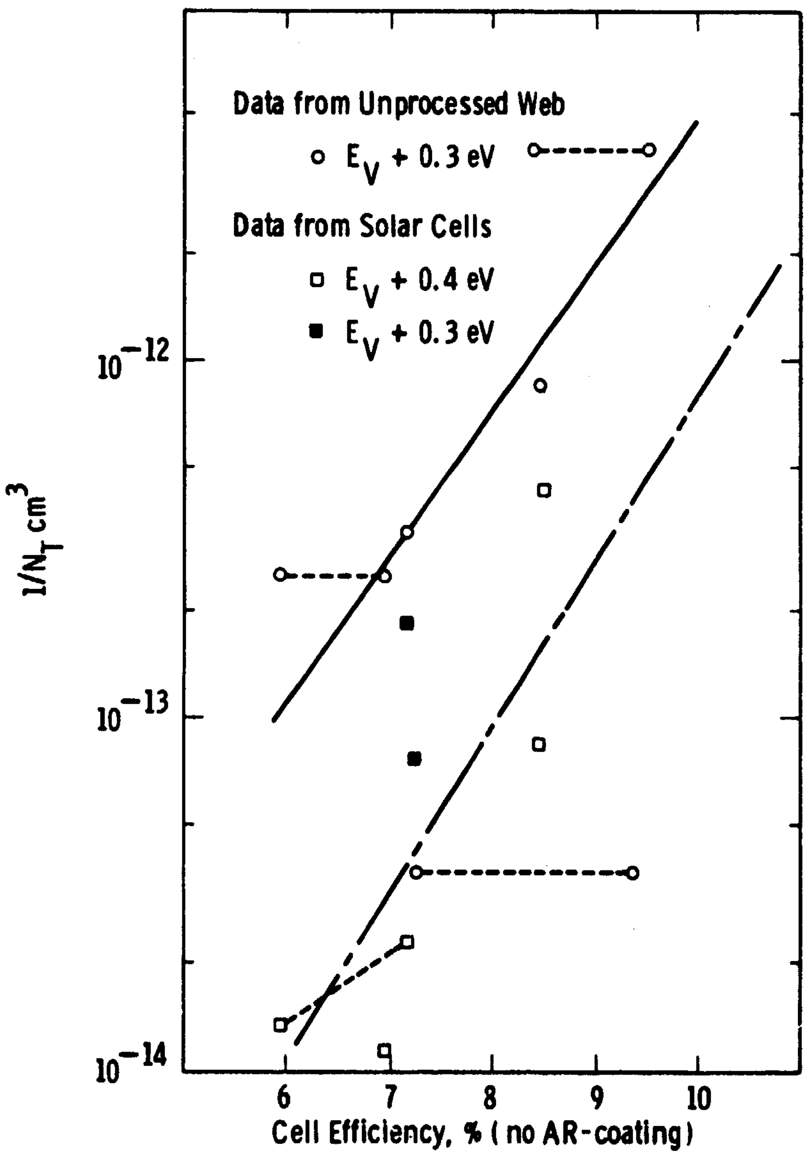

Figure 37 Reciprocal trap density vs solar cell efficiency for unprocessed web and the same material made into solar cells.

Curve 715029-A

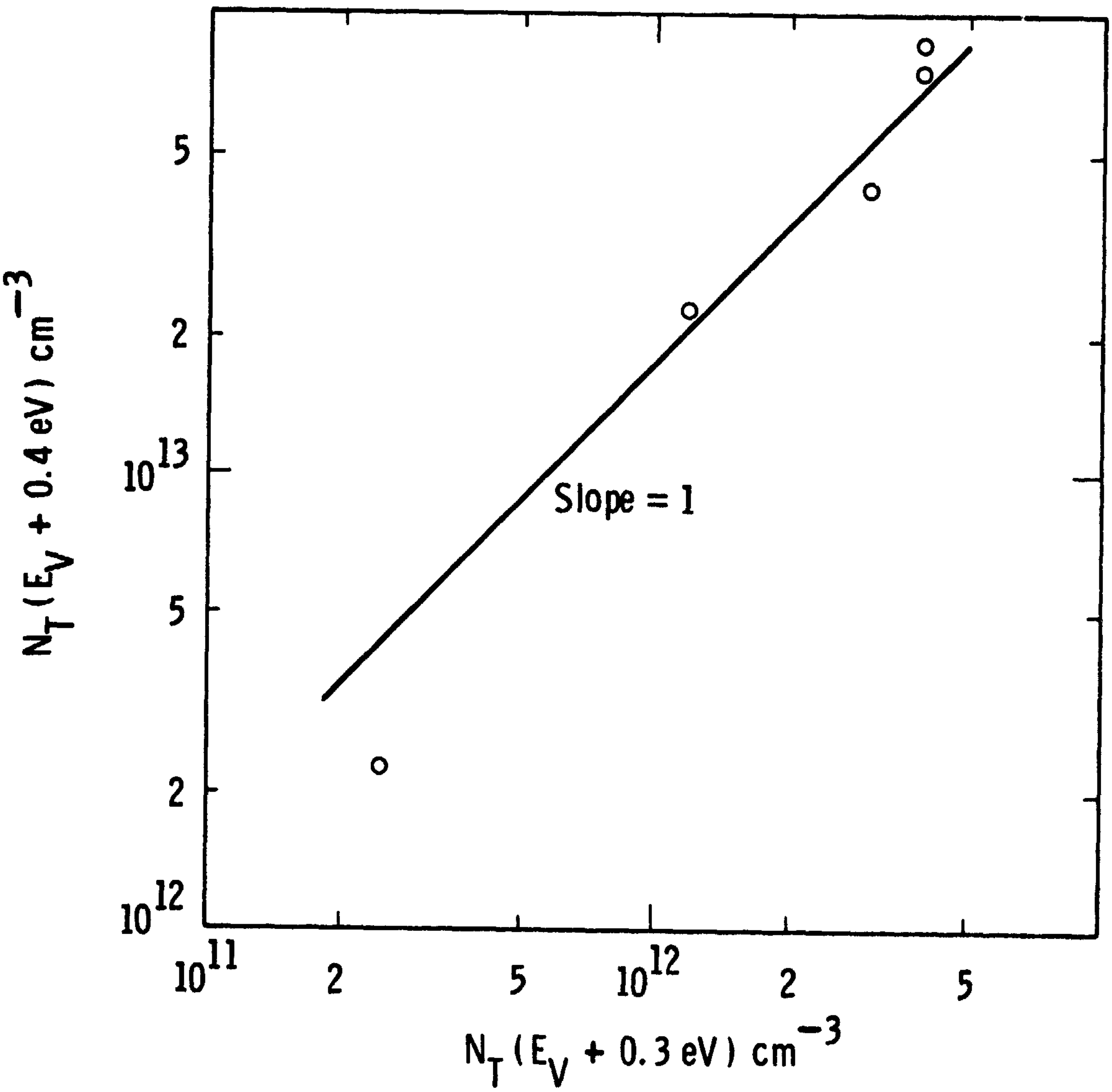

Figure 38 Relation between trap density in unprocessed material E_V + 0.3ev) and trap density in solar cells (E_V + 0.4ev).

behaviour of the material may be related to the growth apparatus, e.g. impurity transport by the gas phase as in the case of the argon flooding system.

Additional work is contemplated to verify and expand these conclusions. If the source of contamination can be identified, then it can be eliminated to produce web solar cells with even higher efficiencies.

3.3.3 Microstructural Evaluation

In order to better understand the mechanisms of structural degradation and possible deformation of the web crystals by high stresses during growth, studies were made of the dislocation density in dendritic web crystals having different residual stresses. Etch pits were formed by immersing cleaned web samples in Sirtl etch (2 parts chromic acid to 1 part HF) for 6 minutes at room temperature. This preparation gave high contrast pits which were easily counted using automatic quantitative metallography.

The actual determination of etch pit density was done with a Leitz Classimat automatic image analyzer. The apparatus counted the number of pits in a 680 μm square area, then moved in programmed steps to adjacent areas; the process repeated until a total area 6.8x10.2 mm in size had been covered. When the etch pit density distribution across the width of the sample was examined it was found to have a distinct central maximum, examples of which are shown in Figure 39. When the value of this maximum (obtained by averaging the three highest individual values) is plotted as a function of the residual stress, a direct relation between the two parameters is found (Figure 40).

Two important conclusions can be drawn from these results. First, dendritic web with small residual stress also has very few dislocations; in fact,it is dislocation free over large areas. Second, the dislocation density is largest in the central region of the web where the lateral stresses are predicted from our thermal model to be largest. This provides strong evidence that this is the stress component responsible for the observed residual stress.

Curve 715027-A

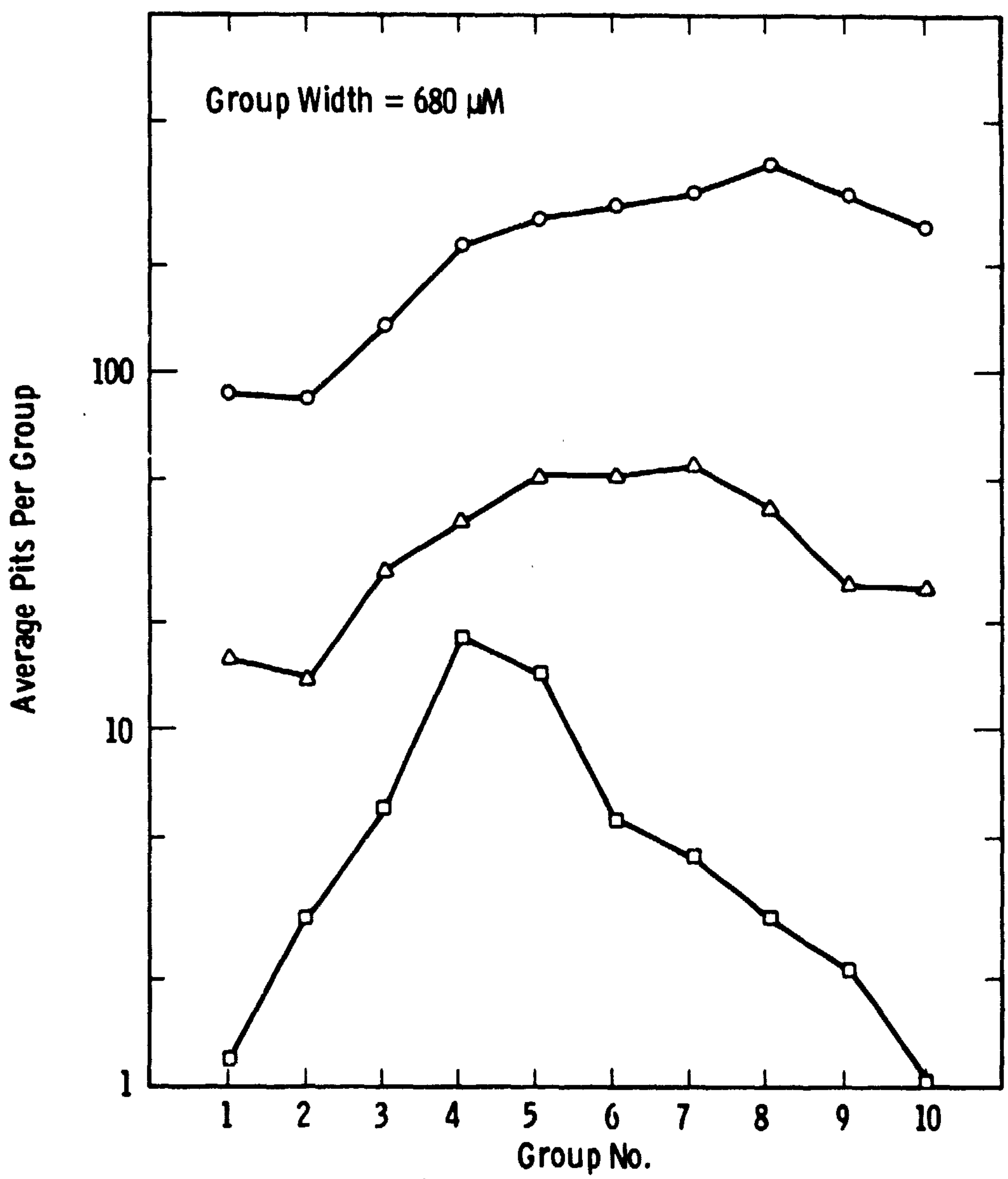

Figure 39 Average etch pit density across central area of several web crystals. Group width is 680 μm.

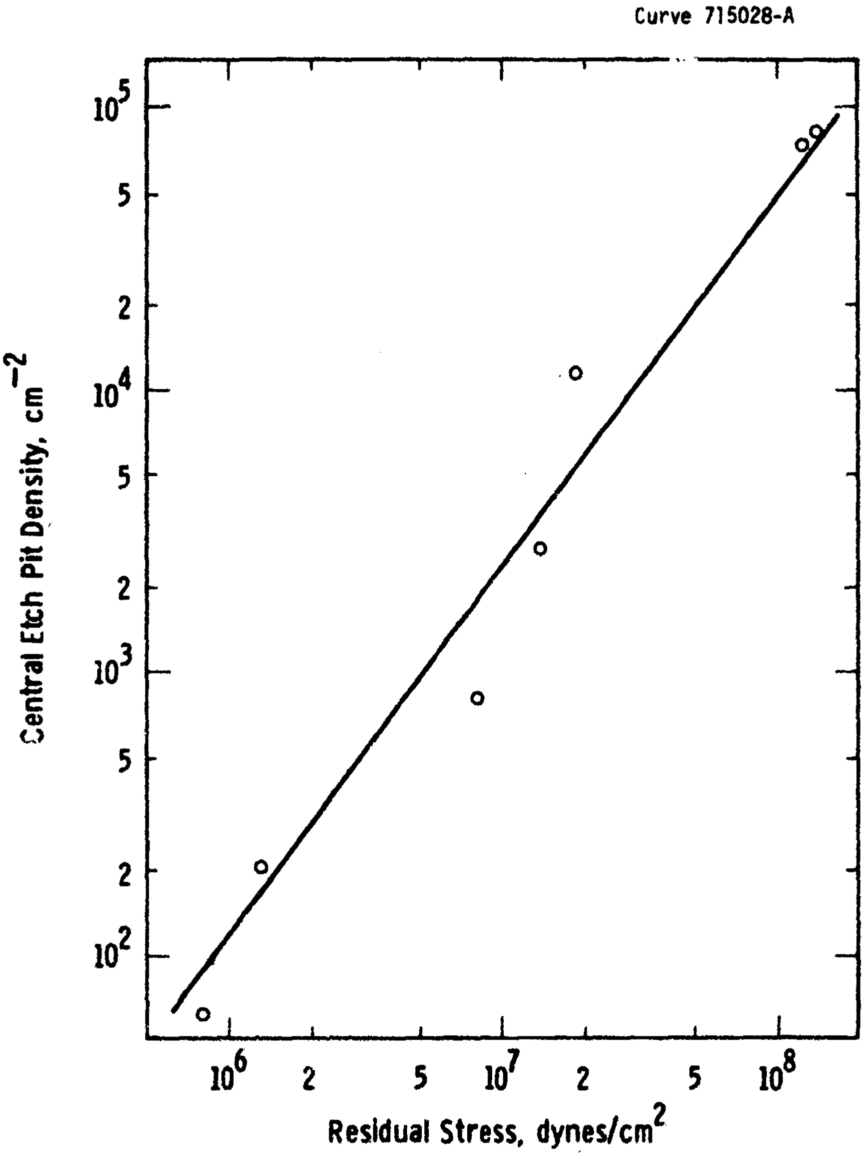

Figure 40 Relationship between etch pit (dislocation) density and residual stress in web crystals.

4. CONCLUSIONS

Experimental results as well as computer simulation indicate that an afterheater placed above the susceptor lid raises rather than reduces residual stress in silicon web. The afterheater, *per se* is not a viable approach to reduce deformation of web and thus to promote web widening. However, the analyses suggest that a cold aftertrimmer will provide the appropriate vertical temperature profile in the ribbon needed to reduce deformation. First experiments confirm that the residual stress indeed is low in webs grown with an aftertrimmer comprised of two flat parallel water cooled plates. Insufficient experiments have been conducted yet to verify the expected improvement in web widening.

Lid slots with bevels or larger slot widths increase the speed at which web can grow (at any given thickness). This is because the latent heat of fusion is more effectively dissipated by slot configurations with large radiative view factors. Slots which produce growth speeds to 7cm/min were recently tested. By combining slot designs which favor flat temperature profiles in the liquid with large radiative view factor web output rates of 12 to 13 cm^2/min are readily achieved (15 cm^2/min rates were obtained shortly after the end of the report period.)

Both experiment and computer simulation show the critical effect of changing melt level on web growth stability. As the melt is depleted by crystal growth, the freezing front falls deeper and deeper into the hot growth cavity. Thermal conditions change making control of growth difficult, particularly at high output rates. More important, as the melt level drops, the beneficial effects of lid design and thermal trimming are lost. Since less heat can be dissipated from the crystal, growth velocity is reduced. As the portion of the crystal acted upon by the lid and trimmer is displaced, stresses in the web increase; widening is hindered. Overall,the impact is to reduce the maximum output rate. Development of and operational melt sensing and replenishment system should be accelerated to increase the effectiveness of the output rate, of technology development studies,and to provide stable growth conditions for long run operation.

Recent preliminary melt replenishment studies show it is feasible to grow web and feed silicon pellets simultaneously. Growth for periods longer than an hour has been hampered by the carry over of oxide from the pellet feed port to the growth chamber. This apparently occurs when a silicon pellet dislodges oxide accumulated at the bottom of the feed tube; the gas flow through the feed tube then sweeps the oxide to the vicinity of the crystal-liquid interface. Growth is terminated by pull out of the web or degradation of crystal quality.

We have developed and tested a unique venturi flow system by which an inert gas can be drawn past the growing web, then away from the crystal to be exhausted elsewhere. This technique keeps furnace components oxide free and should be adaptable to prevent oxide carry over during melt replenishment.

An alternative gas flow system, in which gas passed between the hot growth shields impinged on the web also prevented oxide deposition. However, contamination of the crystals occurred probably by impurity transport from the molybdenum shields. This sort of contamination could occur in other crystal growth equipment depending on the geometry and direction of gas flow.

Web solar cell performance, aside from the contaminated material described above, continues to lie in the 13-14% range for the unoptimized process used to monitor the crystal growth studies. Deep level spectroscopy indicates the presence of trap levels in web solar cells with efficiencies below about 14%. This suggests that further improvements in crystal growth and processing will result in web solar cell efficiencies above the 15.5% maximum value achieved to date.

5. PLANS FOR FUTURE WORK

During the final quarter of Phase II, the emphasis of the effort will be to blend the thermal trimming technology developed to increase web width with "fast" lid designs to reach the 25cm^2/min web output rate goal. Concurrently the mechanized feeder will be combined with a venturi growth lid system in the W furnace. Tests will be carried out to evaluate this arrangement and to increase to 10 meters the amount of web which can be grown while simultaneously feeding silicon. Studies of lid geometries and growth parameters to facilitate the control of seeding for high output rate systems will continue.

6. NEW TECHNOLOGY

Two items of new technology have been identified and are being reported separately to JPL under the New Technology provisions of contract number 954654. One item concerns the design concepts of the Mod 2 JPL web growth facility. The other item concerns the new concepts for susceptor and crucible systems. Both have been described in previous quarterly reports.

7. REFERENCES

1. C. S. Duncan, et al., Annual Report, Silicon Web Process Development. DOE/JPL-954654-78/2 June (1978).
2. A. D. Morrison et al., Annual Report, "Large Area Silicon Sheet by EFG," ERDA/JPL 954355-76/11 (Sept. 1976).
3. A. Baghdadi et al., Annual Report, "Laser Dope Growth in a Ribbon-to-Ribbon Process, etc." DOE/JPL 954376-78/4 (Sept. 1978).
4. C. S. Duncan, et al. Quarterly Report (April-June 1978), Silicon Web Process Development, DOE/JPL 954654-78/3 July (1978).
5. C. S. Duncan, et al. Quarterly Report (July-September 1978) Silicon Web Process Development, DOE/JPL-954654-78/4 October (1978).
6. C. D. Graham, et al., Final Report, Research and Development of Low Cost Processes for Integrated Solar Arrays, ERDA/SE/EC (11-1)-2721/FR/76-1 (1976).
7. R. H. Hopkins, et al., Eleventh Quarterly Report, Silicon Materials Task (Part 2) DOE/JPL-954331-78/3 July (1978).
8. C. L. Miller, D. V. Lang, L. C. Kimmerling, Annual Rev. Materials Sci. p. 377-448 (1977).

8. APPENDICES

8.1 Growth Run Summaries

8.2 Updated Program Plan

8.2.1 Milestone Chart

8.2.2 Program Labor Summary

8.2.3 Program Cost Summary

8.1 Growth Run Summaries

GROWTH RUN SUMMARY

The runs in the J Furnace had two major objectives this quarter (1) Tests of hardware, e.g aftertrimmers to reduce web stress and hence improve width (2) Tests of lid designs to improve web velocity. Generally growth speeds in aftertrimmer tests were held at about 2cm/min. In some runs output rate data were specifically the objective and this is noted.

RUN	NO. OF CRYSTALS	LENGTH (cm)	MAX. WIDTH (mm)	MAX. VELOCITY (cm/mm)	DESCRIPTION/RESULT
J77	2	70	18.1	2.1	Afterheater Test. Full beveled lid, 80x6mm slot, dogbones, 5x5mm bevel. Continue test of afterheater vertical position: 1.5cm above lid. Lineage structure limited widening. Oxide collection on lid shields.
J78	3	292	25.5	2.2	Test effect of shield on oxide accumulation for lid used in J77. Lower shield bent upward. Widening fair but still some oxide accumulation.
J79	2	137	21.3	1.9	Retest of shield configuration in J78. Similar result. Conclude no improvement in oxide control, web speed or width with this shield arrangement.
J80	5	538	30	2.0	Test behavior of new RE-1 lid. for later experiments with afterheater. Baseline behavior verified.
J81	2	148	16.1	2.3	Test shield arrangement to minimize oxide accumulation on long beveled, growth slot. Lower top shield bent up along slot. New top shield. Oxide well controlled but difficult to seed without third dendrities or pull out. Conclude not a useful configuration.
J82	3	123	22	2.0	Afterheater test with RE-1 lid. Evaluate effect of heater vertical position on growth: 2.5cm above lid. Dendrite probe revealed slightly cupped profile in liquid limited widening.

GROWTH RUN SUMMARY

RUN	NO. OF CRYSTALS	LENGTH (cm)	MAX. WIDTH (mm)	MAX. VELOCITY (cm/min)	DESCRIPTION/RESULT
J83	2	114	19.6	2.0	Test effect of 3rd top shield to flatten melt temperature profile with long, beveled lid. Profile flattened but not sufficiently to increase width. Adjust shielding.
J84	4	385	34.7	2.0	Retested 3 shield configuration used in J83. Produced web to 34.7 mm.
J85	2	274	22.9	1.9	Afterheater test. RE-1 baseline lid. Heater 1.5cm above. Remove outside shields on afterheater to raise available ΔT. Very little improvement in ΔT or widening of web.
J86	1	41	14.4	1.9	Afterheater test. RE-1 lid. Lower heater temperature raised (increase ΔT by $\sim$ 100°C) Web did not widen. Run terminated by oxide collection on afterheater.
J87	1	42	14.5	1.9	Ran RE-1 lid without afterheater to check if melt profile was flat. Conclude profile flat enough to get wide web. Failure of afterheater not due to effect in RE-1 lid. Icing terminated run.
J88	5	463	24.0	2.7	Test of dished lid (variable bevel angle across slot length) 8mm thick. 76x5mm slot, 12.7mm dogbones. Center of lid dished to 4mm thickness. Evaluate effect of lid on web widening. Width up to 24mm. Dendrite probe gave flat profile. Webs deformed due to stress.
J89	1	84	17.4	2.0	Test of dished lid (J88) with 2 top shields instead of three. Attempt to reduce web stress. Dendrite profile showed asymmetric temperature profile. Could not widen.

GROWTH RUN SUMMARY

RUN	NO. OF CRYSTALS	LENGTH (cm)	MAX. WIDTH (mm)	MAX. VELOCITY (cm/min)	DESCRIPTION/RESULT
J90	4	423	19.4	5.4	Test shorter lid slot for width control in feeding experiments. Collect velocity-thickness data. Dendrite probe reveals dished profile. Width kept below 20mm. Some oxide accumulation.
J91	3	298	23.5	1.9	Retest of dished lid. Use narrower slots in top shield to reduce stress in web and test widening behavior. Web still deformed.
J92	1	48	13.9	1.7	Retest short slot of Run J90. Argon flow added to reduce oxide. Unstable growth. Tended to produce third dendrites on seeding.
J93	3	444	31.8	2.0	80x6mm, beveled, dogbone lid. Two top shields, bottom large overhang. Argon flow along slot. Test effect of argon flow rate (30 to 100 cm^3/min) on oxide accumulation. Higher flow rate gave better results.
J94	4	309	15.5	2.0	Retest of short slot for feed runs. Difficult to control growth: pullout or third dendrites
J95	4	295	24.6	5.5	Retest of beveled lid for high speed growth. Less overhang on lower top shield to reduce oxide. No oxide problems. Combined output rate over 12 cm^2/min.
		Output >	12cm^2/min.		

GROWTH RUN SUMMARY

RUN	NO. OF CRYSTALS	LENGTH (cm)	MAX. WIDTH (mm)	MAX. VELOCITY (cm/min)	DESCRIPTION/RESULT
J96	5	329	28.3	2.7	Test new lid bevel. Several crystals run to get velocity-thickness characteristics. Lid employs directed argon flow to minimize oxide accumulation in overhanging shield. Data collected. No oxide accumulation.
J97	2	177	21.5	> 5 cm/min	Use same slot-shield configuration as previous run. Raise melt level to improve speed characteristics. Take velocity-thickness data to characterize thermal geometry. Crystals consistent with increased speed attained.
J98	3	156	16.3	2.7	(Runs 98 to 100 were tests of a shorter slot length designed to keep the width smaller for subsequent feed experiments in RE facility). Test 3.8 cm long slot for width control in feeding-target width 2.5cm. Crystals did not widen well enough. Dendrite probe revealed steep dip in melt temperature profile.
J99	2	86	14.2	2.3	Test of 3.8 cm slot with lower melt level to flatten melt profile. Melt temperature profile showed some improvement but still not enough to get to desired constant width. Some temperature fluctuations during growth run.

GROWTH RUN SUMMARY

RUN	NO. OF CRYSTALS	LENGTH (cm)	MAX. WIDTH (mm)	MAX. VELOCITY (cm/min)	DESCRIPTION/RESULT
J100					Test of 3.8 cm slot. Argon flow to top shields reduced to minimize any temperature fluctuations. Temp profile remained dipped. Conclude this lid design ineffective for width control in feeding experiments.
J101	2	138	23 (> 12 cm^2/min output)	7	Test new lid bevel with argon flow under top shields for increased growth speed. Achieved 7 cm/min maximum velocity. Same instability in seeding control, repeatability
J102	1	83	18.5	2.1	Retest of lid used in 101 with slightly lower melt level to improve seeding. Run relatively unproductive. Vibration in melt (cause undetermined) and some temperature control problems.
J103	2	182	21	2.0	Replace thermocouple in system. Reran configuration of J102 with larger shield overhang (cooler shields improve heat transfe Tests restricted by free floating ice in melt
J104	2	241	27.6	2.0	Retest of larger shield overhang as per J102 and J103. Width improved. Melt pulled away from crucible before speed test complet meltlevel too low.
J105	2	170	18.6	2.2	Raised melt level to more stable regime. Retest shields used in J102-J104. Some oxide collection and icing. Conclude shield lid configuration improves speed and output rate but results are not sufficiently reproducible to achieve goals.

GROWTH RUN SUMMARY

RUN	NO OF CRYSTALS	LENGTH (cm)	MAX. WIDTH (mm)	MAX. VELOCITY (cm/min)	DESCRIPTION/RESULT
J106	3	477	27.7	2.1	First test of cold after trimmer designed to reduce elastic bending of web. Test conducted with RE-1 lid, a baseline configuration. Initial trimmer position 2.5 cm above lid. Widest crystal decanted spontaneously. No bending.
J107	2	442	19	1.9	Second test of cold after trimmer. Position 2.0 cm above lid. Oxide collection on trimmer later in day reduced run effectiveness

GROWTH RUN SUMMARY

RUN	NO. OF CRYSTALS	LENGTH (cm)	MAX. WIDTH (mm)	MAX. VELOCITY (cm/min)	DESCRIPTION/RESULT
J108	3	190	23	2.0	Test repeat J106 Cold aftertrimmer (angled plates,45°) Evaluate any effects of aftertrimmer melt temperature profile with RE-1 lid. Mount trimmer modified to improve vision during seeding. Melt probe indicated temperature dipped in liquid, asymmetric also.
J109	1	78	23.8	1.7	Test cold aftertrimmer. Evaluate effect of trimmer vertical position on melt profile. Melt dipped with trimmer at extreme lower and higher position. Also asymmetric.
J110	2	91	17.4	2.0	Test cold afterheater. Evaluate effect of coil position on melt profile with afterheater 1.6cm. Temperature profile dipped and asymmetric in low position. Slightly dipped in high position.
J111	2	86	15.1	2.1	Evaluate melt profile for RE-1 lid with cold aftertrimmer removed. Melt profile flat. Melt vibration limited growth.
J112	7	716	26.3	2.1	Retest melt profile and growth with RE-1 lid, aftertrimmer removed. Flat profile. Concluded angled plates on aftertrimmer interact with induction field and perturb [illegible] temperature profile.
J113	Not productive of web				Cold aftertrimmer modified to vertical parallel plate configuration to reduce inductive effects. Probe melt as a function of coil height. Profile flatter but asymmetric at coil positions tested. Conclude trimmer should be inserted at end of furnace opposite coil leads.

GROWTH RUN SUMMARY

RUN	NO. OF CRYSTALS	LENGTH (cm)	MAX. WIDTH (mm)	MAX. VELOCITY (cm/min)	DESCRIPTION/RESULT
J114	3	125	19.8	2.1	Cold aftertrimmer test. Trimmer inserted at end of furnace opposite cool to reduce inductive effects further. Melt profile nearly flat and symmetric.
J115	3	464	23.7	1.9	Cold aftertrimmer test. Evaluate position of trimmer above lid on melt profile and growth. Trimmer 2.1cm above RE-1 lid. Crystals under better than previous run. Growth ended by pullout.
J116	5	433	26.4	2.0	Cold aftertrimmer test. Trimmer set 1.0 cm above RE-1 lid. Width improved. Lineage in widest crystal due to bad start.
J117	3	247	23.4	1.9	Cold aftertrimmer test. Retest conditions of run J116 trimmer 1.0 cm above lid. Run dendrite probe a low and medium coil positions. Slight asymmetry at medium position; slight dip no asymmetry at low position. Conclude slight dip still limiting widening.
J118	2	276	24.1	2.0	Cold aftertrimmer test. Run at higher coil position to reduce thermal dip.
J119	Abort run				Cold aftertrimmer test. Continue evaluation of aftertrimmer vertical position on melt profile and web growth. Melt wet lid.
J120	5	549	31.3	2.0	Cold aftertrimmer test with new RE-1 lid. Continue evaluation of trimmer vertical position. Trimmer 1.6cm to 2.1cm above lid.

GROWTH RUN SUMMARY

The majority of runs in the RE furnace this quarter were to develop melt replenishment techniques and hardware. For these runs growth speed was fixed at about 2cm/min and width was kept below that at which web bending might occur (so longer lengths could be gotten while feeding). A few other runs were devoted to test lid designs for improved width or speed and argon purge system for oxide control. These runs are annoted with appropriate width and speed data.

RUN	NO. OF CRYSTALS	LENGTH (cm)	DESCRIPTION/RESULT
RE50	2	170	Feed system test. Run to evaluate Type A crucible barrier (vertical, narrow slot). Fed and grew web simultaneously. Growth terminated by floating ice in melt. Noted melt rippling during feeding; did not disturb growth. Silicon remained in feed reservoir.
RE51	4	473	Test effect of narrow straight (80x4 mm) slot on web stress. Two full top shields 5mm x 5mm bevel. Web deformed at about 2 cm maximum width and went polycrystalline.
RE52	3	170	Feed system test. Test shorter growth slot(50x4mm) to raise temperature at feed position. Type A barrier in feed reservoir. Oxide collected on right of growth slot. Argon feed rate appeared too high; reduce flow reduced oxide deposition. Silicon remained in feed reservoir.
RE53	3	214	Feed System Test. Initially no silicon in feed chamber to test: (1) thermal symmetry in system (2) melting behavior of pellets. Type A barrier. Dendrite probe indicated thermal asymmetry-feed side hot. Pellets melted in empty reservoir and some flowed over to growth chamber.
RE54	4	470	Test new RE-1 lid to replace damaged lid. Buttoning and growth behavior normal for this lid. Widths 23-28 mm easy to achieve. Lid appears useable in future experiments.
RE55	3	162	Test effects of 80x6mm slot, 5x5mm bevel (12.7 mm dogbone) on melt profile, web stress and width. Dendrite profile indicated temperature is slightly humped in center of melt and some asymmetric. Crystals widened poorly 20mm max. Oxide collected on shield assembly caused ice in melt.

GROWTH RUN SUMMARY

RUN	NO. OF CRYSTALS	LENGTH (cm)	DESCRIPTION/RESULT
RE56	4	372	Verification run on new RE-1 lid. Maximum width 28.5 mm. Melt profile relatively flat as expected. Plan to run lid in after-trimmer experiments.
RE57	6	350	Test effect of vertical coil position on seeding and growth with RE-1 lid. Problems with ice formation negated experiment. Note oxide on bottom of lid after run. Apparently spalled during run. Test new lid cleaning procedure installed.
RE58	3	305	Test effect of directed argon flow to minimize oxide buildup on overlapping shields. Beveled lid, 80mm slot. Considerably reduced oxide laid down on shield. Harder to seed at high flow rates-third dendrites.
RE59	4	464	Verification test of directed argon flow system. Good oxide control. Grew maximum width of 28mm. Good seeding.
RE60	4	389	Test 5cm, beveled lid for subsequent feeding runs. Dendrite probe fairly flat over center 2-3cms. Feed hole clogged in absence of argon flow. Flow is mandatory for this configuration.
RE61	Not Productive of Web		Feed system test with RE60 lid. Type B barrier no silicon in feed chamber. Large amounts of ice. Shields oxidized suspect system leak. Clean and tighten fittings before next run.
RE62	1	96	Test RE58 lid configuration. Lid overhang extended to reduce radiation from hot lid to web. Used argon flow between shields. Excessive oxide accumulation .
RE63	1	88	Feed system test. Beveled lid, 5cm slot, dogbones. Addition of argon flow tubes to minimize oxide accumulation. Type B crucible barrier (60° slant). No silicon in feed reservoir. Fed and grew web; growth terminated by floating ice.

GROWTH RUN SUMMARY

RUN	NO. OF CRYSTALS	LENGTH (cm)	DESCRIPTION/RESULT
RE64	1	70	Retest RE62 configuration (80mm slot, beveled large overlapping shields) without argon flow tubes. Excessive oxide. Conclude cannot run this arrangement without argon purge.
RE65	5	325	Feed System Test. Beveled lid, 5cm slot, dogbones (RE63) without argon purge through shields. Large (6mm) gap below feed barrier. Assess containment characteristics. Got ice when feeding pellets. Some oxide toward end opposite feed tube. Silicon remained in feed reservoir.
RE66	1	95	Test dished growth lid (design to vary radiation view angle along slot length) two top shields. Evaluated widening characteristics Only 21mm width. Excessive oxide on shield made result ambiguous.
RE67	3	264	Feed System Test. 5cm, beveled slot with dogbones (RE63). Test use of $A\ell_2O_3$ ceramic argon flow tubes under shield to replace Mo tubes. Type A barrier. Fed pellets without perturbing growth. Feed chamber empty of silicon after run. Growth slot free of oxide.
RE68	2	88	Rerun test of dished lid (RE66). Still have problem with oxide deposition on shields. Conclude must alter shield configuration or use argon purge.

GROWTH RUN SUMMARY

Essentially all runs in the RE facility were directed at the development of melt replenishment techniques and hardware. Growth Speed was fixed at about 2 cm/min and width was kept at a value below which ribbon deformation occurred (so longer lengths could be attained while feeding).

RUN	NO. OF CRYSTALS	LENGTH cm	DESCRIPTION/RESULT
RE69	5	282	Feed system test. Test type C barrier (6x10 mm hole) as partition for feed reservoir. Crystal growth terminated repeatly by formation of ice in melt during feeding.
RE70	3	203	Feed system test. Feed tube itself submerged in melt to act as pellet insertion mechanism as well as in situ barrier. Feed and in situ grow for periods up to 10 min. Pellets only partially melted and blocked tube to further feeding.
RE71	3	158	Feed system test. Retest of submerged tube with argon flow adjusted. Both oxide and unmelted pellets terminated feeding eventually. Conclude submerged tube ineffective feeding technique.
RE72	4	228	Feed system test. Test type C barrier with extended height to minimize oxide transport to growth chamber Again grew and fed for short periods but ice formation terminated growth. Conclude higher barrier ineffective solution to oxide problem.
RE73	Unproductive		Test of reversed argon flow through lid shields (away from slot) to minimize oxide. Produced temperature fluctuations. Seeding and growth difficult to control. Abort run.
RE74	Unproductive		Feed system test. Type C barrier. Systematic test of argon purge rate through feed tube to control oxide buildup. Unable to grow due to ice throughout run. Suspect furnace leak. After run found that no silicon remained in feed chamber.

GROWTH RUN SUMMARY

RUN	NO. OF CRYSTALS	LENGTH cm	DESCRIPTION/RESULT
RE75	5	350	Feed system test. Repeat of previous run after furnace checkout. No major ice problem. Grew and fed simultaneously for periods over 1 hour. Growth of longer crystal terminated by oxide speck.
RE76	3	98	Feed system test. Test of methods to eliminate outflow of silicon from feed chamber during run: larger hole (7x15 mm) in type C barrier. Result ambiguous due to oxide. Height of hole too close to melt surface to act as effective barrier.
RE77	Unproductive		Feed system test. Test effects of melt down procedure to prevent outflow of silicon from feed chamber. Melt charge from feed end toward center. Silicon in feed chamber at end of run. Oxide and ice in melt made run unproductive for growth.
RE78	4	416	Feed system test. Verification of effects of directional charge melt down procedure. Melt from center to feed end by repositioning coil. Feed reservoir empty at end of run. Conclude must melt material in feed chamber first during start up to keep silicon there during run. Fed and grew during run.

GROWTH RUN SUMMARY

RUN	NO. OF CRYSTALS	LENGTH (cm)	DESCRIPTION/RESULT
RE79	2	273	Feed Run Test. Evaluate melt down procedure on silicon retention in feed chamber. RE-1 type lid. Melt down from feed end first. Silicon remained in feed reservoir throughout run. Web width up to 24mm.
RE80	Not Productive of Web		Test lid for high speed growth. Recessed bevel, ∿ 3mm thin lip (see text, section 3.1.2). Speed to 6cm/min in short lengths. Excessive oxide accumulation on shields. Oxide fell in, run aborted.
RE81	7	471	Retest high speed lid of RE80 but with argon purge to reduce oxide. Speeds up to 4.5 cm/min. Widths 12.3-17.5mm. Lineage.
RE82	2	209	Retest high speed lid (RE81). Evaluate effect of coil height on seeding and growth. Max. speed 3.5cm/min; Max. width 15mm. Problem with lineage structure formed during seeding; limits widening.
RE83	2	123	Test effect of lid-melt distance on speed. Full beveled, dogboned lid recessed 2mm to bring melt level close to growth slot. Collect thickness velocity data. Maximum speed 5cm/min. Hard to control seeding.
RE84	1	42	Test effect of slot width on speed and seeding. Slot configuration. as in RE81. Slot widened from 4.6 to 5.5mm. Tendency for web to go polycrystalline near start of seeding. Harder to control seeding.
RE85	Not Productive of Web		Rerun RE84 configuration. Obtained thickness-velocity data but no long web lengths (due to vibration in melt). Speeds to 5cm/min.
RE86	4	280	Test effect of melt height on growth velocity. Reduced melt height with RE84 lid configuration. Better control of seeding but growth speed reduced.
RE87	Run aborted		Test beveled, recessed lid as used in RE83. Argon flow tubes to minimize oxide. Melt wetted lid; run aborted.

GROWTH RUN SUMMARY

RUN	NO. OF CRYSTALS	LENGTHS (cm)	DESCRIPTION/RESULT
RE88	Not productive of Web		Clean up lid wetted in RE87. Attempt rerun of that configuration. Vibration on melt surface prevented stable growth.
RE89	4	498	Retest of configuration attempted in RE87 and 88. Lower initial melt level to improve melt stability. Growth stability good. Widths up to 24mm.
RE90	1	68	Grow crystal for resistivity check; doping level $3x10^{17}$ DOPESIL compared to $1x10^{17}$ usually employed.

GROWTH RUN SUMMARY

A major objective of the work carried out on the W furnace this quarter was to test the effectiveness and evolve hardware for two directed gas flow methods. The flow techniques then can be applied to any web growth system to (1) minimize oxide accumulation on furnace parts during longer runs (2) improve convective cooling of the web for faster growth. The venturi method draws cold argon over the web and exhausts it. between the lid and shields to an aspirator. The argon flooding technique purges gas into the cavity between the lid and shields then over the web (see text). Other experiments were directed at lid development for web width control and low web stress. Growth speed for the tests was fixed at about 2cm/min and target width was 20 to 25mm.

RUN	MAX. WIDTH (mm)	TOTAL LENGTH (cm)	DESCRIPTION/RESULT
W79	Not Productive of web		Test short dogbone lid and two "open" shields to get a long, low stress crystal. The longest crystal pulled out when the melt became too warm. Oxide grew on the shields.
W80	Not Productive of web		Identical test conditions to W-79. Oxide on shields again stopped growth.
W81	Not Productive of web		Test Venturi system. Two venturi chimneys. Purpose to keep oxide from accumulating on shields by circulating argon over the melt and away from the growth slot. Shields remained clean. Problems with vibration in melt.
W82	Not Productive of web		Venturi system test. Argon feed tubes in the aspirator clogged with oxide the shields accumulated oxide.
W83	Not Productive of web		Venturi system test. Problems with chimney clogging.
W84	Not Productive of web		Venturi system test. Reduce argon flow to aspirator; tubes remained open but some oxide collected on bottom of shield. Very difficult to adjust melt temperature between extremes of pull out and third dendrites.
W85	17.2	82	Venturi system test. Initially no argon flow was used to check effects on growth, but when oxide began to collect on the shield the argon was turned on. Crystal growth remained difficult with argon flow. Thirds or pullout.

GROWTH RUN SUMMARY

RUN	MAX. WIDTH (mm)	TOTAL LENGTH (cm)	DESCRIPTION/RESULT
W86	13.1	114	Venturi system test. The aspirators were closed so that a test could be made to see whether the crystal growth problem was the result of gas flow around the growth interface or was related to the presence of the massive aspirators. Since a crystal over a meter in length was grown before oxide fell into the melt and caused the web to pull out, it appears that gas flow has caused unstable thermal conditions at the liquid-crystal-interface.
W87	16.3	115	Venturi system test. Fabricated new shield with 45° bend along lid bevel to deflect gas flow. Low argon flow to aspirator to improve stability. Heavy oxide collection.
W88	25.8	318	Venturi system test. The aspirator lid was placed over the regular lid to redirect gas flow away from the melt. Experiment successful; stable growth conditions. Web grown was highly stressed due to extra thick lid configuration.
W89	Not Productive of Web		Venturi system test. Use of two lids resulted in large stress values during last run. To reduce this problem but still keep gas flow away from the melt and menicus, the beveled section of the upper aspirator lid was removed. Had to move coil to achieve growth. Only short web grown.
W90	22.7	400	Venturi system test. To improve web stress a shield was interposed between the lids. The crystals grew well, but there was oxide collection on the shield itself.
W91	22	320	Venturi system test. The same lid arrangement as in W-90 was used in order to verify the observed behavior. Oxide collected on the shield and caused the eventual pull out of the 3 meter crystal. Growth stable but web still stressed.

GROWTH RUN SUMMARY

RUN	MAX. WIDTH (mm)	TOTAL LENGTH (cm)	DESCRIPTION/RESULT
W92	15	92	Venturi system test. The aspirator lid was replaced with a 1/16 shield to open the radiation view angle for stress reduction. Web tended to form lineage during seeding meniscus too cold.
W93	21.2	270	Venturi system test. Same lid/shield configuration as W-90, except that a 1/8" space was used instead of 1/4" between the lids. There was some oxide collection on the shield.
W94	Not Productive of web		Venturi system test; retest of configuration in W-93. Again there was some oxide collection on the shields. Conclude arrangement unsatisfactory.
W95	24.7	154	Argon flooding system test-(first trial). Because the aspirators on the lid caused either unstable growth or highly stressed material, depending on particular lid geometry, new aspirators are being designed which will not be set into a lid. In the meantime a different technique is under test. During this run one tube blew argon between the lid and the lower shield towards the outer edge of the susceptor. A solid ring kept the gas from escaping, and directed the flow out to the web. This kept the side of the lid which held the argon tube clean, but oxide grew on the opposite side of the lid.
W96	22.4	353	Test argon flooding system. A second tube was installed to produce symmetric opposing gas flow. With both tubes in use the shields remained clean. The web, which grew easily, had a heavy coating of oxide, in strong contrast to the clear web grown with aspirators.
W97	Not Productive of web		Test argon flooding system. Retest of previous arrangement to verify results. Suspect furnace leak, heavy oxide. Clean-up of furnace carried out after run.

GROWTH RUN SUMMARY

RUN	MAX. WIDTH (mm)	TOTAL LENGTH (cm)	DESCRIPTION/RESULT
W98	23.3	390	Test argon flooding system to keep shields clean. System clean throughout run. Width of web maintained constant to ± 1 mm over 220 cm length.
W99	25	323	Test argon flooding system. Examine flow rate effects. System clean throughout run. Good width control.
W100	16.4	120	Test argon flooding system and controls. Severe vibration in melt precluded good growth.
W101	28.2	381	Test of argon flooding system with inner quartz baffle removed to monitor effects on total system flow (observation of asymmetric oxide deposition on webs after last runs) Result: no effect on oxide on web but produced oxide accumulation on shields. Higher coil position needed for growth but stability maintained.
W102	20	200	Test argon flooding system. Quartz baffle replaced; shields remain clean. Conclude baffle required for system cleanliness.
W103	24.8	374	Argon flooding system. Longer slot in lid used to increase target width for constant growth. Oxide accumulated at start of run. It was removed and shields stayed clean.
W104	18.5	309	Argon flooding system. Attempt to introduce width control with longer lid slot. Width controlled for one meter. Shields remained clean.
W105	22.2	192	Argon flooding system. Returned to shorter slot to obtain more experience with procedures to control width. Width control more difficult with longer slot.
W106	23.7	220	Argon flooding test. Increase gap in flow cavity between shields from 1/8" to 1/4" to reduce flow velocity. Oxide collected on lower shields.
W107	Unproductive of Web		Argon flooding system. Return to 1/8" cavity. Shields clean but icing problem throughout run.
W108	24.1	403	Repeated run W107. Tested effect of tank argon supply vs. liquid argon for flooding. Oxide collected on shields during run although growth was stable.

GROWTH RUN SUMMARY

RUN	MAX. WIDTH (mm)	TOTAL LENGTH (cm)	DESCRIPTION/RESULT
W109	13.8	168	Argon flooding system; 1/8" gap, short slot. Return to liquid argon supply. Width control difficult because of poor visibility through new quartz tube used to replace one broken after a previous run.
W110	23.3	190	Argon flooding system. Test effects of coil position on growth rate and width control. Lower coil positions caused freezout. Return to higher positions.
W111	16.8	116	Argon flooding system. Further test of coil position. Uppermost positions evaluated. Tendency to extra dendrites at extreme positions. Coil position optimized at mid range for this system.
W112	Unproductive of Web		New venturi, system (2 in. aspirator) tested for first time. Flooding system worked well for growth but surface contamination of web reduced cell efficiency. Reversal of gas flow with venturi should keep shields clean but leave web unaffected. First run to debug flow system; little growth.
W113	18.4	241	Venturi system test. Short growth lid. Small amount of oxide on shield. Initial conditions for web growth identified.
W114	16.1	120	Venturi system test. Test effect of coil position on ability to control web growth. Some oxide collected and inhibited growth.
W115	Unproductive of Web		Venturi system test. Leak in piping caused oxidation of furnace parts. Run aborted.
W116	20.4	196	Venturi system test. Retest of system employed in W115 The lid and shields remained clean. Some tendency for web pullout.

GROWTH RUN SUMMARY

RUN	MAX. WIDTH (mm)	TOTAL LENGTH (cm)	DESCRIPTION/RESULT
W117	19.5	241	Venturi system test. The lid and shields as in W115. Parts remained clean. The coil was raised to improve stability of crystal growth.
W118	22.3	227	Venturi system test. The setup was the same as in W-115. Continue the study of cool position on growth. Lower position. Stable growth.
W119	30.5	294	Venturi system test; set up as in W-115 with the short dogbone lid and the usual shields. Run to verify previous results. The lid and shields remained clean and the crystal grew well. Run terminated by pullout.
W120	25.4	145	Venturi system test, setup as in W-115. Test flow rate in aspirator. The lid and shield remained clean.
W121	22.1	256	Venturi system test, setup as in W-115. Test flow rate in aspirator. The lid and shields remained clean.
W122	23	396	Venturi system test, setup as in W-115. Test argon flow rate. Decreased flow-through aspirators. The shields remained clean to fairly low argon flow. When argon was totally turned off, oxide accumulation slowly initiated.
W123	23	102	Venturi system test; setup as in W-115. There was some oxide collection on the shield.
W124	23.5	218	Venturi system test; setup as in W-115. Test ability to control web width. The shields remained clean.
W125	25.7	202	Venturi system test; setup as in W115. Test ability to control width. There was some oxide collection on the shields, but it did not present a growth hazard. Temperature control was extremely stable.

GROWTH RUN SUMMARY

RUN	MAX. WIDTH (mm)	TOTAL LENGTH (cm)	DESCRIPTION/RESULT
W126	24.3	341	Venturi system test; setup as in W115. Test ability to control web width. There was some oxide growth on the shields. Generally good control.
W127	13.5	90	System test; setup as in W115. Test ability to control width. Trouble with extra dendrites.
W128	28.8	437	Aspirator system test using long dogbone lid to increase web target width. Width control was difficult. Either pullout or third dendrites with this lid, but wider crystals grow easily.
W129	26.8	307	Aspirator system, set up as in W128. There was some oxide collection on the shield.
W130	23.8	394	Aspirator system, using short dogbone lid. There was a significant amount of oxide collection on the shield.
W131	25.1	354	Aspirator system using short dogbone lid. The 2" chimneys have been replaced with 2 3/4" long chimneys to try to improve venturi effect. Both shields and web were clean in this run.

8.2 Updated Program Plan

8.2.1 MILESTONE CHART

JPL CONTRACT 954654 - PHASE II

TASKS/MILESTONES

1. EXISTING WEB GROWTH FACILITIES
   a. Operate Facilities
   b. Demonstrate 12 cm^2/minute
   c. Demonstrate 25 cm^2/minute
2. MODIFY EXISTING WEB GROWTH MACHINE
3. OPERATE MODIFIED MACHINE
4. DYNAMIC THERMAL TRIMMING
   a. Develop dynamic thermal trimming capability
   b. Evaluate and modify thermal trimming
5. MELT REPLENISHMENT
   a. Develop and demonstrate melt replenishment
   b. Utilize melt replenishment capability
6. PERFORM SEEDING VARIATIONS AND STRUCTURAL CHARACTERIZATION
7. DEVELOP AND OPTIMIZE LID GEOMETRY AND UTILIZE THERMAL TRIMMING
8. PERFORM THERMAL MODELING
9. PROVIDE SOLAR CELLS AND WEB SAMPLES AS REQUIRED
10. UP-DATE ECONOMIC ANALYSIS
11. SUPPORT MEETINGS AS REQUIRED
12. PROVIDE REQUIRED DOCUMENTATION

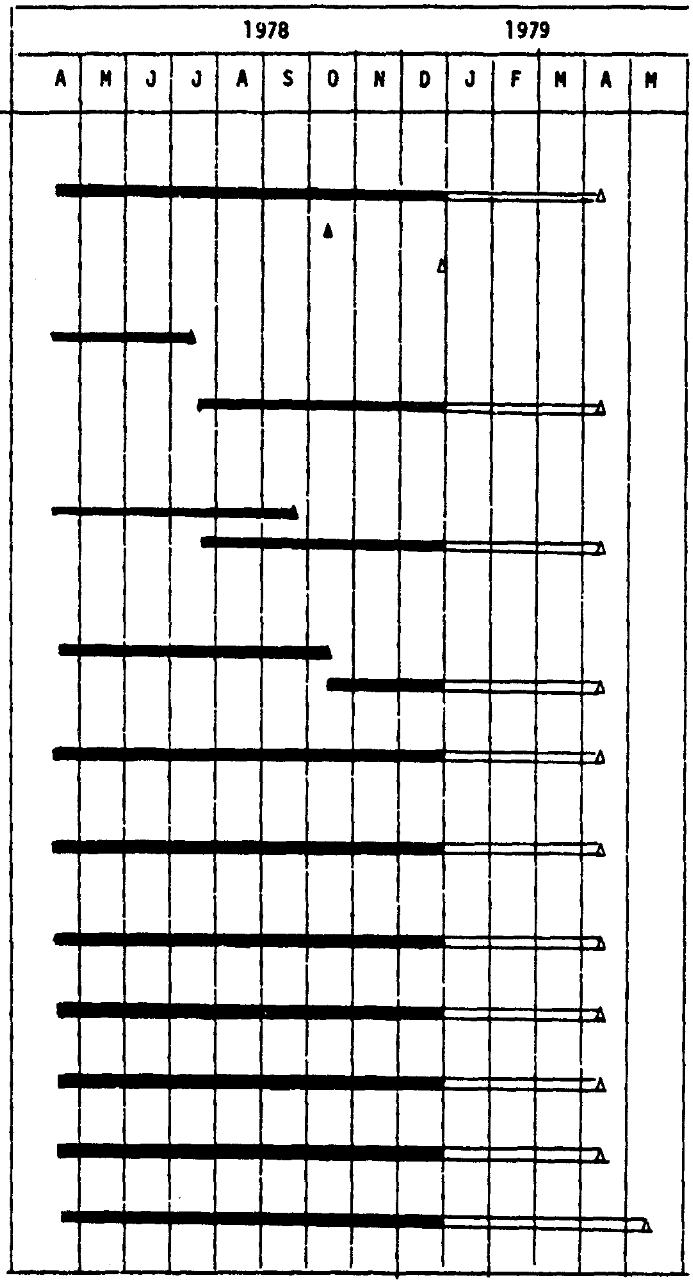

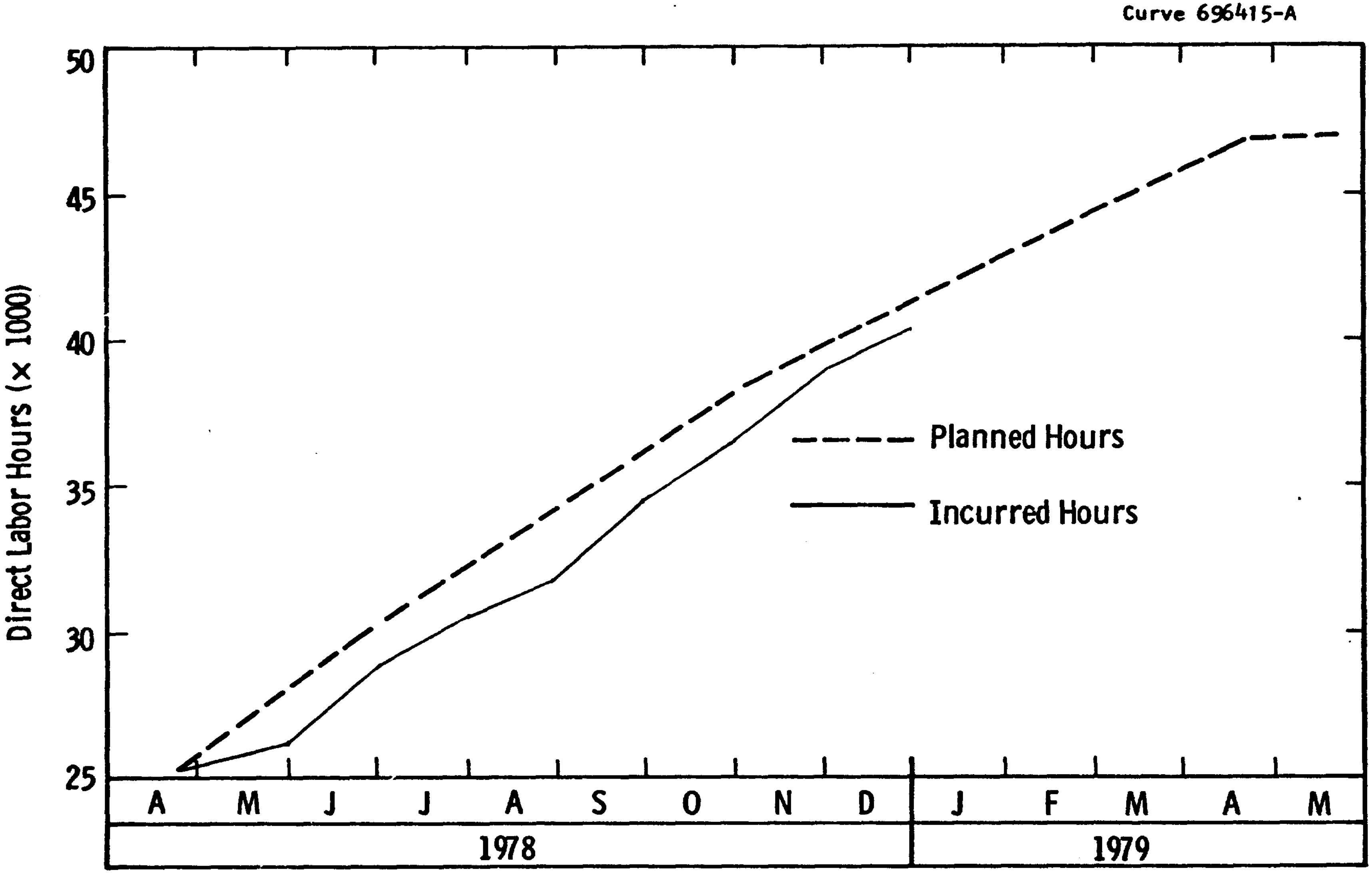

8.2.2 Program Labor Summary JPL 954654, Phase II

Curve 696416-A

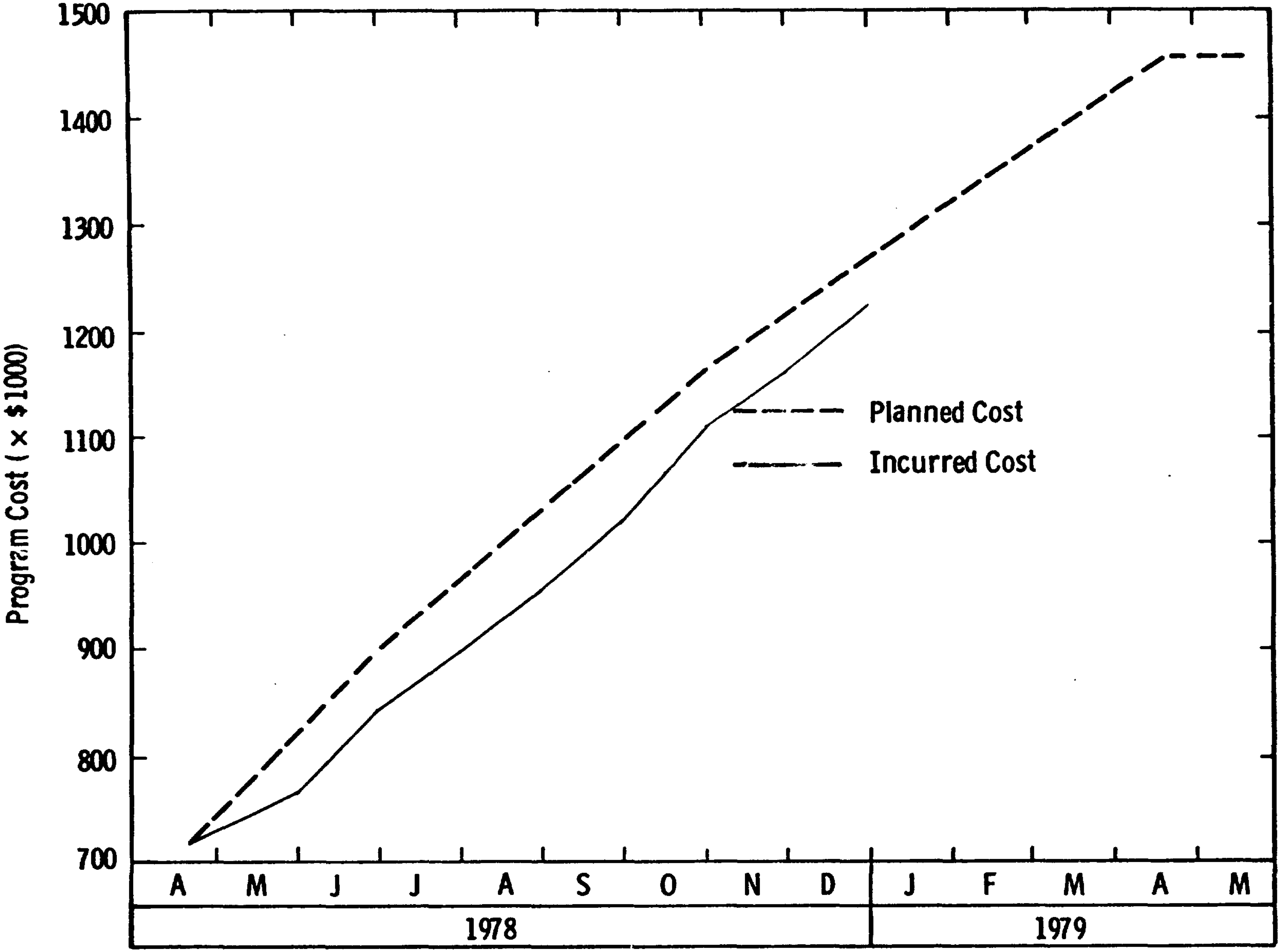

8.2.3 **Program Cost Summary JPL 954654 Phase II**